



Characterisation of Absorbatox™ as a wound healing agent

by

Khulekani Mncube
BSc: Human Physiology
BSc (Hons) Pharmacology

Dissertation submitted in partial fulfilment of the requirements for the degree of:

MSc with specialisation in Pharmacology

April 2013

Faculty of Health Sciences
Department of Pharmacology
University of Pretoria
Pretoria

Supervisor: Dr A.D Cromarty

DEDICATION

I dedicate this dissertation to my Lord, the risen Saviour, Jesus Christ without Whom my entire university career would not have been possible.

“And I am convinced *and* sure of this very thing, that He Who began a good work in you will continue until the day of Jesus Christ [right up to the time of His return], developing [that good work] *and* perfecting *and* bringing it to full completion in you.”

- Philippians 1:6 (Amplified Bible)

ACKNOWLEDGEMENTS

- I would like to express my gratitude to my supervisor, Dr Duncan Cromarty, for lending his expertise and extending his support, encouragement, and advice throughout my post-graduate studies.
- I would like to thank Professor Opper BW Greeff for his support and words of encouragement throughout my post-graduate studies.
- My sincere thanks goes to Dr Markus Stoeckli, Dr Rocco Falchetto Dr Brendan Prideaux, Mr Gregory Morandi, Dr Dieter Staab and the rest of the Analytical Chemistry unit of Novartis Pharma AG (Basel, Switzerland) for hosting me in their lab as an intern, their patience in training me in MALDI MSI, their support and encouragement even after my internship, and also for helping me comfortably integrate into their laboratory. Thank you especially to Dr Stoeckli for teaching me the importance of balance between life and work.
- I wish to thank Dr Marie-Claude Djidja for her help in troubleshooting my sample preparation for the MALDI analysis and to Dr Melanie Ceci and Ms Nicole Ehrhard for all their help in preparing my histological slides.
- My heartfelt gratitude goes out to Novartis Pharma AG, especially to the Diversity and Inclusion Team for their vision to create the Novartis Next Generation of Scientists Internship and giving me the opportunity to be a part of this program.
- I am truly thankful to Dr Caprioli of Vanderbilt University for hosting me in his lab and to Dr Erin Seeley and Mrs Jamie Allen for introducing me to and getting me acquainted with MALDI mass spectrometry and popular American culture.
- I owe sincere thanks to the Chemistry Department of Tshwane University of Technology and Professor Josef Heveling for hosting me in their lab. My thanks go

out to Mr Joshua Malobela and Mr Benias Nyamunda for teaching me and helping me perform my BET-nitrogen adsorption-desorption experiments.

- I am obliged to Mr Charles Noakes and Poretech for laser particle sizing analysis work done on my samples and to Mr Noakes for his assistance in analysing the results.
- I am very grateful to University of the Witwatersrand for facilitating my animal study and especially to Dr Leith Meyer for performing the surgeries.
- I am thankful to Professor Francois Steffens and Mrs Joyce Jordaan for their assistance in regards to statistical analysis and to Professor Steffens for patiently explaining the statistical results to me.
- I wish to thank the Library staff of the Basic Medical Sciences Library, University of Pretoria for their assistance in acquiring research material.
- I wish to thank Mr Aaron Baloyi and Mr Solly Mahlangu of the Pathology Department, University of Pretoria for training me in preparing FFPE tissues.
- I am sincerely thankful to the NRF for financial support by way of a DAAD bursary and KIC travel grant.
- I wish to thank my family, friends and members of my church congregation for their encouragement and prayers as well as Ms Nelsa Da Silva for providing me with a home away from home in my final year of study.
- Finally, my endless, sincere and heartfelt gratitude to my parents and little sister for their love; emotional and spiritual support; encouragement; prayers; and faith in my ability to achieve. I appreciate every sacrifice made on their part to ensure my success. God showed me great favour when He gave me you all. Thank you.

TABLE OF CONTENTS

UNIVERSITY OF PRETORIA - DECLARATION	vii
ABSTRACT	viii
GLOSSARY OF ABBREVIATIONS	x
LIST OF TABLES	xvi
LIST OF FIGURES	xvii
CHAPTER 1: INTRODUCTION	1
Literature review	1
Importance of Work.....	12
AIM	15
OBJECTIVES	15
CHAPTER 2: PHYSICAL CHARACTERISATION	16
INTRODUCTION	16
Nitrogen Gas Adsorption	16
Laser Particle Sizing and Size Distribution	21
MATERIALS AND METHODS	26
Nitrogen Adsorption	26
Laser Particle Sizing	27
RESULTS AND DISCUSSION	29
Nitrogen Adsorption	29
Laser Particle Sizing	35
CONCLUSION	37
CHAPTER 3: ANIMAL STUDY	38
INTRODUCTION	38
MATERIALS AND METHODS	41
Animals	41
Wound induction	43
Wound measurements	44
Statistical analysis	44
RESULTS	46

DISCUSSION.....	51
CHAPTER 4: MALDI-MSI.....	56
INTRODUCTION	56
MATERIALS AND METHODS	63
Formalin-Fixation Paraffin-Embedding (FFPE).....	63
Mass Spectrometry	65
RESULTS AND DISCUSSION.....	73
CONCLUSION	88
CHAPTER 5: PROTEIN IDENTIFICATION	91
INTRODUCTION	91
MATERIALS AND METHODS	94
RESULTS AND DISCUSSION.....	96
Proteins identified on tissue from wound repair DAY THREE	98
Proteins identified on tissue from wound repair DAY SIX	101
Proteins identified on tissue from wound repair DAY SEVEN.....	103
Proteins identified on tissue from wound repair DAY NINE	106
Proteins identified on tissue from wound repair DAY THIRTEEN	108
Proteins identified on tissue from wound repair DAY SIXTEEN	109
CONCLUSION	112
CONCLUDING REMARKS	117
IMPROVEMENTS TO CURRENT STUDY.....	124
REFERENCES.....	126
APPENDIX: Letters of ethical approval and statistical analysis	149

UNIVERSITY OF PRETORIA

FACULTY OF HEALTH SCIENCES

DEPARTMENT OF PHARMACOLOGY

I, Khulekani Mncube,

Student number: 25150392

Subject of the work **“Characterisation of Absorbatox™ as a wound healing agent”**

Declaration

1. I understand what plagiarism entails and am aware of the University’s policy in this regard.
2. I declare that this dissertation is my own, original work. Where someone else’s work was used (whether from a printed source, the internet or any other source) due acknowledgement was given and reference was made according to departmental requirements.
3. I did not make use of another student’s previous work and submitted it as my own.
4. I did not allow and will not allow anyone to copy my work with the intention of presenting it as his or her own work.

Signature _____

ABSTRACT

Introduction. Chronic wounds are a great burden to care-givers and patients alike and are the main cause of many preventable amputations. Such wounds are treated with wound dressings but providing a wound environment that is conducive to proper wound healing is not always possible with such dressings. Absorbatox™ is a natural zeolite that has been manipulated to increase its cationic exchange capacity and has its main functionality as a potential wound healing agent in its strong capillary action. This quality enables the zeolite to absorb excess wound exudate and thus prevent wound infection and maceration. Absorbatox™ was characterised to determine its effects on wound healing.

Methods. The physical characterisation of two grades of Absorbatox™ - granular and micronised - was conducted using nitrogen adsorption to determine pore size and surface area, and laser particle sizing to determine the particle sizes of the Absorbatox™ particles. Full-thickness wounds of 8 x 8 mm were created on the backs of pigs and treated with Absorbatox™, a positive and a negative control. The wound dimensions were measured and recorded. The wounds were then excised on selected days of each phase of wound healing and fixed in formalin. The wound sections were analysed by mass spectrometry imaging and abundant wound proteins were identified from the tryptic digests using BLAST against the Swiss-Prot database.

Results. The surface areas of the micronised and granular Absorbatox™ were 14.43 and 11.23 m²/g, respectively. The micronised Absorbatox™ particle sizes ranged between 0.8 µm to approximately 300 µm with an average pore diameter of 28.2 nm. The granular Absorbatox™ particle sizes ranged between 2 µm and 875 µm with average pore diameters of 43.8 nm. Absorbatox™ showed better wound healing by delaying wound contraction and causing more rapid shallowing of the wound depths compared to the negative control. The difference observed in the wound healing rates of the Absorbatox™-treated and positive control groups were statistically significant and the histological evaluations of the wounds treated with Absorbatox™ showed wound closures that were associated with qualities that more closely resembled normal, healthy tissue than the positive control wounds. The protein

activity in the trypsin-digested tissue including within the wound area and the surrounding healthy tissue was successfully imaged using MALDI-MSI. BLAST software was used at an e-value of 30 to identify possible proteins from the tryptic digests and were identified as proteins involved in wound healing.

Discussion. Micronised Absorbatox™ treated wounds showed more rapid healing than the other treatments most likely due to the smaller particles and pores which results in strong capillary action to absorb excess exudate. Mass spectrometry imaging allowed monitoring of the protein fluctuations that occur during wound healing. The proteins detected were then identified using BLAST and MASCOT database comparison tools which identified that the abundant proteins detected by mass spectrometry were not those typically observed in wound healing but rather those involved in molecular aspects of wound healing like nerve regeneration, cell proliferation, survival, and migration.

Keywords: Nitrogen-adsorption, Wound healing, MALDI-TOF, trypsin digestion, BLAST

GLOSSARY OF ABBREVIATIONS

µg/mL	Microgram per millilitre
µm	Micrometres
3D	Three-dimensional
AESC	Animal Ethics Screening Committee
AlO ₄	Aluminate
ANOVA	Analysis of Variance
ASAP	Accelerated Surface Area Porosity
AUCC	Animal Use and Care Committee
BdB	Broekhoff and de Boer
BET	Brunauer, Emmett, and Teller
BJH	Barrett, Joyner, and Halenda
BLAST	Basic Local Alignment Search Tool
BLNK	B-cell linker protein
BSA	Bovine Serum Albumin
CAS	Central Animal Service
CCD	Charge-coupled device
CEC	Cation exchange capacity
CHCA	α-cyano-4-hydroxycinnamic acid

Cl	Cranston and Inkley
cm ³ /g	Cubic centimetre per gram
CO ₂	Carbon dioxide
Cr	Chromium
Da	Dalton
DH	Dollimore and Heal
DNA	Deoxyribonucleic acid
dpi	Dots per inch
EGF	Epidermal growth factor
EGFR	Epidermal growth factor receptor
EtOH	Ethanol
EZS	Electrical Zone Sensing
FFPE	Formalin-Fixed Paraffin-Embedded
g	Gram
H	Hysteresis
H&E	Haematoxylin and Eosin
HIV/AIDS	Human Immunodeficiency Virus / Acquired Immunodeficiency Syndrome
IL	Interleukin
ITO	Indium tin oxide
IUPAC	International Union of Pure and Applied Chemistry

K	Kelvin
kDa	Kilodalton
KGF	Keratinocyte growth factor
L	Litre
l/m	Litres per minute
LS	Light scattering
LSHU	Liquid Sample Handling Unit
M	Molecular weight of the adsorbate
m/z	Mass-to-charge ratio
m ² /g	Square metre per gram
mA	Milliampere
MALDI-MSI	Matrix-assisted laser desorption/ionisation mass spectrometry imaging
MALDI-TOF	Matrix-assisted laser desorption/ionisation time-of-flight
MAPK	Mitogen-activated protein kinase
MASCOT	Modular Approach to Software Construction Operation and Test
mg/kg	Milligrams per kilogram
ml	Millilitre
mm	Millimetre
mM	Millimolar
mmHg	Millimetres of Mercury

MMPs	Matrix metalloproteinases
MS	Mass spectrometer
MS/MS	Tandem mass spectrometry
NCBI	National Centre for Biotechnology Information
Nd/YAG	Neodymium-Doped Yttrium Aluminum Garnet
NF- κ B	Nuclear factor kappa-light-chain-enhancer of activated B cells
NH ₄ CO ₃	Ammonium carbonate
NK	Natural Killer
nm	Nanometre
NP	Nucleoprotein
°C	Degree Celsius
P/P ₀	Partial / relative pressure
Paf1C	Polymerase-associated factor 1 complex
PDGF	Platelet-derived growth factor
PF4	Platelet factor 4
PMF	Peptide mass fingerprinting
PSD	Pore size distribution
PTMs	Post-translational modifications
PVD	Peripheral Vascular Disease
R	Gas content

RBP	RNA-binding proteins
r_k	Radius (of the largest cylindrical capillary filled with condensate)
RNA	Ribonucleic acid
ROI	Region of interest
r_p	Radius into which condensation occurs
rRNA	Ribosomal ribonucleic acid
s	Second(s)
SEM	Scanning electron microscope
SEM	Standard error of the mean
SF	Splicing factor
SiO ₄	Silicone tetraoxide
T	Temperature
T-cell	Thymus cell
TFs	Transcription factors
TGF- β	Transforming growth factor beta
Ti	Titanium
TIMPs	Tissue inhibitors of metalloproteinases
TLC	Thin layer chromatography
TNF- α	Tumour necrosis factor alpha
TPM	Tropomyosin

UV	Ultraviolet
VEGF	Vascular endothelial growth factor
V_m	Monolayer capacity
vs.	Versus
γ	Surface tension of the adsorbate
θ	Contact angle
ρ	Density of the adsorbate

LIST OF TABLES

Table 1

Surface, external, and micropore areas of granular and micronised Absorbatox™.

Table 2

Total pore volumes and pore size distributions of granular and micronised Absorbatox™.

Table 3

Wound width measurements (mm).

Table 4

Wound length measurements (mm).

Table 5

Wound depth measurements (mm).

LIST OF FIGURES

Figure 1

Illustration of the wound healing process as well as the estimated time for which each phase lasts (Broughton *et al.*, 2006).

Figure 2

Prevalence of Peripheral Vascular Disease (PVD) amongst diabetic patients in Africa (Abbas and Archibald, 2007).

Figure 3

Three-dimensional tetrahedral structure of a zeolite (Woodford, 2012).

Figure 4

Graphical representation of methods used to determine surface area, pore volume, and pore size distribution (Micromeritics® Instrument Corporation, n.d).

Figure 5

A) Low-angle light scattering from a particle larger than the light source wavelength following the Fraunhofer theory. B) A combination of high- and low-angle light scattering from a particle slightly smaller than the light source wavelength in accordance to the Mie theory (Young, 2005).

Figure 6

Nitrogen adsorption-desorption isotherm for granular Absorbatox™ zeolite.

Figure 7

Nitrogen adsorption-desorption isotherm for micronised Absorbatox™ zeolite.

Figure 8

The IUPAC classification of adsorption isotherms and hysteresis loops (Sing *et al.*, 1982).

Figure 9

Granular Absorbatox™ (left) and micronised Absorbatox™ (right).

Figure 10

Cumulative finer volume percent vs. particle diameter (μm).

Figure 11

Pattern of wound treatments.

Figure 12

Comparison of the effects of each treatment: Absorbatox™ vs. Negative control and Cerdak™ (positive control) on wound widths.

Figure 13

Comparison of the effects of each treatment: Absorbatox™ vs. Negative control and Cerdak™ (positive control) on wound lengths.

Figure 14

A line graph comparison of the wound contraction rates of each treatment group.

Figure 15

Comparison of the effects of each treatment: Absorbatox™ vs. Negative control and Cerdak™ (positive control) on wound depths.

Figure 16

Histological comparison of wound tissue treated with Cerdak™ (positive control), negative control, and the two Absorbatox™-treatments used in the study by Oosthuizen *et al.* (2009).

Figure 17

Graphical description of the process of the generation of ions and their subsequent translation into ion-density distribution images (Seeley and Caprioli, 2011).

Figure 18

Difference in matrix application for both protein profiling and imaging (Chaurand *et al.*, 2005).

Figure 19

Simplified scheme of formaldehyde reaction with proteins. (a) Formaldehyde is added to a protein with the formation of a reactive hydroxymethyl molecule. (b) Formation of an imine group (Schiff's base). (c) Methylene bridge formation between a lysine residue (lysyl group) and nitrogen of a peptide linkage. Formaldehyde is depicted as methylene glycol, formed by reaction with water (D'Amico *et al.*, 2009).

Figure 20

The above diagram shows the protein effects of formalin fixation and that of antigen retrieval (Yamashita, 2007).

Figure 21

Diagram of the embedded tissue and the approximate areas at which sections were made for MALDI-MS analysis.

Figure 22

Screen shot of the stacked mass spectra of the wound (blue), healthy (red), and the CHCA matrix (green) as seen in TissueView 1.0.

Figure 23

Histology-directed MALDI-MS images of full-thickness wounds showing the progression of wound healing following the intensity of selected peptides with m/z 373 and m/z 413.

Figure 24

Histology-directed MALDI-MS images of full-thickness wounds showing the progression of wound healing following the intensity of selected peptides with m/z 486 and m/z 607.

Figure 25

Histology-directed MALDI-MS images of full-thickness wounds showing the progression of wound healing following the intensity of selected peptides with m/z 644 and m/z 795.

Figure 26

Histology-directed MALDI-MS images of full-thickness wounds showing the progression of wound healing following the intensity of selected peptides with m/z 833 and m/z 1044.

Figure 27

The figure above shows the “top-down” (right) and “bottom-up” (left) methods that can be used to identify and characterise proteins (Thiede *et al.*, 2005).

Figure 28

Graphical description of the workflow for collecting “bottom up” proteomic data. On-tissue trypsin digestion resulted in tryptic digests which gave spectra that were fed into databases to give positive identification of the proteins detected in the wound tissue (adapted from Fenyö, 2000).

Figure 29

An output table of possible proteins identified from the data submitted to the BLAST database.

Figure 30

A graphical description illustrating the overlap seen in the wound healing process in terms of the proteins detected in the animal models used in this study.

CHAPTER 1: INTRODUCTION

Literature review

“Healing is a matter of time, but it is sometimes also a matter of opportunity.”

– Hippocrates

Wounds result from either thermal or mechanical damage to the skin (Boateng *et al.*, 2008; Gibson and Schultz, 2009). This damage interferes with the normal anatomical and physiological function of the wounded area, for example, by compromising the protective barrier against infection. Wound healing is an important and complex but necessary process that aims to restore the anatomical and physiological integrity of the skin through a series of sequential but overlapping phases. These are the inflammatory, proliferatory, and remodelling or maturation phases. A healed wound is one that is completely covered by scab (Tian *et al.*, 2007). The process involves several mediators of inflammation, many different enzymes, growth factors and several localised cell types like keratinocytes, fibroblasts and endothelial cells as well as immune cells (Diegelmann and Evans, 2004; Blakytyn and Jude, 2006; Boateng *et al.*, 2008; Gibson and Schultz, 2009).

When tissue injury is sustained, the underlying blood vessels are damaged and bleeding can occur. Bleeding helps flush out foreign particles (Boateng *et al.*, 2008). Blood flow brings platelets that undergo aggregation and release of important factors that initiate the formation of a clot to discontinue the blood flow but also to facilitate the release of a variety of cytokines which lead to vasodilation and increased permeability of local blood vessels. This is an important part of the maintenance of

homeostasis and the beginning of the inflammatory phase (Singer and Clark, 1999; Diegelmann and Evans, 2004; Blakytyn and Jude, 2006).

The inflammatory phase begins immediately after the wound is sustained and lasts three to four days during which protein-rich exudate is released into the wound to promote vasodilation through the release of histamine and serotonin (Broughton *et al.*, 2006; Boateng *et al.*, 2008). Vasodilation allows for the infiltration of neutrophils which are drawn into the wounded tissue by locally released cytokines such as interleukin-1 (IL-1), transforming growth factor beta (TGF- β), tumour necrosis factor alpha (TNF- α), platelet factor (PF4) and bacterial by-products (Broughton *et al.*, 2006). The neutrophils not only play a phagocytic role in the wound area but also condition the area for healing by releasing proteolytic enzymes to eliminate bacterial debris and contaminants as well as damaged and necrotic tissue (Diegelmann and Evans, 2004; Broughton *et al.*, 2006; Boateng *et al.*, 2008; Sibbald and Woo, 2008). Macrophages start replacing the neutrophils as the process progresses and dominate during the end stages of the inflammatory phase. The macrophages release platelet-derived growth factor (PDGF), vascular endothelial growth factor (VEGF), and TGF- β all of which facilitate angiogenesis. The presence of the macrophages is also important for the transition into the proliferatory phase of the wound healing process (Diegelmann and Evans, 2004; Broughton *et al.*, 2006; Sibbald and Woo, 2008; Kyriakides *et al.*, 2009).

The proliferatory phase occurs from approximately day four through to day fourteen (Broughton *et al.*, 2006) and includes the major healing processes (Hunt *et al.*, 2000). During this period, fibroblasts, keratinocytes, and endothelial cells are the most dominant cells undergoing proliferation (Broughton *et al.*, 2006). Epithelial cells on the edge of the wound begin to proliferate to create a new protective barrier against fluid loss and potential infection (Singer and Clark, 1999; Broughton *et al.*, 2006). There is also an increase in skin strength due to the appearance of newly synthesised collagen by the fibroblasts (Boateng *et al.*, 2008). This cell proliferation is stimulated by epidermal growth factor (EGF) and TGF- α produced by activated platelets and macrophages (Broughton *et al.*, 2006) as well as keratinocytes

(Diegelmann and Evans, 2004). The secretion of mediators such as PDGF, results in the chemotaxis of neutrophils then macrophages (Diegelmann and Evans, 2004). PDGF is also a potent chemoattractant for monocytes, fibroblasts, and smooth muscle cells and is associated with accelerated wound healing and enhanced tensile strength across the wound (Ashraf *et al.*, 2009). TGF- β is a major mediator in wound healing by regulating fibroblasts (Diegelmann and Evans, 2004). It has a three-fold effect on extracellular matrix deposition by increasing the overall production of matrix by enhancing collagen synthesis (Diegelmann and Evans, 2004; Broughton *et al.*, 2006) as well as that of proteoglycans and fibronectins (Diegelmann and Evans, 2004) thus playing a role in scar formation (Ashraf *et al.*, 2009); decreasing the production of matrix metalloproteinases (MMPs); and increasing the production of tissue inhibitors of metalloproteinases (TIMPs) (Diegelmann and Evans, 2004; Broughton *et al.*, 2006). TGF- β – especially TGF- β_1 also plays an important role in this stage of wound healing by acting as a potent chemoattractant for monocytes, macrophages, neutrophils, keratinocytes, and fibroblasts. TGF- β_1 also induces the release of other growth factors from these leukocytes (Singer and Clark, 1999; Blakytyn and Jude, 2006). The MMPs are a family of zinc endopeptidases that are responsible for degrading components of the extracellular matrix; eliminating damaged protein; promoting movement of certain cellular components into the centre of the wound; destroying provisional extracellular matrix; regulating the activity of some growth factors; and playing a role in angiogenesis (Osman *et al.*, 2002). The MMPs are divided into subgroups depending on their substrate. The MMPs that play a key role in wound healing are the collagenases (MMP-1 and -8) and the gelatinases (MMP-2 and -9) (Muller *et al.*, 2008). Other mediators involved in wound healing include the eicosanoids such as the prostaglandins which mediate inflammation; cytokines which regulate cellular activities and function; and nitric oxide – a physiologically active molecule released by macrophages (Diegelmann and Evans, 2004; Broughton *et al.*, 2006).

The maturation (remodelling) phase is the final stage of wound healing and can last anything from a few days to two years (Broughton *et al.*, 2006; Boateng *et al.*, 2008) depending on the size and depth of the wound tissue. During this phase, the pro-collagen precursors synthesized during the proliferatory phase are converted from

the immature but predominant collagen III to the mature, organised collagen I network that ensures a wound that is strong and resistant to sheer forces thus limiting the chance of reopening (Diegelmann and Evans, 2004; Broughton *et al.*, 2006; Sibbald and Woo, 2008). This phase also results in the development of scar tissue which is determined by the strength of the new epithelia (Hunt *et al.*, 2000; Boateng *et al.*, 2008).

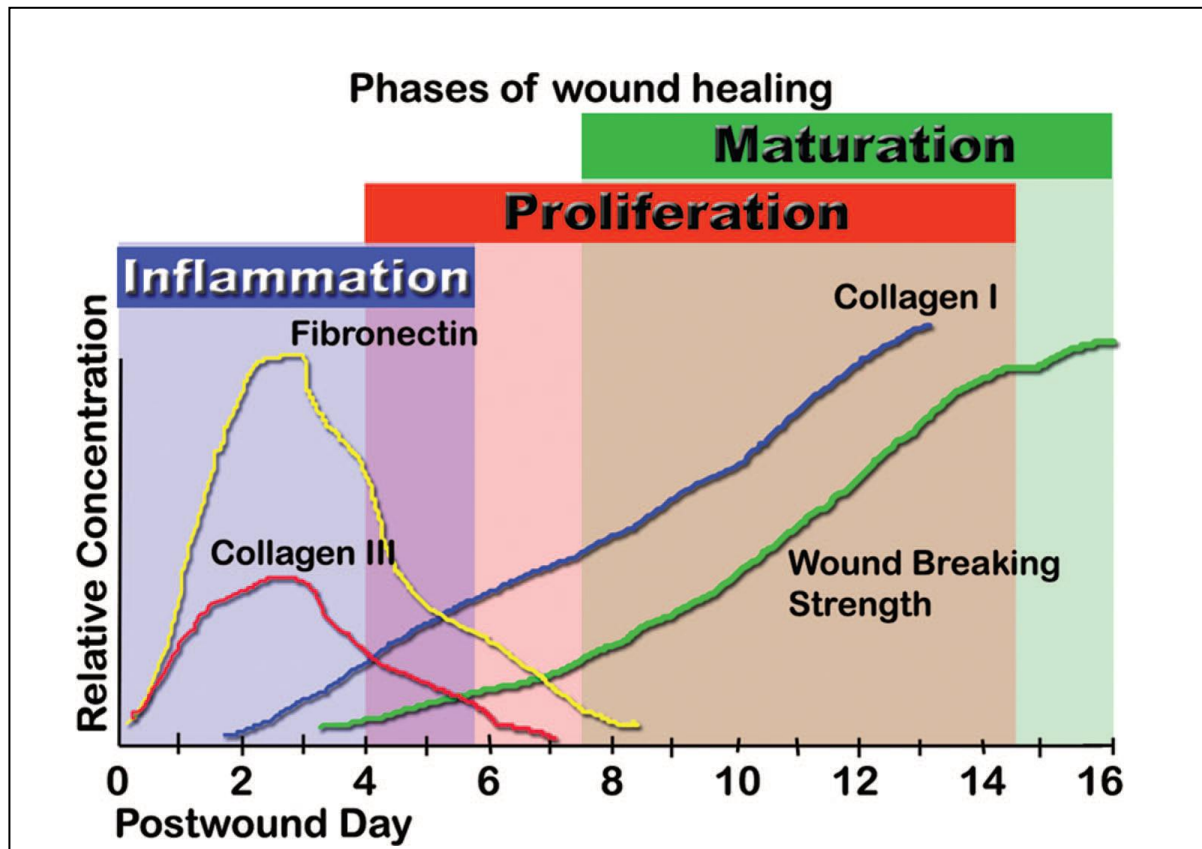


Figure 1: Illustration of the wound healing process as well as the estimated time for which each phase lasts (Broughton *et al.*, 2006).

Despite the complexity of the wound healing process, its effectiveness can be significantly affected by several factors such as arterial insufficiency, growth factors, inadequate perfusion, infection, low oxygen tension, neuropathy, nutritional state, oedema, as well as systemic factors and metabolic disorders (Hunt *et al.*, 2000) (example: diabetes). The presence of underlying physiological and biochemical defects and imbalances such as those seen in diabetes, often leads to impaired

healing of wounds. Muller *et al.* (2008) state a “unifying pathophysiological hypothesis” supported by Blakytyn *et al.* (2005), Diegelmann and Evans (2004), and Singer and Clark (1999), that in chronic wounds, the wound healing process is arrested in a state of inflammation. This typically results in profuse neutrophil and macrophage infiltration associated with the extensive discharge of reactive oxidative species and degrading enzymes (proteases) and pro-inflammatory cytokines leading to the formation of wounds that do not heal completely within the average 8-12 weeks and/or are recurring (Blakytyn and Jude, 2006; Boateng *et al.*, 2008). Diabetic ulcers are also prone to repeated infection owing to the inadequate neutrophil and macrophage migration and impaired function (Singer and Clark, 1999; Blakytyn and Jude, 2006; Hirsch *et al.*, 2008).

Chronic wounds are managed to prevent or treat infection that could lead to amputation (Hunt *et al.*, 2000). In the case of diabetic patients, *Staphylococcus aureus* (*S. aureus*) is the most abundant single isolate from diabetic wounds, and this often leads to the poor wound healing seen in these instances (Hirsch *et al.*, 2008).

In general, treatment of wounds is done by debridement of necrotic tissue and occlusive dressings (Hunt *et al.*, 2000) but this has not always been so. The treatment of wounds has evolved over centuries from the application of traditional healing agents such as plants and animal fat, to tissue engineered skin substitutes (Boateng *et al.*, 2008). The use of some crude plants and animal fat however, often led to bacterial infection thus defeating the purpose of using a wound dressing (Boateng *et al.*, 2008). Despite the development of skin substitutes, wound dressings are still the mainstay of chronic wound treatment (Singer and Clark, 1999; Boateng *et al.*, 2008), although dressing such wounds appropriately is a challenge. The goal of wound dressings is to provide an environment that is conducive to proper wound healing. A dressing should readily absorb excessive wound exudate, so as to prevent bacterial overgrowth, exudate leakage and maceration at the edges of the wound, yet should not cause excessive drying of the wound. The rationale behind this is that wound exudate helps facilitate the healing process by providing

the wound bed with nutrients and assists in the migration of the epithelial cells (Singer and Clark, 1999; Sullivan *et al.*, 2001; Boateng *et al.*, 2008).

Systemic pharmacological agents can also be used in wound healing but these have the potential to cause toxic side effects and therefore direct application of healing agents to the wound is preferred (Boateng *et al.*, 2008).

Absorbatox™ embedded in the wound dressing helps to create a wound healing environment ideal for rapid and positive wound healing; and since it is a topical wound treatment, does not have the potential to cause systemic toxicity.

Absorbatox™ is a synthetically enhanced, hydrated aluminosilicate and a clinoptilolite of the zeolite family which has limited natural activity but has been subjected to a patented process that increases its cation exchange capacity (CEC) to 5 times its original capacity. Like all zeolites, Absorbatox™ is composed of aluminium, oxygen, and silicon in a tetrahedral arrangement resulting in pores and a cage like structure since the tetrahedral units cannot fill the available space entirely (Kaneko, 1994). The three-dimensional arrangement of AlO_4 and SiO_4 tetrahedra in Absorbatox™ enclosing a porous cage like complex (Dutta *et al.*, 2005) exemplifies this. The porous complex provides Absorbatox™ with specific physicochemical properties including: ion exchange capacity, adsorbent nature, size exclusion framework, and catalytic properties. The advantage of Absorbatox™ in wound healing lies in its ability to draw wound exudate out of the wound by strong capillary forces but still keep the wound from becoming overly dry.

With the aim of further investigating Absorbatox™ as a wound healing agent, the processed zeolite was subjected to physicochemical characterisation. The Brunauer, Emmet, and Teller (BET)-nitrogen adsorption-desorption experiments were performed to determine the average surface area and total pore volume of two Absorbatox™ samples of different physical dimensions – micronised (fine powder)

and granular. Laser particle sizing was used to determine the average particles sizes of the same two Absorbatox™ samples.

At present, gas adsorption is the best and one of the more commonly used adsorption methods to investigate the characteristics of porous materials such as surface area, total pore volume, and pore size distribution (PSD) (Sing, 1998; Choma *et al.*, 2002) such as Absorbatox™. The BET theory upon which the BET-nitrogen adsorption-desorption experiments are based, is that gas molecules physically adsorb on a solid surface in layers infinitely; that no interaction between these layers exist; and that the Langmuir theory can be applied to each layer. The resulting BET equation is used to calculate the surface area and pore volume of solids by the physical adsorption of gas molecules (Brunauer *et al.*, 1938).

While knowledge of a material's surface area gives insight into how it will react with another substance and is thus an important quality to investigate when characterising porous materials (Bae *et al.*, 2010), it is, in fact, the pore size distribution which is the strongest determinant of adsorption (Wang *et al.*, 2005). The method of Barrett, Joyner, and Halenda (BJH) (Micromeritics® Instrument Corporation, n.d.) is used to determine pore size distribution from experimental isotherms using the Kelvin model for pore filling (Micromeritics® Instrument Corporation, n.d; Choma *et al.*, 2002).

The BJH method of determining pore size distribution analyses the nitrogen desorption isotherm at liquid nitrogen temperature based on the assumption that the mechanisms of physical adsorption on the pore walls and capillary condensation in the pore can be employed to establish equilibrium between the adsorbed and gas phases during the process of desorption (Barrett *et al.*, 1951; Choma *et al.*, 2002).

Particle size plays an important role in many industries including the pharmaceutical and mining industries (Micromeritics®, n.d). Numerous techniques exist to

determine particle size (Bowen, 2002) however, light scattering techniques such as laser particle sizing are more widely used due to their high levels of accuracy and reproducibility, and also that these analysis techniques are generally faster than microscopy for example (Barth and Flippen, 1995; De Ridder *et al.*, 2000; Vanderhallen *et al.*, 2002; Micromeritics®, n.d). Laser particle sizing uses the principle of light scattering to determine particle size and light scattering instruments are often based on the Mie theory. The Mie theory is a mathematical-physical theory of the scattering of electromagnetic radiation by isotropic, spherical particles as a function of the angle at which light is scattered at the point of interaction with the particle. The intensities of light at each scattering angle are measured and are correlated to particle size (Webb, 2004; Ferraris *et al.*, 2004).

Further exploration into a possible mechanism of action of Absorbatox™ included actual examination of wound tissue from an animal study at the subcellular level using a technique called matrix-assisted laser desorption/ionisation mass spectrometry imaging (MALDI MSI).

MALDI MSI is a soft-ionisation technique that has gained popularity in modern proteomics (the analysis of proteins in a living system) (Liu *et al.*, 2010) largely because it allows researchers to study biological processes extensively by the systematic analysis of proteins expressed in a cell or tissue (Yates, 1998). The technique came as a result of many years of investigation into the use of lasers for the soft ionisation of biomolecules (Caldwell *et al.*, 2008) such as proteins (Tarran *et al.*, 2007). MALDI-time-of-flight-MS (MALDI-TOF-MS) has made possible the sensitive detection and measurement of large, intact proteins from tissue sections and even plasma as they fluctuate during the various biological processes and even stages of wound healing (Jemal and Xia, 2006; Zhao *et al.*, 2006). In addition to being able to measure the protein fluctuations in tissue, MALDI MSI, another sensitive and robust technique, allows researchers to image tissue by the quantitation of proteins present in thin histological tissue sections. MALDI MSI and MALDI-TOF enable analysis of tissue sections by detecting the presence, relative concentration, location, and spatial orientation of small molecules and lipids in

addition to proteins and other macromolecules in biological structures (Yates, 1998; Aebersold and Goodlett, 2001). This makes following the changes occurring during physiological processes at molecular level possible, which makes MALDI-TOF and MALDI MSI each an ideal tool to investigate the biological effects that Absorbatox™ has on wounds with respect to its ability to provide an environment that results in improved wound healing.

MALDI-MSI works as follows: An organic material (termed matrix) is applied to a thin (10 µm – 30 µm) tissue section that was previously mounted on to a plate and dehydrated. The plate, upon which the section is mounted, is introduced into a mass spectrometer, where a focused laser beam is pulsed along the surface, resulting in the ejection of ions from the tissue. These ions are accelerated into a flight tube and strike, thereafter, a detector at different times. The lighter ions travel faster and thus hit the detector sooner. This difference in flight time is translated into spectra. Distribution images for specific ions are then extracted from the thousands of acquired spectra.

Ion-intensity distribution images, despite being a graphical representation of the spectra analysed, do not offer information on the proteins present in the tissue. For this reason, protein and peptide identification is necessary. Protein identification is typically performed using tandem mass spectrometry (MS/MS). However, the identification of intact proteins – regarded as the “top-down” approach – raises some serious challenges. For this reason, it is not uncommon to introduce an enzyme to digest the protein into peptides and then measure the tandem mass spectra of the peptides (Worley *et al.*, 1995; Resing and Ahn, 2005; Xu and Ma, 2006). From here, a number of methods can be employed to identify the proteins: *de novo* sequencing, sequence tagging, database searches, and consensus of multiple search engines (Xu and Ma, 2006). While MALDI has made possible the analysis of significantly large proteins, the greatest impact still remains in the analysis of peptides generated by proteolytic digestion. A reason for this is, while the mass accuracy of the MALDI MS is high, it is not sufficient to identify a protein with confidence based only on its molecular weight (Veenstra *et al.*, 2006). It is thus the mass spectrum of the peptide

fragments resulting from the use of a proteolytic enzyme such as trypsin, that gives the “peptide mass fingerprint” that is used to identify the proteins in a tissue sample (Veenstra *et al.*, 2006).

Trypsin is the favoured enzyme for peptide mass fingerprinting as it is moderately cheap, extremely effective, and produces tryptic digests of, on average, 8-10 amino acids which are ideally suited for MS analysis (Thiede *et al.*, 2005). This is exemplified by its use in almost all large-scale projects in mass spectrometry to give more easily analysable peptides (Olsen *et al.*, 2004). Trypsin belongs to the serine protease family and shows primary structural similarity to chymotrypsin. The enzymatic mechanism requires that the target amino acid be recognised in the binding pocket of the trypsin. The substrate binding pocket of the trypsin has a negatively charged aspartate at the bottom of it and binds basic amino acids by means of an ionic interaction. The target amino acids for trypsin cleavage need to have long side chains and be positively charged to permit this formation of the ionic bonds. Arginine and lysine both fulfil the criteria necessary for the ionic interaction required for trypsin to work and it is at these regions that trypsin lyses unless either the arginine or lysine is followed by a proline (Olsen *et al.*, 2004; Fremout *et al.*, 2010). The resultant peptides are characteristic, specific, and unique for each given protein thus identifying the peptide means identifying the protein as a whole. Identifying the protein from the peptide fragments is termed “bottom-up” or “shot-gun” proteomics. This method is also advantageous in terms of its sensitivity and proteome coverage (Fremout *et al.*, 2010; Mallick and Kuster, 2010). The peptides identified by this method are then fed into a bioinformatics algorithm which allows for the proteins to be identified after comparing a query sequence with a library or database of sequences. Two examples of bioinformatics algorithms that can be used to identify the peptides are MASCOT and BLAST which correlate mass spectra with peptides in sequence databases to return a positive identification. MASCOT is a probability-based search engine for peptide identification and peptide sequence assignment (Olsen *et al.*, 2004; Weatherly *et al.*, 2005). BLAST is a similarity search program that matches similar peptide sequences and either identifies the protein or confirms a vague hit produced by MASCOT (Shevchenko *et al.*, 2001).

The wound healing model used for the study is a Large White Female pig. While using a human model for the study would be ideal, it is obvious that such a study would raise serious ethical debate. Other wound healing studies use rodents such as rabbits or mice for such studies due to the ease of handling and the cost of housing for these animals. The main disadvantage of using rodents as models is that they simply do not properly represent wound healing as seen in humans due to the many differences between rodent and human skin profiles. Porcine skin, however, shows greater similarity to human skin than other species (Hirsch *et al.*, 2008; Velandar *et al.*, 2008).

The main similarities between the skins of the two species with regards to wound healing are those of the epidermis, skin vascularisation, and epidermal collagen. This similarity in structure was most evident in a study conducted by Moritz and Henrique in 1946 during which skin sections from both humans and pigs treated with benzidine were seen to be virtually indistinguishable (Vardaxis *et al.*, 1997).

With respect to wound healing, porcine skin also heals similarly to human skin. Rodent skin heals mainly through contraction whereas both human and porcine skins heal primarily through re-epithelialisation. Another important aspect of pigs as wound healing models is that pigs are also more closely representative of chronic wounds in patients with serious illnesses since they too are placed under a great deal of physiological stress with the induction of numerous wounds, the regular and repeated handling, as well as the frequency of general anaesthesia (Sullivan *et al.* 2001).

Importance of Work

“My grandma lost both legs to diabetes; my mama already lost her foot and now I got diabetes. I figured I would just lose my legs, too. I never knew there was anything I could do to stop it.”

- Quote from a REACH focus group participant (1999)

According to Diabetes South Africa, 4-6 million people in South Africa have diabetes. While a diagnosis of diabetes does not necessarily mean that one will develop a chronic wound, much less undergo an amputation because of it, it is important to note that diabetic patients are at a higher risk of developing peripheral vascular disease – the primary cause of chronic wounds. Figure 2 is a graph summarising the high prevalence of peripheral vascular disease in diabetic patients in selected African countries.

In addition to diabetes, HIV/AIDS should also be considered in the development of chronic wounds. The development of a chronic wound in an HIV/AIDS patient can result from a simple cut from a non-sterile edge. Because the HIV/AIDS patients are immune-compromised, the immune response that is normally seen when a wound is sustained may not occur or may not be quite as efficient as in a healthy person. This results in the bacteria that would ordinarily be eliminated by the neutrophils and macrophages, proliferating unchecked and causing a localised infection. In such a case, it is not necessarily the infection that leads to the chronic wound, but rather that the absence of critical immune responses prevents release of chemotactic cytokines and growth factors necessary for the wound to progress from the inflammatory phase to the proliferatory phase and finally to be properly healed. According to the mid-year report of Statistics South Africa of 2011, 16.6% of the adult population in South Africa were living with HIV; this is an increase of 1.17 million since 2001 with almost a quarter of these being due to new infections.

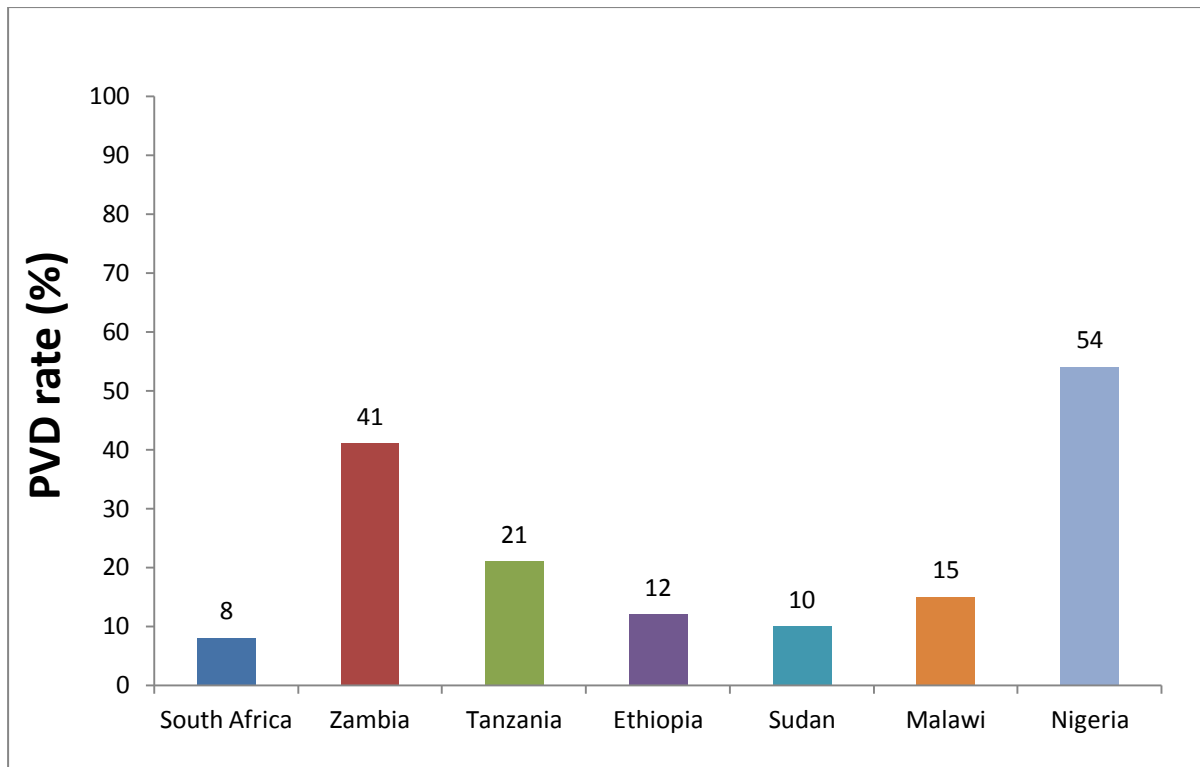


Figure 2: Prevalence of Peripheral Vascular Disease (PVD) amongst diabetic patients in Africa (Abbas and Archibald, 2007).

Both diabetes and HIV/AIDS are on the increase, not just in South Africa, but throughout the whole of Africa where chronic wounds are a considerable burden to both patients and healthcare systems. In Africa (Abbas and Archibald, 2007) the increasing number of diabetic patients and rate of HIV infection with their related complications including poor wound healing are leading to numerous preventable amputations. These health problems are the driving force for this project in investigating wound healing on the proteomic level where an understanding of the differences in wound healing kinetics and phase-dependent proteomics could lead to identifying targets for early interventions that could prevent exacerbation of wound status to the point where drastic intervention measures are required.

Determining the mechanism of action of Absorbatox™ as a wound healing agent could greatly benefit South African patients. The potential outcome of this research is not only to achieve effective wound management which is much needed, but also

to create a marketable, safe, and effective wound dressing that will contribute to healing of chronic wounds and thus the prevention of amputations and the reduction in loss of employment due to disability.

While it could be argued that disability does not equal loss of employment, when the number of people in South Africa whose only income is from manual labour (such as: mechanics, construction workers, miners) is considered, it becomes very clear that this research does indeed hold promise to decrease unemployment due to preventable amputation, and essentially protect the South African economy.

The importance of this research is not only limited to Africa, however, since an estimated 5 million patients in the United States suffer from chronic wounds (Velandar *et al.*, 2008). In both the African and American contexts, this often results in lost time from work and hefty health care costs. Unfortunately, these high incidence and prevalence rates are not likely to decrease significantly any time soon with increasing sedentary lifestyles and unhealthy diets and the resultant cases of obesity: a cause of type II diabetes. Interestingly enough, a parallel increase in the incidence of foot complications in the diabetes populations has been documented (Abbas and Archibald, 2007).

To quote from a wound healing research group (Velandar *et al.*, 2007): “We need better ways to treat diabetic wounds”.

AIM

To assess changes in wound tissue and possibly identify possible mechanisms by which Absorbatox™ induces wound healing.

OBJECTIVES

1. Physical characterisation

- 1.1. Analysis of nitrogen adsorption isotherms to determine surface area of the Absorbatox™ samples as well as their average pore volumes and distribution.
- 1.2. Laser particle sizing to determine the average particle size of the Absorbatox™ samples.

2. Biological characterisation

- 2.1. Conduct an *in vivo* wound study using a porcine model from which tissue will be excised for MALDI-MS analysis.
- 2.2. Perform MALDI MSI of tissue sections of excised wound tissue at different stages of the healing process to visualise fluctuation of proteins during the different stages of wound healing.
- 2.3. Identify the protein species found in the wound tissue samples at different stages of wound healing.

CHAPTER 2: PHYSICAL CHARACTERISATION

INTRODUCTION

Nitrogen Gas Adsorption

Zeolites are naturally occurring hydrated minerals which were discovered and named in 1756 by the Swedish mineralogist, Baron Cronstedt and later defined by Smith (1984) as aluminosilicate frameworks based on a three-dimensional arrangement of AlO_4 and SiO_4 (Breck, 1964; Smith, 1984). Zeolites are formed in cavities in lava flows and in plutonic rocks and are made up of a multiple tetrahedral structure (Breck, 1964). The resulting lattice encloses a network of cavities and channels which provide the zeolites with a variety of physicochemical properties that include: ion exchange capacity, a size exclusion frame, catalytic properties, as well as a large internal surface area allowing for an adsorbent nature (Kaneko, 1994; Sakintuna *et al.*, 2003; Dutta *et al.*, 2005). The dimensions of the three-dimensional channels and the pore sizes of the zeolites determine the size exclusion and catalytic activity of a zeolite (Sakintuna *et al.*, 2003; Dutta *et al.*, 2005). The structure of the zeolites possesses a negative charge which can contain a variety of cations, such as sodium, calcium, and magnesium (Breck, 1964).

Absorbatox™ is a zeolite; a specific member of the clinoptilolite family of zeolites and thus possesses the characteristics of zeolites.

At present, gas adsorption is the best technique to assess total surface area of adsorbent materials such as Absorbatox™ and one of the more commonly used methods to investigate the characteristics of porous materials including surface area, total pore volume, and pore size distribution (PSD) (Sing, 1998; Choma *et al.*, 2002). Both the physical structure (surface area) and chemical properties (cation type) influence the gas adsorption characteristics of a zeolite (Burevski and Poceva, 1994; Sing, 1998; Choma *et al.*, 2002).

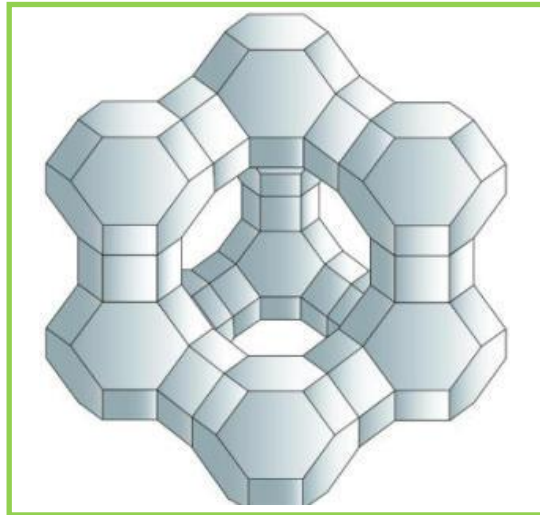


Figure 3: Three-dimensional tetrahedral structure of a zeolite (Woodford, 2012).

Surface area and pore volume

The surface area of a material affects the way that it interacts with another substance and is thus an important parameter to investigate when characterising porous materials (Bae *et al.*, 2010). As a rule the greater the surface area the greater the amount of a different compound can interact with the porous material.

The Brauner-Emmett-Teller (BET)-nitrogen absorption method of determining surface area remains the favoured method of determining overall surface area of porous materials (Sing, 1998; Bowen, 2002). The Langmuir theory determines surface area based on monolayer coverage of a complete surface by the adsorbate. The BET theory expands on this theory by incorporating multilayer adsorption (Sing, 1998; Bae, 2010). The assumptions upon which the BET theory is based are that gas molecules adsorb on a solid surface in an infinite number of layers and that no interaction exists between the different adsorption layers (Brunauer *et al.*, 1938).

To determine surface area, an adsorbate – most often, nitrogen at a subzero temperature of 77 K (Sing, 1998) – is compressed in the presence of a solid in

steadily increasing quantities. After each quantity of adsorbate is applied, the pressure is allowed to equilibrate while the amount of nitrogen adsorbed to the surface is computed. The amount of nitrogen adsorbed at each temperature and pressure defines the adsorption isotherm. Using this defined isotherm, the quantity of gas required to form a single layer on the surface of the material being studied is determined and with the area covered by the newly calculated amount of gas known, the overall surface area of the material can be calculated (Micromeritics® Instrument Corporation, n.d).

The large surface area of zeolites is due to their highly porous nature. The pore dimensions play a vital role in the physicochemical properties of solid adsorbents (Kaneko, 1994). This is exemplified by the ability of Absorbatox™ to draw up and hold wound exudate by strong capillary forces. Thus, the most essential data is with regards to the pore dimensions of the Absorbatox™.

During the process of adsorption, filling of the pores occurs. The course of adsorption is dependent on the pore volume available. In the case of macropores, (pores that exceed 50 nm in width) pore filling takes place via multilayer formation. In the case of micropores (pores smaller than 2 nm in width), adsorption occurs via a volume-filling process at a lower relative pressure. In mesopores, pores between 2 and 50 nm in width, both adsorption mechanisms occur; multilayer pore filling occurs first which is then followed by volume-filling (Kaneko, 1994; Jaroniec and Kaneko, 1997; Sing, 1998; Sakintuna *et al.*, 2003). While it was initially thought that capillary condensation and (micropore) volume-filling are the same, it is now widely accepted that this is not the case (Sing, 1998; Dutta *et al.*, 2005). The surface area of zeolites is dependent on the pore number and pore volumes and since high porosity provides a greater surface area a higher adsorptive capacity is expected for these materials (Kusumaningtyas, 2006).

Pore size distribution

Pore size distribution is defined as “the population of pores as a function of pore width” (Kaneko, 1994). The method of Barrett, Joyner, and Halenda (BJH) is used to determine pore size distribution from experimental isotherms using the Kelvin model for pore filling (Choma *et al.*, 2002; Micromeritics® Instrument Corporation, n.d) and is only applicable to open pores assuming the cylindrical pore model (Barrett and Joyner, 1951; Allen, 1997). The Kelvin equation-based method incorporates methods put forward by Barret, Joyner, and Halenda (BJH), Dollimore and Heal (DH), Cranston and Inkley (CI), and also Broekhoff and de Boer (BdB) (Choma *et al.*, 2002) and takes into consideration statistical film thickness (t-curve) as a function of relative pressure as well as the relationship between the evaporation (condensation) pressure and the pore width (Choma *et al.*, 2002). This is represented by the Kelvin capillary condensation equation (Roberts, 1967):

$$r_k = \frac{-2\gamma\rho M \cos\theta}{RT \ln P/P_0}$$

where, " r_k " is the radius of the largest cylindrical capillary filled with condensate; " γ " represents the surface tension of the adsorbate; " ρ " is the density of the adsorbate; " M " is the molecular weight of the adsorbate; θ is the contact angle between the condensed phase and the surface of the solid and is usually assumed to be equal to zero; " R " is the gas constant, and " T " is the temperature measured in Kelvin and P/P_0 is the partial pressure.

The thickness " t " of the adsorbate layer is considered in the equation used to determine the pore radius " r_k ":

$$r_k = r_p + t$$

where r_p indicates the radius into which condensation occurs at the required relative pressure (Broekhoff and de Boer, 1968; Yağşı, 2004; Dutta *et al.*, 2005).

The BJH method of determining pore size distribution analyses the nitrogen desorption isotherm at liquid nitrogen temperature based on the assumption that the mechanisms of physical adsorption on the pore walls and capillary condensation in the pore can be employed to establish equilibrium between the adsorbed and gas phases during the process of desorption (Barrett and Joyner, 1951; Choma *et al.*, 2002). During adsorption, the quantity of nitrogen required to form a monolayer on a surface is calculated as a function of gradually increased pressure of nitrogen gas at a constant temperature of 77 K. As the pressure increases, the gas condenses first in the smallest pores. This continues until all the pores are filled with liquid. This is known as the point of saturation (Micromeritics® Instrument Corporation, n.d). The reverse occurs in desorption. The pressure is gradually reduced allowing for capillary condensation; or in other words, for the nitrogen that had originally saturated the open pores to now evaporate (Brunauer *et al.*, 1938; Barrett and Joyner, 1951; Kaneko, 1994; Allen, 1997; Dutta *et al.*, 2005). So, both adsorption and desorption isotherms are necessary to ascertain pore size distribution using the BJH method.

Figure 4 gives a concise description of the methods typically employed to determine surface area, pore volume, and pore size distribution.

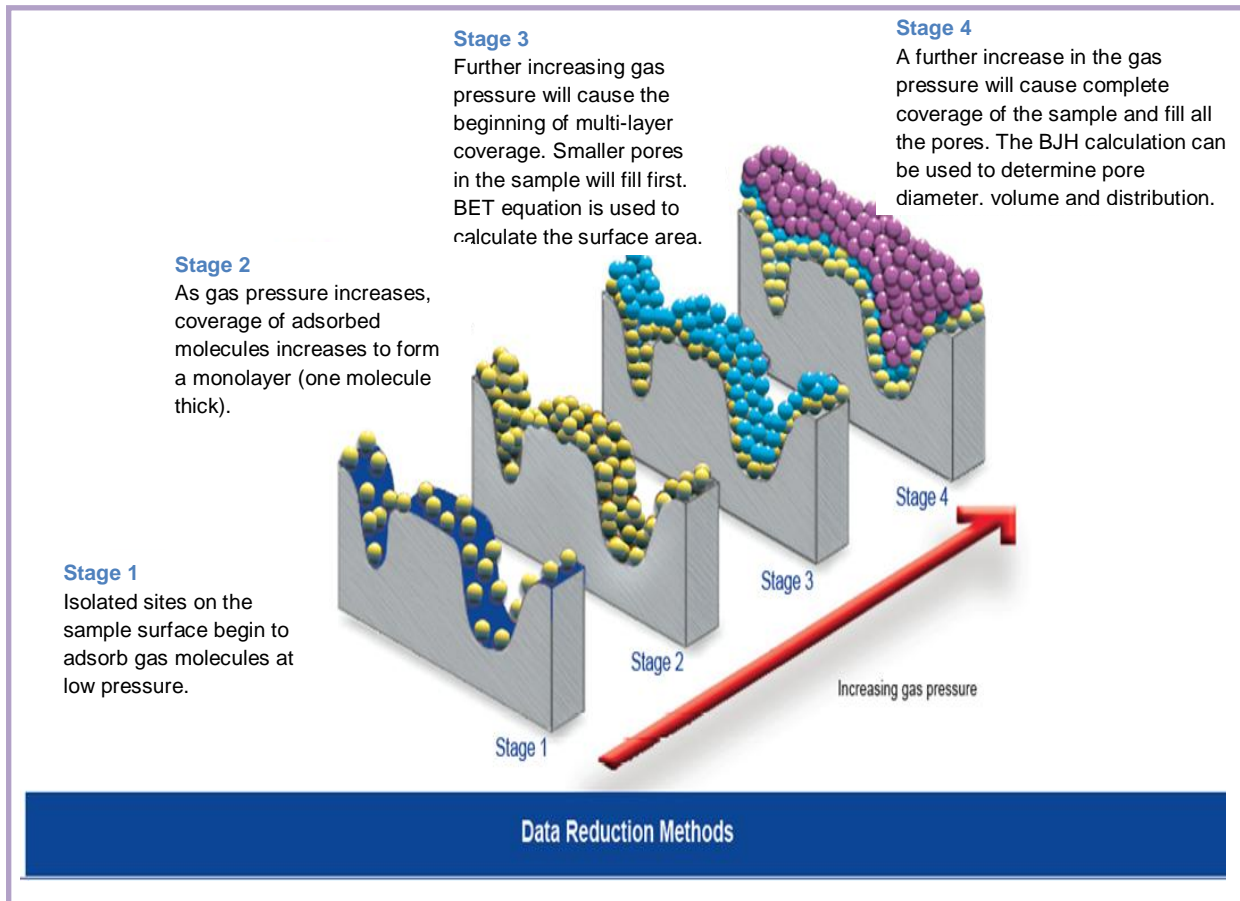


Figure 4: Graphical representation of methods used to determine surface area, pore volume, and pore size distribution (Micromeritics® Instrument Corporation, n.d).

Laser Particle Sizing and Size Distribution

Webb (n.d) cites McGraw Hill’s Dictionary of Scientific and Technical Terms (Third Edition) to define a particle as “any relatively small subdivision of matter, ranging in diameter from a few angstroms to a few millimetres.” The size of a particle gives important information on its behaviour such as performance as an abrasive, application in the case of cosmetics, dissolution rate in the case of pharmaceuticals, and flow properties of fluid-cracking catalysts (Micromeritics® Saturn Digsizer ® II, n.d).

Numerous techniques exist to determine particle size (Bowen, 2002) such as scanning electron microscopy (imaging), electrical zone sensing (Coulter principle), sedimentation (centrifugation), and light interaction methods which include laser particle sizing (laser diffraction) (Barth and Flippen 1995; Bowen, 2002; Ferraris, 2004; De Clerq, 2004; Webb, n.d).

Scanning electron microscopy (SEM) is an analytical tool that uses a focused beam of electrons to give a magnified image. If the conditions are ideal, this technique can produce images with feature resolution at the nanometre level simultaneously giving insight into both the morphology as well as the size distribution of the particles. SEM also gives information into any possible absence of homogeneity present in the sample (Tsapatsis *et al.*, 1995; Bowen, 2002; Ferraris, 2004).

Sedimentation using either gravity or centrifugation is a very popular method based on the application of Stokes' Law. This law describes the terminal velocity of a spherical particle settling in a fluid medium under the influence of a gravitational force. Sedimentation with centrifugation can result in a lower range of around 10 nm and even further down towards a nanometre if an analytical ultracentrifuge is used (Barth and Flippen, 1995; Bowen, 2002; Ferraris, 2004; Webb, n.d).

Electrical zone sensing (EZS) is based on the Coulter principle. This well-established method works down to approximately 0.5 μm and allows for the measurement of both the volume and number distribution. In this technique, the suspended particles in an electrolyte at a highly dilute concentration are passed through an orifice of a defined volume in an insulating wall between two electrodes. Voltage pulses proportional to the particle's volume are produced for each particle as the particles enter the orifice (the sensing zone). The accumulation of pulses over a period of time gives the particle size distribution. EZS has also been used to establish emulsion stability (Barth and Flippen, 1995; Bowen, 2002; Ferraris, 2004; Webb, n.d).

Laser diffraction measures the angular distribution of light scattered from a particle in a dilute medium (Ferraris, 2004).

While reliable information is obtainable from processing images acquired from using direct methods such as microscopy (both light and electron), the methods are slow and do not always yield statistically significant results (Vanderhallen *et al.*, 2000; De Ridder *et al.*, 2002). Indirect methods such as laser diffraction are fast and highly reproducible and are thus more widely used. In addition to this, light scattering techniques are also useful for kinetic and *in situ* studies since they are often non-destructive and non-perturbative to the species under investigation (Barth and Flippen, 1995; Vanderhallen *et al.*, 2000; De Ridder *et al.*, 2002).

Laser particle sizing uses the principle of light scattering to determine particle size. Light is defined as the energy residing in the narrow and very specific region of the electromagnetic spectrum which, depending on its interaction with matter, can produce various visual effects (Webb, 2004). That is, light can be reflected, refracted (bent), absorbed, diffracted (slight deviation from its original path upon interaction with matter), and even scattered (Ferraris, 2004; Webb, 2004). Scattered light is made up of reflection, refraction, and diffraction and can thus be defined as a change of the direction and intensity of a light beam when it strikes an object due to the combined effects of reflection, refraction, and diffraction (Ferraris 2004; Webb, n.d). Light scattering (LS) can either be dynamic or static. Dynamic light scattering (also known as quasi-elastic light scattering) uses the correlation of light intensity variations and the Brownian movement of the particles to determine particle size. Techniques that rely on this type of light scattering vary widely depending on sample concentration and conditions as well as environmental factors. Static LS establishes particle size using intensity characteristics of the scattering pattern at various angles (Twomey *et al.*, 1994; Ferraris, 2004; Webb, n.d).

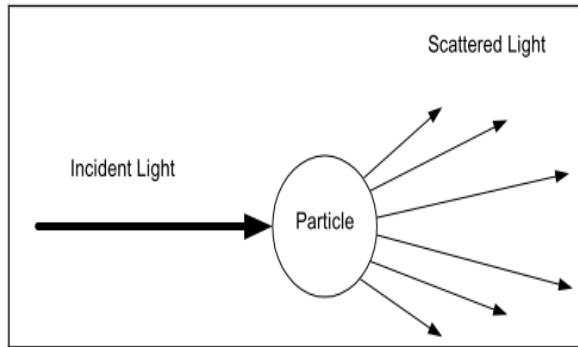
During the 1800s, many advances were made in understanding light scattering. Diverse theories were developed that related to particles of certain shapes and sizes in a particular medium (Webb, n.d). In the 1970's, these developments and

knowledge resulted in the advent and commercialisation of the first laser light scattering instruments (Micromeritics® Saturn Digsizer ® II, n.d).

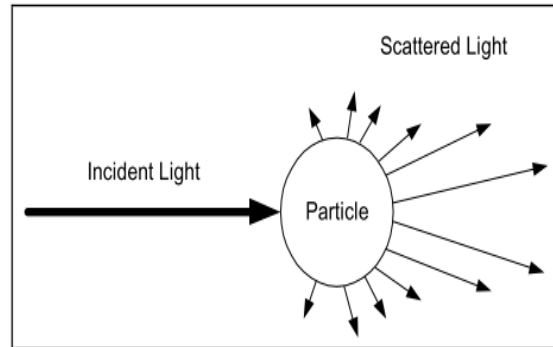
These laser light scattering instruments use two fundamental methods of data analysis: the Mie and Fraunhofer theories.

In 1906, Gustav Mie worked out a comprehensive mathematical-physical theory of the scattering of electromagnetic radiation by isotropic, spherical particles as a function of the angle at which light is scattered at the point of interaction with the particle. When Mie developed the theory, it could only be applied with boundary conditions: (i) only monochromatic light (light of a single colour or wavelength) is considered; (ii) the particle must be isotropic and (iii) spherical; (iv) the incident light is composed of plane waves; (v) both scattering and absorption are considered; (vi) only static light is considered; and (vii) no quantum effects such as Raman or Doppler effects, are considered (Ferraris, 2004; Webb, n.d). Despite the constraints of the Mie theory, it can still be applied to determine particle size even if the particle does not meet all the conditions since the current availability of computing software means that particle-sizing instruments based on this theory are guided by expressed conditions of Mie theory so as to construct a scattering pattern reducible by the Mie theory (Webb, n.d).

Joseph Von Fraunhofer developed a theory that predicts the diffraction of light at the edges of objects - in particular opaque objects. The theory describes scattering occurring when the particles investigated are far larger than the wavelength of the light source in use. The outcome of this low-angle light scatter is that light is scattered off axis in a forward direction. For this method, the refractive index need not be known since it is based only on the diffraction effect (Ferraris, 2004; Young, 2005; Webb, n.d). In contrast, the general rule for the Mie theory is that the particles are slightly smaller than the wavelength giving higher angles of refraction and a broader range over which scattering occurs. In this case, forward (low-angle) scatter is still predominant but the refractive index must be known (Ferraris, 2004; Webb, n.d).



A. Fraunhofer Light Scattering



B. Mie Light Scattering

Figure 5: A) Low-angle light scattering from a particle larger than the light source wavelength following the Fraunhofer theory. B) A combination of high- and low-angle light scattering from a particle slightly smaller than the light source wavelength in accordance to the Mie theory (Young, 2005).

The sizes of the zeolite particles were determined using laser light scattering technology which gives high levels of resolution, accuracy, reproducibility, and repeatability. The laser light scattering instrument used - a Micromeritics Saturn DigiSizer® - employs a laser diode and a modern charge-coupled device (CCD) detector which allows a high-resolution, digital representation of the light scattering pattern to be captured. Data reduction is then executed on the resulting information using the Mie Theory (Micromeritics® Saturn DigiSizer ® II, n.d).

MATERIALS AND METHODS

Nitrogen Adsorption

Instrumentation

A Micromeritics Accelerated Surface Area Porosity (ASAP) 2020® was used to conduct the nitrogen adsorption-desorption experiments. This instrument is equipped with two independent vacuum systems, a vacuum system for sample preparation and another for sample analysis which allows for the concurrent preparation and analysis of samples without the one procedure interrupting the other. The ASAP 2020® also has an elevator that raises and lowers the analysis bath fluid Dewar automatically and a shield that encloses each Dewar as a means of protection. Instrument-grade nitrogen was used for the adsorption-desorption study.

Experimentation

Two Absorbatox™ samples were analysed: a granular sample which looks like sugar granules and the micronised sample which looks like talcum powder.

Absorbatox™ is a hygroscopic compound – that is – it absorbs moisture from the atmosphere when left exposed. The Absorbatox™ was stored in a large, sealed bucket which was apparently not moisture tight. Small samples of the zeolite were removed from the bucket and placed in open petri dishes and placed in a desiccator overnight. The Absorbatox™ samples were then transferred to sealed centrifuge tubes when not being used. It was later observed that, even in these sealed tubes, the zeolite was able to absorb moisture from the atmosphere. With this in mind, both the zeolite samples were kept in a Petri dish in an oven at 85°C overnight in an attempt to ‘dry’ the samples before degassing. During the sample analysis process of degassing on the instrument, the sample is heated and placed under the vacuum to remove moisture and possible contaminants. A mass of 25

mg of granular or micronised Absorbatox™ was weighed out and each was placed in its own tube. A filler rod was placed in each tube to decrease the volume within the tube and thus to accelerate degassing of the sample. A rubber stopper was used to plug the sample tube, and the tube was attached to the degassing port. The sample tube was pushed into the degassing port fully and secured. A heating mantle was placed over the bulb of the sample tube and secured using a mantle clip. The initial degassing parameters (temperature: 200°C and degassing time: 3 hours) used were as in the method published by Salama *et al.* (2009). These parameters did not result in proper degassing as was observed in the initial degassing analysis graphs. Since Absorbatox™ had proven to be highly hygroscopic before, the failure to properly degas the sample was attributed to high moisture content in the sample. With this in mind, both the zeolite samples were kept in a Petri dish in an oven at 115°C for a period of three days in an attempt to further 'dry' the samples before degassing. The initial degassing parameters were then adjusted; temperature, pressure, and degassing times were increased to 300°C, 100 mmHg, and 12 hours, respectively. The micronised samples were degassed under the same temperature and pressure parameters but for an extended time of 24 hours.

BET analysis was performed at 77 K and the BJH method applied to determine pore diameters after which nitrogen-adsorption isotherm graphs were obtained.

Laser Particle Sizing

Instrumentation

A Micromeritics Saturn DigiSizer 5200 VI.II® was used to conduct the laser particle sizing experiments. This instrument has a sizing range of 0.1 µm to 1000 µm and is equipped with a liquid sample handling unit (LSHU) which has several automated features, one of which is a sample recirculation system that maintains particle dispersion. The unit is also equipped with an ultrasonic probe, an auto-

dilution function which monitors the concentration of the sample and adds liquid as needed until optimum concentration is achieved, as well as a device that sprays residue from the reservoir walls so as to prevent sample carry-over. Filtered water was used for laser particle sizing experiments.

Experimentation

A mass of 2.5 g of each Absorbatox™ sample (granular and micronised) was suspended in water to a final concentration of 0.08% (granular) and 0.002% (micronised) which gave an obscuration of 18.1% for the granular sample and 10.2% for the micronised sample. Before analysis, the samples were agitated ultrasonically to disperse the sample and break up agglomerates. After the ultrasonic treatment at 60% intensity for 60 seconds for the granular Absorbatox™ and 30 seconds for the micronised Absorbatox™, the samples were recirculated for a period of 120 seconds to remove any air bubbles that may have formed in the sample and tubing. Recirculation is necessary since bubbles also scatter light and cannot be distinguished from solid particles by the system (Webb, 2004).

The granular and micronised samples were pumped at a flow rate of 16.0 litres per minute (l/m) and 12.0 l/m, respectively through the sample cell past a laser beam where the light scattering occurs. The scatter pattern in both cases was recorded by a 3.1 megapixel CCD detector and then used in the Mie theory calculation to determine particle size distribution. The refractive indices used were (Re) 1.57 and (Im) 1.00 for the Absorbatox™ and 1.331 for the water. Water temperature and viscosity was approximately 24°C and 0.798 cp respectively.

RESULTS AND DISCUSSION

Nitrogen Adsorption

Initial characterisation of the Absorbatox™ zeolites was performed using nitrogen adsorption-desorption isotherms. This is a standard technique preferred for pore size, pore size distribution, micropore volume, and surface area determination.

The surface area of both zeolite samples was assessed using isotherm data using the method developed by Brunauer, Emmett, and Teller (BET). The BET method is used for multilayer adsorption but is based on the Langmuir equation where adsorption is limited to a monolayer. After the analysis, nitrogen adsorption-desorption isotherm graphs of each Absorbatox™ sample were obtained.

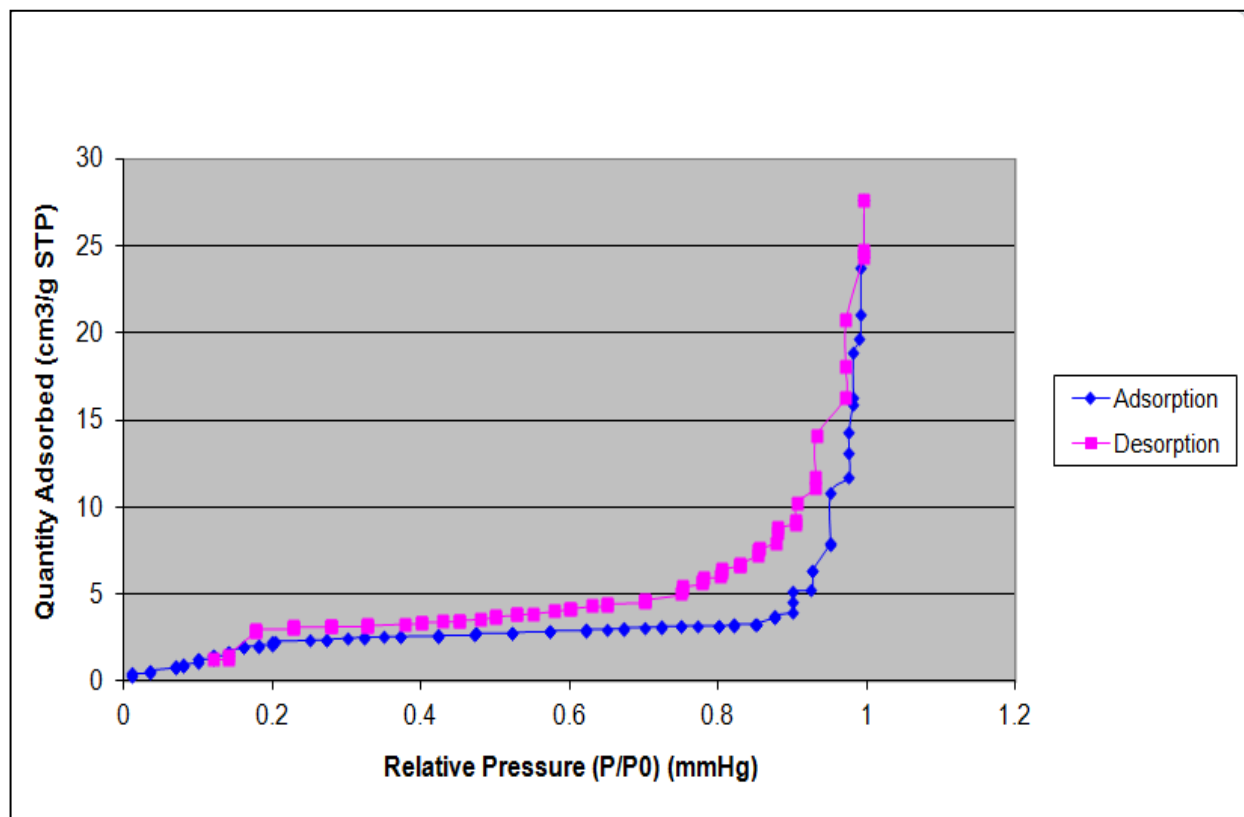


Figure 6: Nitrogen adsorption-desorption isotherm for granular Absorbatox™ zeolite.

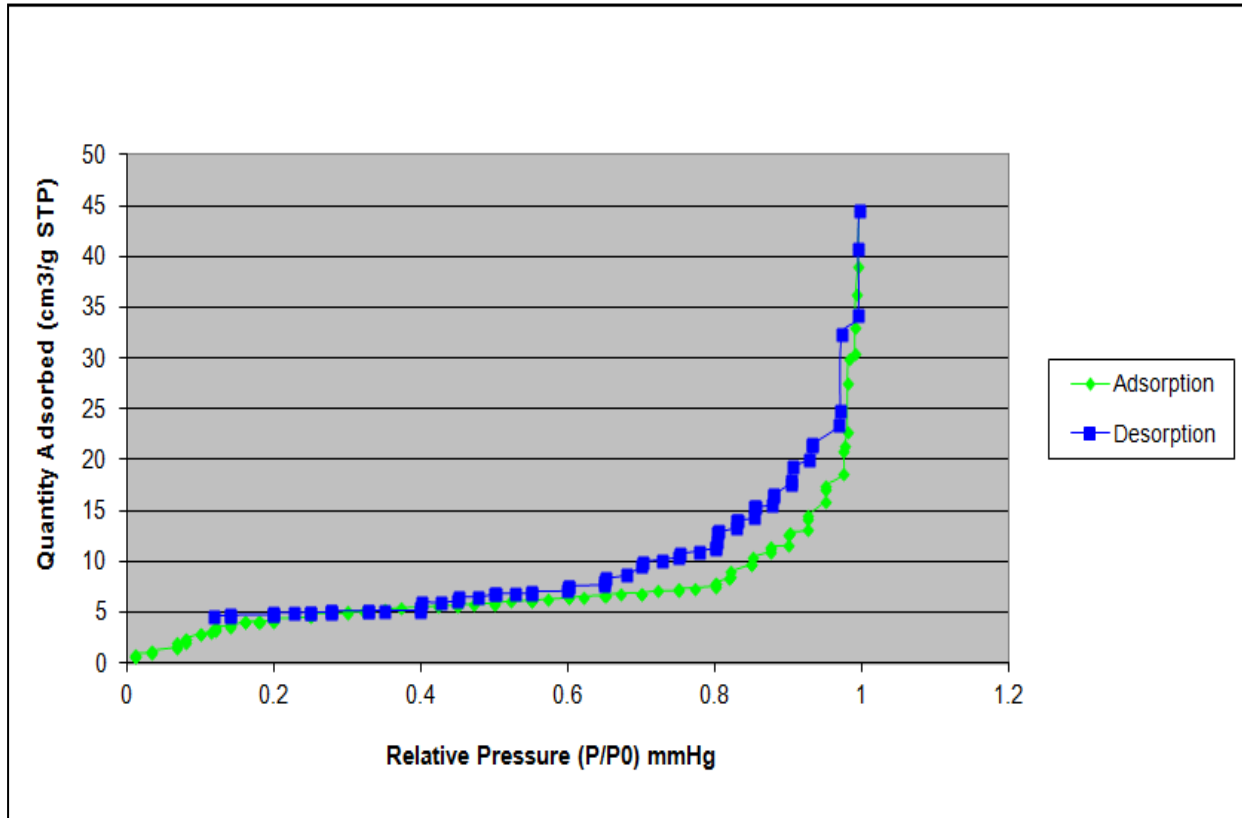


Figure 7: Nitrogen adsorption-desorption isotherm for micronised Absorbatox™ zeolite.

In both cases, the Absorbatox™ nitrogen adsorption-desorption isotherms have similar shapes. Isotherm shapes were originally defined by Brunauer *et al.* (1940) and classified into five groups and later reviewed and incorporated into a more practical classification by the IUPAC which added an additional (sixth) isotherm shape (Donohue and Aranovich, 1998; Sing, 1998; Storck *et al.*, 1998; Barton, 1999).

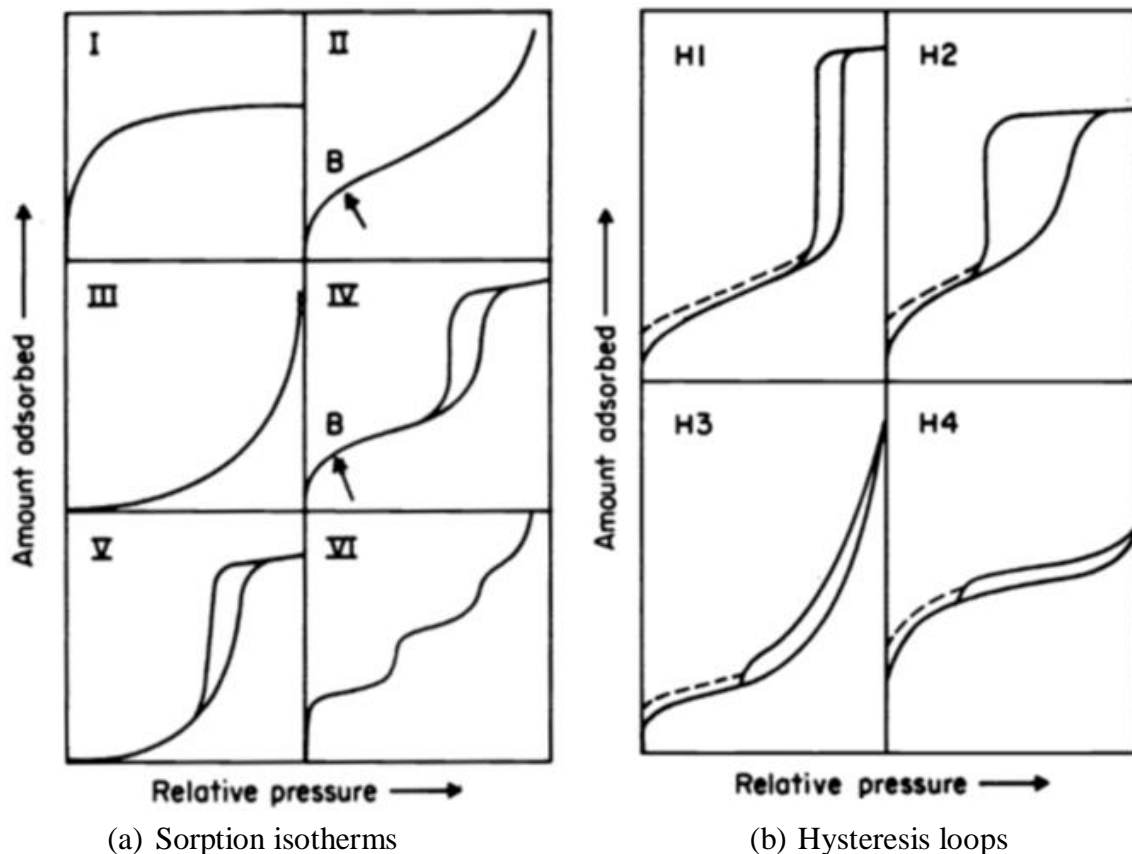


Figure 8: The IUPAC classification of adsorption isotherms and hysteresis loops (Sing *et al.*, 1982).

Based on the isotherm classification (Figure 8), both the nitrogen adsorption-desorption isotherms of the granular and micronised zeolites show similarity to Type IV isotherms. This type of isotherm is found with many mesoporous adsorbents (Allen, 1997). Literature states that zeolites are microporous materials (Kaneko, 1994; Sakintuna *et al.*, 2003) and should thus exhibit Type I isotherms (Hodson, 1998). However, Absorbatox™ exhibits Type IV adsorption-desorption isotherms which is in line with studies by Barton *et al.* (1999) and Floquet *et al.* (2003) that report Type IV isotherm characteristics have been observed in tight-fitting molecules in silicate materials. At low pressures, an absorbate layer forms on the pore surface followed by sequential layers that eventually make up the multilayer. The knee (the first bend) in the adsorption isotherm is indicative of the point at which the monolayer-multilayer forms (Sing *et al.*, 1982). A characteristic feature of this type of isotherm is the hysteresis loop which is the non-overlapping region of the adsorption-

desorption branches (Figures 6 and 7). The loop exhibits different paths followed by the adsorption and desorption isotherms. The loop closes in both the Absorbatox™ isotherms at different relative pressure ratios (P/P_0); the granular material at 0.12 and the micronised material at 0.2. The onset of the Type IV hysteresis loop marks the start of capillary condensation in the mesopores (Sing *et al.*, 1982).

The adsorption isotherm is the quantitative description of the amount of adsorbate adsorbed by a material (V) at a constant temperature, at the adsorption pressure (P) (Allen, 1997; Barton *et al.*, 1999). The amount adsorbed is dependent on the characteristics of the solid (adsorbent): porous vs. non-porous, and the pressure at which adsorption occurs. The amount of adsorbate involved in the adsorption can be determined using a gravimetric or volumetric method after the sample is degassed. The ASAP 2020® was set to measure the amount of adsorbate volumetrically – that is, the volume of gas adsorbed was determined by calculating the amount of gas removed from the system by applying standard gas laws. The alternative method - the gravimetric method - assesses the increase in the weight of the test material after adsorption. The surface area is typically determined by deducing the total adsorbate required to cover the test material with a monolayer of adsorbate molecules. This is termed the monolayer capacity (V_m) (Allen, 1997).

Using the BET method, the total surface area including the external and micropore surface areas were determined for both the granular and micronised Absorbatox™ samples. These are expressed in Table 1 below.

Table 1: Surface, external, and micropore areas of granular and micronised Absorbatox™.

SAMPLE DESCRIPTION	GRANULAR ABSORBATOX™	MICRONISED ABSORBATOX™
BET Surface area (m ² /g)	11.23	14.43
t-Plot external surface area (m ² /g)	4.95	4.61
t-Plot micropore area (m ² /g)	6.28	9.82

When observing the two Absorbatox™ samples, it is evident even at the macroscopic level that the granular particles are larger than the micronised particles (Figure 9). Even without further analysis, the BET surface area values for the two samples are in agreement with the surface area-to-volume ratio: the larger particles – the granular Absorbatox™ - have a smaller surface area than the smaller, micronised Absorbatox™ per unit mass.



Figure 9: Granular Absorbatox™ (left) and micronised Absorbatox™ (right).

The BJH method using the Kelvin equation is the most common way of determining pore size distribution from nitrogen isotherms (Sing, 1998). Pore size distribution is obtained by decreasing the pressure at which adsorption occurred i.e.: induce desorption. The starting point for this method is with an isotherm at saturated vapour pressure when the pores are completely filled with nitrogen. A slight decrease of the pressure results in desorption of a measurable amount of the vapour and a residual layer, the thickness of which is used to calculate pore size distribution (Allen, 1997).

Both Absorbatox™ samples exhibit Type IV desorption isotherms. This isotherm type is due to strong fluid-solid attractive interactions and gives insight into the mesopore through its hysteresis loop. Molecules form a liquid-like adsorbed layer within the mesopore that has a meniscus, the curvature of which is associated with the Kelvin equation and is related to pore shape and size. The hysteresis is attributed to capillary cracks from which the adsorbate molecules (nitrogen in this case) do not desorb as readily as they adsorb and gives an indication of the pore filling or emptying mechanisms (Kaneko, 1994; Allen, 1997; Barton *et al.*, 1999). The hysteresis loops in the isotherms of both samples are consistent with Type H3 hysteresis. The adsorption isotherms are steep at saturation pressure (Allen, 1997) with asymptotic character not exhibiting limiting adsorption at high relative pressures (0.8 – 1.0 mmHg) (Medioroz and Pajares, 1987; Yu, 2002; Yu *et al.*, 2004) while the desorption isotherms slope are steep at high relative pressures and almost parallel to the X-axis at intermediate and low relative pressures (0.2 – 0.8 mmHg). This type of hysteresis is observed in open, slit-shaped capillaries with parallel walls, wide pores and short necks and corresponds to a narrow size distribution of lamellar mesopores (Yu *et al.*, 1996; Bérend *et al.*, 1995; Allen, 1997) of non-uniform size and shape (Leofanti *et al.*, 1998).

The pore volumes and pore size distributions were calculated using the BJH method and are represented in Table 2.

Table 2: Total pore volumes and pore size distributions of granular and micronised Absorbatox™.

SAMPLE DESCRIPTION	GRANULAR ABSORBATOX™	MICRONISED ABSORBATOX™
BET adsorption average pore diameter (Angstrom)	437.89	282.12
t-Plot micropore volume (cm ³ /g)	0.01	0.03
BJH adsorption cumulative volume of pores (cm ³ /g)	0.04	0.05
BJH desorption cumulative volume of pores (cm ³ /g)	0.04	0.05

The values obtained from the BJH adsorption average pore diameter are in agreement with the implication of the general shapes of the adsorption-desorption isotherms of the Absorbatox™ samples. The Type IV isotherms suggested that the particles are mesoporous; that is, having a distribution of pore widths between 2 and 50 nm (Kaneko, 1994; Jaroniec and Kaneko, 1999; Barton *et al.*, 1999; Sing, 2001; Sakintuna *et al.*, 2003). The granular Absorbatox™ has a pore diameter of approximately 45 nm while the micronised Absorbatox™ has an average pore diameter of 28 nm.

Laser Particle Sizing

Laser particle sizing was employed to measure particle size distribution (PSD) in both Absorbatox™ samples using a Micromeritics Saturn DigiSizer® designed to measure particle sizes in the range of 0.1 µm to 1000 µm (Webb, n.d;

Micromeritics® Saturn Digisizer ® II, n.d). The diluted sample suspensions were introduced into the instrument and the particle sizes at each counting interval were recorded. The data referring to particle sizes and frequency with which each size occurred were processed by the software.

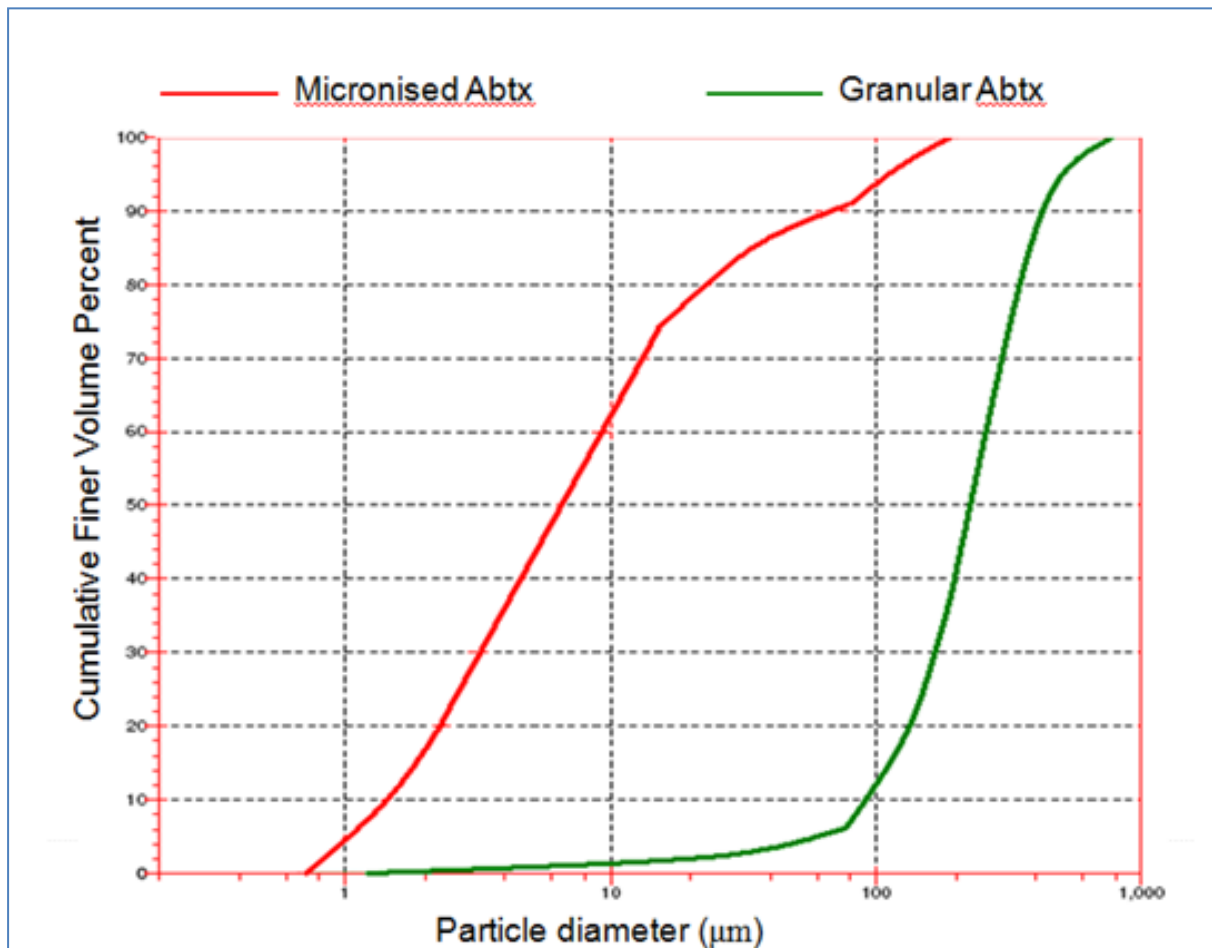


Figure 10: Cumulative finer volume percent vs. particle diameter (µm).

Figure 10 (above) shows the distribution of diameters of the particles present in each of the tested Absorbatox™ samples. It is immediately evident when looking at the graphs that the particles within the samples are not uniform in size. This is in agreement with the findings of the nitrogen adsorption-desorption experiments in which the adsorption-desorption isotherms for both samples exhibited Type H3 hysteresis which corresponds to non-uniformly sized particles (Leofanti *et al.*, 1998).

The granular Absorbatox™ particle sizes (green graph) range between 2 µm and 875 µm with the majority of the particles exceeding 90 µm in diameter. These particle sizes would have the capacity to accommodate the average pore diameters of 43.8 nm as calculated using the BET method. The micronised Absorbatox™ particle sizes (red graph) are between 0.8 µm to approximately 300 µm. This would enclose the average pore diameter of 28.2 nm calculated using the BET method.

As previously mentioned, the micronised Absorbatox™ does have smaller particles than the granular Absorbatox™. The light particle sizing gives more precise measurements. In addition to this, the laser particle sizing results relate well with those obtained from the nitrogen adsorption-desorption experiments and to the surface area-to-volume ratios: the larger particles of the granular Absorbatox™ have a smaller total surface area while the smaller particle micronised Absorbatox™ has a larger total surface area per unit mass.

CONCLUSION

Absorbatox™ was characterised in terms of total surface areas and pore volumes using the BET nitrogen adsorption-desorption method and particle size distribution by laser particle sizing, respectively. It was established from the BET nitrogen adsorption-desorption isotherms that both the granular and micronised Absorbatox™ samples, although different, have mesoporous characteristics. The results obtained from the laser particle sizing experiments also related well to, and supported some characteristics identified by the nitrogen adsorption-desorption study by establishing that the smaller particles have a larger surface area than the larger (granular) particles and also showing non-uniformity in the particle sizes of the Absorbatox™ as was suggested by the BET nitrogen adsorption-desorption isotherms.

This work has not only culminated in the successful physical characterisation of the Absorbatox™ zeolites but has also shown that the results from both BET nitrogen adsorption-desorption and laser particle sizing experiments relate well to each other.

CHAPTER 3: ANIMAL STUDY

INTRODUCTION

The ability to closely predict the human biological response to a treatment or even the efficacy of that treatment to combat a human disorder is the ultimate determinant of a good *in vivo* model (Sullivan *et al.*, 2001). The choice of an animal model is also dependent on various factors including the cost and ease of handling, animal availability, as well as anatomical and physiological likeness to humans. While small mammals such as mice and rabbits easily meet the first three criteria, and are often used in wound healing studies, they are significantly different structurally and functionally. More specifically, humans heal mainly through re-epithelialisation whereas these rodents heal largely through wound contraction (Sullivan *et al.*, 2001). In addition to this, rodents and even primates – despite their phylogenetic closeness to humans – do not develop cheloids, and hypertrophic scar formation is very rare as these are not typical wound healing responses in these mammals (Wang *et al.*, 2001).

Pig skin, on the other hand, has been reported to be notably similar to human skin both anatomically and physiologically (Moritz and Henriques, 1946; Sullivan *et al.*, 2001; Wang *et al.*, 2001; Hirsch *et al.*, 2008; Velandar *et al.*, 2008). This similarity was especially noted in a study conducted by Moritz and Henricque in 1946 during which skin sections, from both humans and pigs, treated with benzidine were seen to be virtually indistinguishable from each other (Vardaxis *et al.*, 1997).

The main similarities between the skins of the two species with regards to wound healing are those of the epidermis, skin vascularisation, and epidermal collagen.

Human and pig epidermis are similarly thick ranging between 50 and 120 μm and 30 – 140 μm , respectively depending on the location of the skin on the body (Vardaxis *et al.*, 1997; Sullivan *et al.*, 2001). The porcine epidermis, like that of man, has

irregularities in the contour of both the upper and lower surfaces of the epidermis (Moritz and Henriques, 1946). Total turn-over time of porcine epidermis is approximately 30 days and is about 27-28 days in humans. Vardaxis *et al.*, (1997) also noted that the epidermis of both species has the same number of layers in both the viable and the horny layers.

The vascular organisation of porcine and human skin has a lower, mid-epidermal, and a sub-epidermal vascular plexus. These structures – while similarly organised – differ in the density of their distribution. More specifically, the sub-epidermal plexus of the pig dermis is less dense than the human sub-epidermal plexus. The lower region of the hair follicles and other appendages in the pig are not as well vascularised as the hair follicles and glands in the human skin (Vardaxis *et al.*, 1997; Sullivan *et al.*, 2001).

Porcine collagen exhibits significant biochemical similarity to that of human collagen. This similarity is illustrated in the usage of porcine skin and porcine skin products both as biological wound dressings and in xenografts in humans both of which trigger minimal or no immune response in the human subject (Vardaxis *et al.*, 1997; Sullivan *et al.*, 2001).

An additional but somewhat trivial fact to further illustrate the similarity in porcine and human skin: pigs are the only animals that experience sunburn in the same way as in humans (Vardaxis *et al.*, 1997).

The use of a porcine model also allows for the evaluation of the role and presence of growth factors in wound healing given that the wound healing patterns are physiologically comparable (Sullivan *et al.*, 2001).

Pigs can also more closely represent chronic wounds in patients with serious illnesses since they too are placed under a great deal of physiological stress with the

induction of numerous wounds, the regular and repeated handling, as well as the frequency of general anaesthesia (Sullivan *et al.*, 2001).

Although using human subjects to study wound healing in humans would most likely give more accurate results, this would raise ethical issues as patients' wounds cannot go untreated in order to serve as controls for experiments. It would also be difficult to find a large enough number of people with similar types of wounds that could be compared to each other (Vardaxis *et al.*, 1997; Sullivan *et al.*, 2001).

Despite the many technological advances that have occurred such as the use of tissue engineered skin substitutes, the mainstay of wound treatment is still wound dressings; a crucial characteristic of which is to remove excess wound exudate while retaining wound moisture (Boateng *et al.*, 2008). Boateng *et al.* (2008) classify wound dressings as traditional (e.g.: synthetic bandages and gauzes) which are dry and do not provide the moist wound environment conducive to proper wound healing; and modern dressings such as hydrogels and hydrocolloidal dressings. The hydrocolloidals are preferred in paediatric wound management because of the pain-free removal of this adhesive dressing. Hydrogels are active wound healing agents suitable for cleansing dry and necrotic wounds. This type of dressing is also permeable to metabolites and is typically non-irritating (Boateng *et al.*, 2008; Papazoglou *et al.*, 2010).

In this study, the efficacy of Absorbatox™ and Cerdak™ wound dressings in the treatment of full-thickness wounds were compared. Full thickness wounds are wounds causing damage to the epidermis, the dermal layers and the underlying subcutaneous fat and deeper tissues (Boateng *et al.*, 2008).

Cerdak™ is described as a device consisting of a non-woven fabric sachet filled with microporous ceramic granules. The ceramic granules work by capillary action. The interstitial voids between the granules also lead to the absorption and retention of wound exudate. The anti-bacterial action of ceramic helps to clean the wound while

maintaining optimal conditions for normal wound healing. Cerdak™ is designed to treat various wound types from diabetic and pressure wounds to surgical wounds (Cerdak™, n.d).

Absorbatox™ - a modified, naturally occurring clinoptilolite of the zeolite family - is a synthetically enhanced, hydrated aluminosilicate mineral which has been put through a patented process that increases its cation exchange capacity (CEC) to five times its original capacity. Absorbatox™ is at least as safe as the other naturally occurring clinoptilolites since no evidence exists to suggest that clinoptilolites in general are changed in structure or otherwise even in the gastrointestinal tract (Pond *et al.*, 1989). The insolubility of this compound further exemplifies its safety as a wound healing agent. Its activity is due to its adsorbing and binding properties. Absorbatox™ comprises of aluminium, oxygen, and silicon atoms in a tetrahedral arrangement arranged in way that creates cage-like open pores since the tetrahedral units cannot take up all the available space entirely (Kaneko, 1994). The wound healing functionality of Absorbatox™ lies in its ability to draw up wound exudate by strong capillary forces but still keep the wound from becoming overly dry. The use of Absorbatox™ has been proven safe in both animals and humans (Absorbatox™, n.p).

MATERIALS AND METHODS

Animals

The animal study was conducted at the University of the Witwatersrand (Medical School) at the CAS (Central Animal Service). Two female Large White pigs, with an initial weight of 25–30 kg were used. On arrival, the pigs were set up in individual, smooth-walled pens with stainless-steel gates and allowed to acclimatize to their new surroundings for 7 days before initiation of any experiments. A supervising

veterinarian was in charge of the study insofar as ensuring the general health and well-being of the animals and performing biopsies.

The study was conducted according to the guidelines set out in the national standards document SANS 10386:2008 with ethical approval having been obtained from the AESC (Animal Ethics Screening Committee) of the University of the Witwatersrand (reference no: 2008-47-04) and from the AUCC (Animal Use and Care Committee) of the University of Pretoria (reference no: H027-08).

The study was divided into three phases correlating to the three phases of wound healing and conducted over a period of sixteen days.

On day one, twenty 8 mm diameter full thickness (skin) wounds were made along the back of each pig (10 above each psoas muscle on either side of the vertebrae). The pigs were under general anaesthesia and opioid-based analgesic therapy during this procedure. Experimental treatment was in the form of wound dressings which consisted of a porous sachet containing one of two different granular sizes of Absorbatox™ and attached to an adhesive strip applied directly to the skin with the sachet in direct contact with the wound. The sachets were covered with a thick gauze pad and the entire area was stabilized with a stretchable, porous, adhesive covering (OpSite). This made provision for the collection of the wound exudate. The control wounds were treated in the same way except that the Absorbatox™ sachets were not applied.

The treatments that were used were: negative control (empty sachet), Absorbatox™ micronised, Absorbatox™ granular, and Cerdak™. Each pig served as its own control and wounds were randomised to receive accurate results.

Wound induction

The animals were anaesthetised by injecting Dormicum (0.3 mg/kg) and Anaket (11 mg/kg) before wound induction. An inhalation agent, Isoflur, was used to maintain anaesthesia during surgery. The pigs received Temgesic (0.3 - 0.6 ml) administered post-operatively as an analgesic for pain management.

After induction of anaesthesia, the hair on the backs of the animals was shaved off using an electric shaver and the skin was subsequently scrubbed with a non-antibiotic-containing soap. Wounds were induced using an 8 mm punch biopsy (full-skin thickness) along the psoas muscle ridge. Full-thickness wounds were created through both the epidermis and the full thickness of the dermis, revealing the subcutaneous fat. Twenty wounds were created on the psoas muscle ridges on the first day of the study (Figure 11). Wound dressings were applied directly after surgery. During dressing changes, the wound dimensions were measured by measuring the edges across two diagonals in addition to the depth. On selected days, specific wounds and surrounding tissue were completely excised with a narrow region of healthy tissue as follows:

	Pig 1	Pig 2
Day 3	4 wounds: one per treatment	
Day 6	4 wounds: one per treatment	4 wounds: one per treatment
Day 7		4 wounds: one per treatment
Day 9	4 wounds: one per treatment	4 wounds: one per treatment
Day 13	4 wounds: one per treatment	4 wounds: one per treatment
Day 16	4 remaining wounds	4 remaining wounds

All areas from which wounds were excised were sutured closed. After surgery, new experimental dressings were applied to each experimental wound but not from where biopsies had been taken as these areas had already been sutured closed. On the final day of the study, the remaining experimental wounds were excised.

Some wounds were snap-frozen while others were fixed in 10% formalin.

Wound measurements

Measurements of the wounds were taken to serve as indicators of wound closure. Wound lengths (head to tail direction) and widths (side to side direction) were measured using a digital calliper, and recorded. This was an indication of the rate of wound contraction. A calibrated depth indicator was utilised to measure the depths of each wound.

Statistical analysis

Statistical analysis was conducted by an internal consultant of the Department of Statistics. The data analysis consisted of two-way Analysis of Variance (ANOVA) and Repeated Measures of General Linear Model analysis to compare the effects of the experimental treatments (Absorbatox™ vs. Control – positive and negative). The level of significance was set at 0.05.

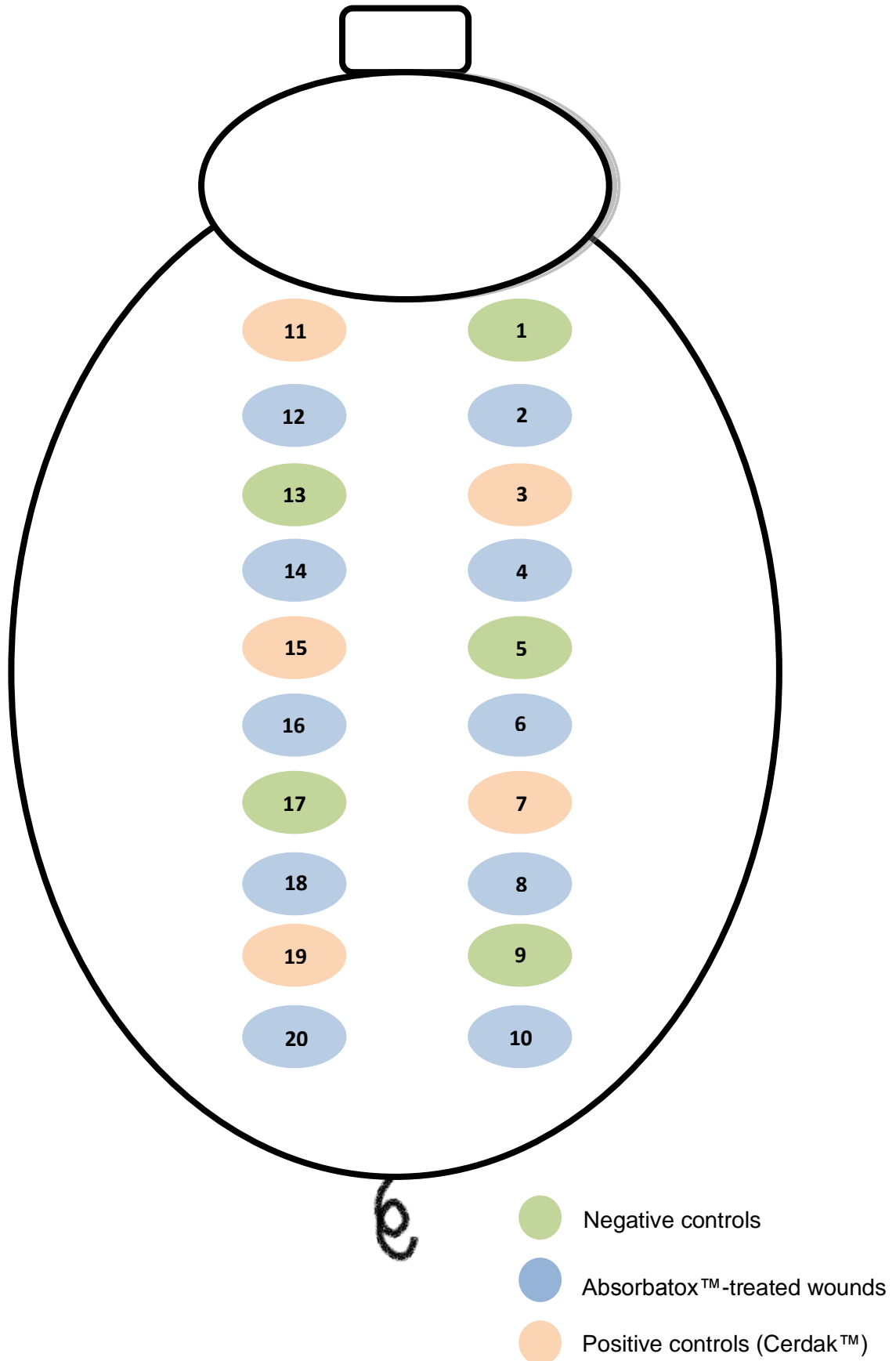


Figure 11: Pattern of wound treatments.

RESULTS

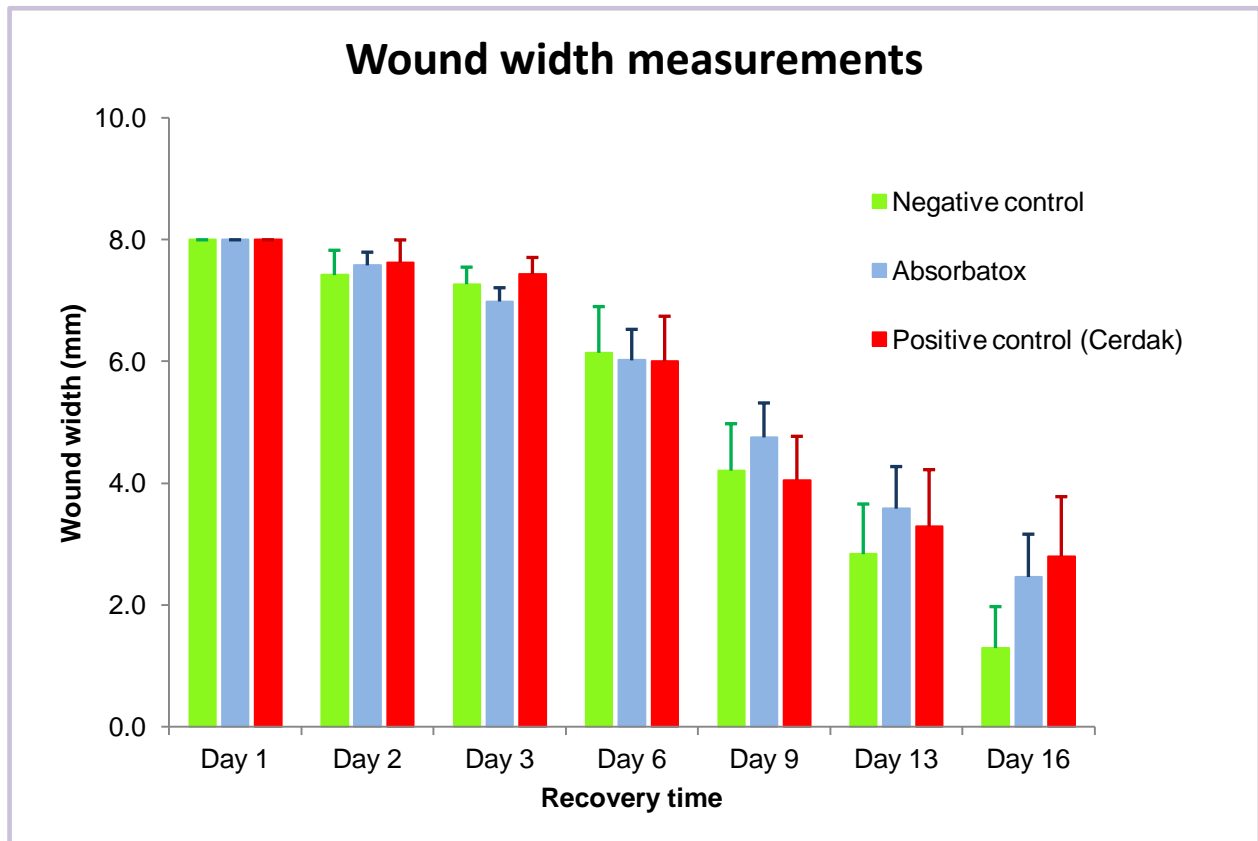


Figure 12: Comparison of the effects of each treatment: Absorbatox™ vs. Negative control and Cerdak™ (positive control) on wound widths. Measurements expressed as mean width (mm) ± SEM.

All the wounds of the different treatment groups started at a symmetrical diameter of 8 mm. The negative control wounds exhibit a more rapid decrease in the wound width than the two experimental treatments. The Absorbatox™ group demonstrated a decrease in wound width, very similar to the Cerdak™ treated group used as a positive control.

Table 3: Wound width measurements (mm).

Average wound widths (mm) ± SEM							
Treatment	Day 1	Day 2	Day 3	Day 6	Day 9	Day 13	Day 16
Negative control	8.0 ± 0.0	7.4 ± 0.4	7.3 ± 0.3	6.1 ± 0.8	4.2 ± 0.8	2.8 ± 0.8	1.3 ± 0.7
Absorbatox TM	8.0 ± 0.0	7.6 ± 0.2	7.0 ± 0.2	6.0 ± 0.5	4.8 ± 0.6	3.6 ± 0.7	2.5 ± 0.7
Positive control (Cerdak TM)	8.0 ± 0.0	7.6 ± 0.4	7.4 ± 0.3	6.0 ± 0.7	4.1 ± 0.7	3.3 ± 0.9	2.8 ± 0.9

The widths of the wounds were consistently lower in the AbsorbatoxTM-treated groups than the positive control until Day 6. Thereafter, the wound widths were comparable between the two groups. The difference between the wound widths on Day 9 was shown to be statistical significant.

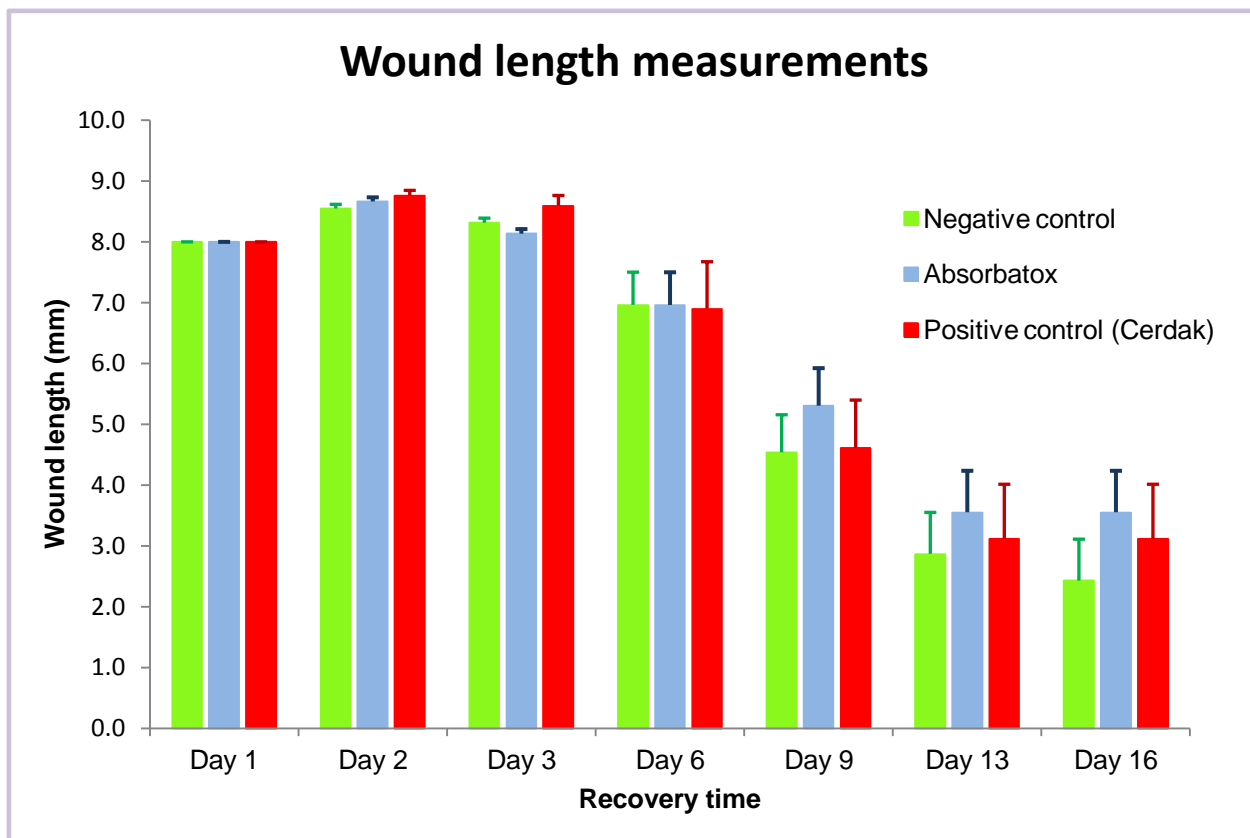


Figure 13: Comparison of the effects of each treatment: Absorbatox™ vs. Negative control and Cerdak™ (positive control) on wound lengths. Measurements expressed as mean length (mm) ± SEM.

Table 4: Wound length measurements (mm).

Average wound lengths (mm) ± SEM							
Treatment	Day 1	Day 2	Day 3	Day 6	Day 9	Day 13	Day 16
Negative control	8.0 ± 0.0	8.6 ± 0.1	8.3 ± 0.1	7.0 ± 0.8	4.5 ± 0.8	2.9 ± 0.8	2.4 ± 0.8
Absorbatox™	8.0 ± 0.0	8.7 ± 0.1	8.1 ± 0.1	7.0 ± 0.5	5.3 ± 0.6	3.6 ± 0.7	3.6 ± 0.7
Positive control (Cerdak™)	8.0 ± 0.0	8.8 ± 0.1	8.6 ± 0.2	6.9 ± 0.8	4.6 ± 0.8	3.1 ± 0.9	3.1 ± 0.9

The wound lengths in the Absorbatox™-treated group were consistently lower than the positive control group until Day 6 and showed statistical significance in this regard on Days 3 and 9. On Days 9 and 13, statistical significance was observed between the negative control and Absorbatox™-treated groups with the negative control showing lower mean values for the wound lengths.

The wound lengths and widths were taken into account together to determine the rate of wound closure. To better visualise this data, a line graph of the values was constructed. See Figure 14.

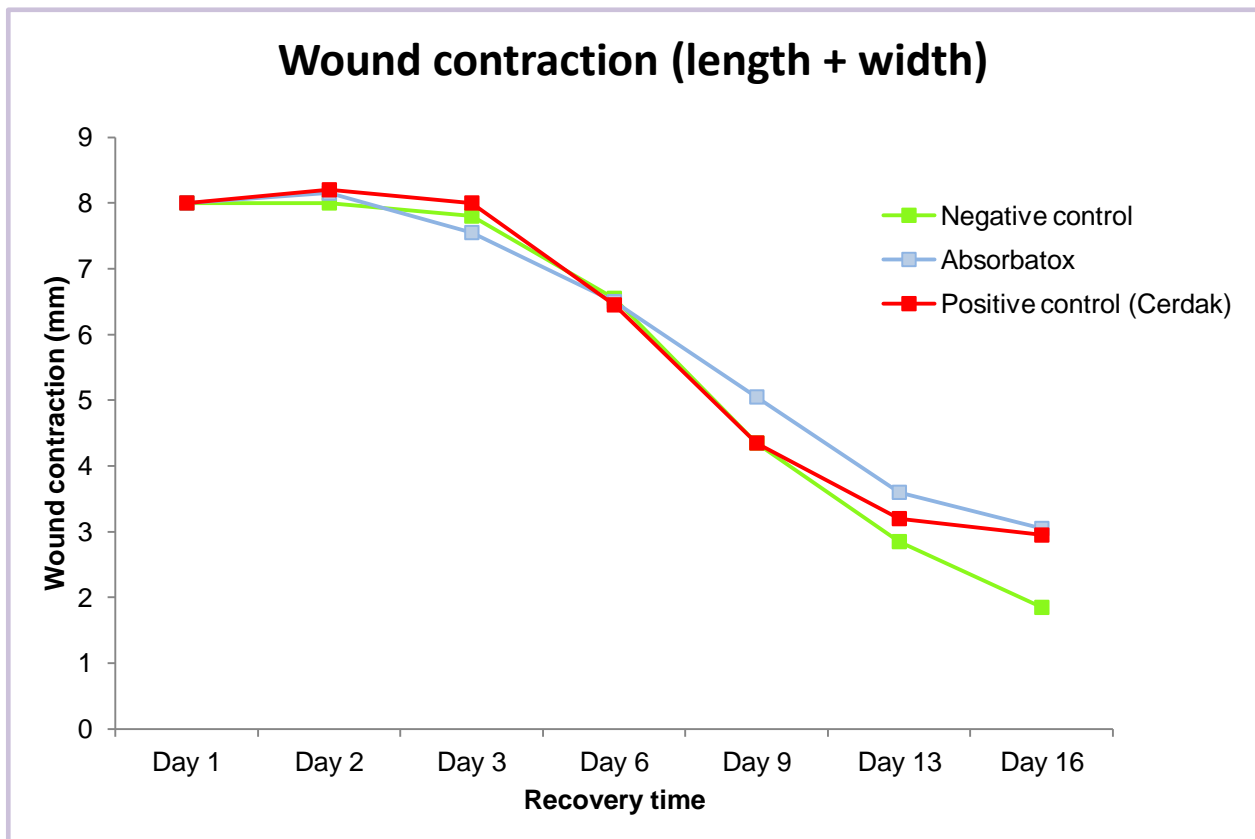


Figure 14: A line graph comparison of the wound contraction rates of each treatment group.

The faster wound closures seen in the negative control groups are indicative of wound contraction. A wound that closes faster may appear to point towards rapid wound healing, however, despite the surface being closed, the wound is weaker and

more prone to re-opening under even slight tensile force since it has little “foundation”.

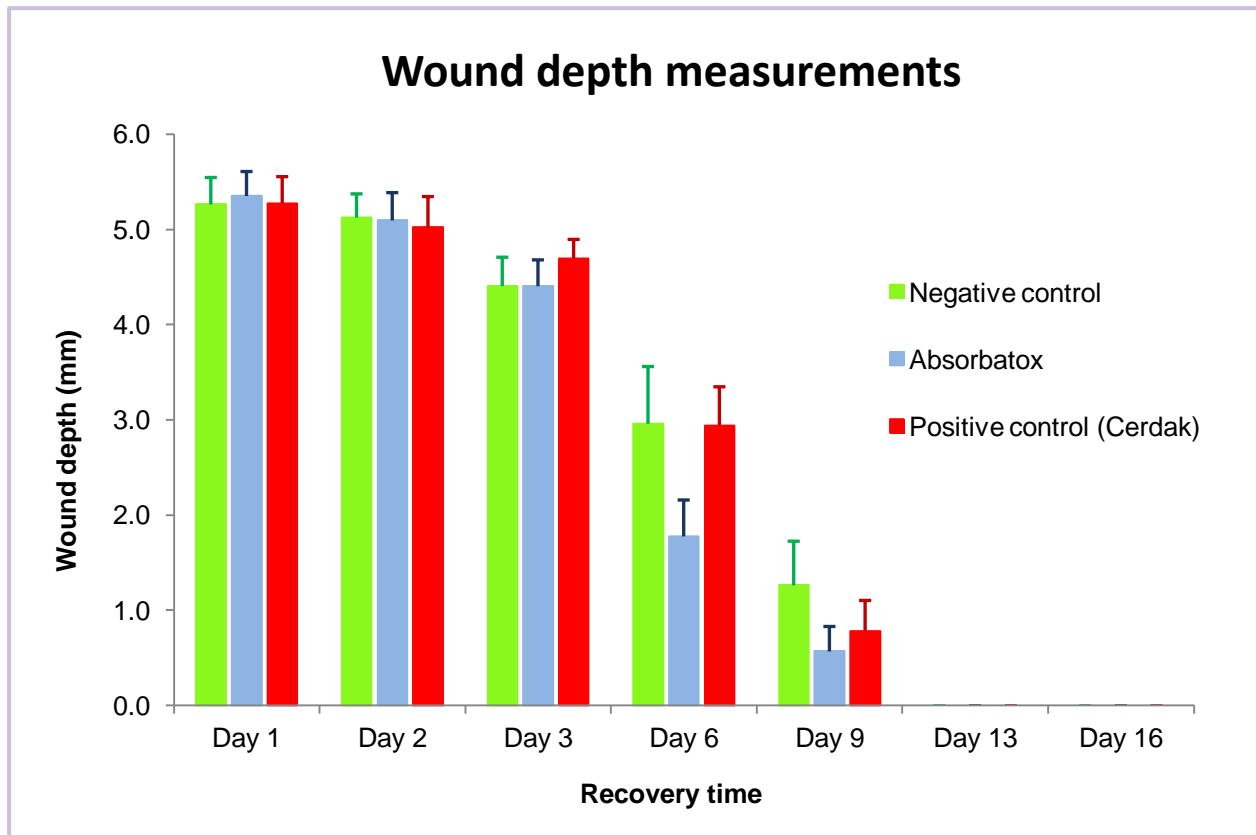


Figure 15: Comparison of the effects of each treatment: Absorbatox™ vs. Negative control and Cerdak™ (positive control) on wound depths. Measurements expressed as mean depth (mm) ± SEM.

Table 5: Wound depth measurements (mm).

Average wound depths (mm) ± SEM							
Treatment	Day 1	Day 2	Day 3	Day 6	Day 9	Day 13	Day 16
Negative control	5.3 ± 0.3	5.1 ± 0.3	4.4 ± 0.3	3.0 ± 0.6	1.3 ± 0.5	0.0	0.0
Absorbatox™	5.4 ± 0.3	5.1 ± 0.3	4.4 ± 0.3	1.8 ± 0.4	0.6 ± 0.3	0.0	0.0
Positive control (Cerdak™)	5.3 ± 0.3	5.0 ± 0.3	4.7 ± 0.2	2.9 ± 0.4	0.8 ± 0.3	0.0	0.0

The wounds were of comparable depths when initially excised and varied slightly but did not exceed 6 mm.

From Table 5, it is evident that the Absorbatox™-treated wounds started off with a slightly greater depth than the negative- and positive-treated wounds. Despite this, these wounds were shallower from the third day onwards; the Absorbatox™- treated groups exhibited consistently lower wound depth measurements than the negative control and Cerdak™ (positive control) groups. This suggests that the wounds treated with Absorbatox™ heal more rapidly from the bottom as opposed to wound contraction from the edges inwards. This implies that Absorbatox™ promotes repair in the lower layers of the dermis with new cell development and collagen deposition; characteristics that are reputed to lead to a stronger healed wound.

The Absorbatox™-treated groups showed statistically significant differences compared to the negative and positive control groups between Days 3 and 9. On Day 3, there was a 20% reduction in the mean wound depths in the Absorbatox™ vs. positive-controlled groups. On Day 9, the Absorbatox™-treated group showed 78% – 100% mean depth reduction vs. the 72% – 90% mean depth reduction observed at this time point for the positive control treatment.

DISCUSSION

Although the study compared limited numbers of samples, it appears that treatment with Absorbatox™ resulted in a more rapid decrease of wound depths compared to the positive (Cerdak™) and negative control treatment groups. Furthermore, less wound contraction was observed in the Absorbatox™ treatment groups than in the negative group and this wound contraction was, although similar to the positive control, slightly slower in the Absorbatox™ group than in the positive control group. The wound depth decreases brought about by Absorbatox™ treatments were more rapid than the control groups and these changes were statistically significant. These factors are positive indicators that Absorbatox™ brings about good wound healing.

During the proliferation phase of wound healing, fibroblasts and epithelial cells migrate into the wound to replace lost and damaged tissue (Boateng *et al.*, 2008). Macrophages express PDGF and TNF- α and initiate the provisional formation of extracellular matrix which contributes to a wound becoming shallower. The fibroblasts also synthesise proteoglycans and fibronectin to further contribute to extracellular matrix generation. A further function is to synthesise immature collagen with the aim of increasing wound strength; however at this stage there is also increased epithelial thickening to help close the wound until sufficient collagen has formed to bridge the wound (Broughton *et al.*, 2006; Schultz and Wysocki, 2009; Guo and DiPietro, 2010). The matrix contains latent TGF- β in the form of pro-TGF- β which requires a protease to activate the inactive TGF- β for its effects to be brought about. The required protease is expressed by macrophages and fibroblasts. The activated TGF- β stimulates influx of fibroblasts and enhances collagen synthesis (Broughton *et al.*, 2006; Schultz and Wysocki, 2009).

Wound contraction, resulting in surface wound closure (Broughton *et al.*, 2006; Guo and DiPietro, 2010), is brought about by macrophage-directed initiation of fibroblast differentiation into contractile fibroblasts (myofibroblasts) triggered by PDGF and TGF- β_1 (Broughton *et al.*, 2006; Guo and DiPietro, 2010).

The final phase of the healing process (remodelling) is characterised by the formation of mature collagen under the influence of TGF- β causing the thickening of the extracellular matrix as the immature collagen III, seen in earlier stages of wound healing, is replaced with mature collagen I (Broughton *et al.*, 2006). TGF- β plays a pivotal role in scar formation by stimulating the deposition of collagen, elastin, and fibronectin in the extracellular matrix. This protein expression, as well as the additional formation of cellular connective tissue and strengthening of the new epithelium, determines the characteristics of the final scar (Broughton *et al.*, 2006; Schultz and Wysocki, 2009; Ashraf *et al.*, 2009).

While no examination of wound exudate or histological sections was conducted for the present study, a previous study conducted in the Department of Pharmacology,

University of Pretoria by Oosthuizen *et al.* (2009) included histological evaluations of cellular and extracellular matrix changes. These histological evaluations showed that the wound closures observed in the Absorbatox™ and Cerdak™ groups (positive control) were associated with the establishment of new epithelium with well-defined basal layers, normal collagen arrangement and neovascularisation (Figure 16).

These sought after healing characteristics were absent in the negative control groups.

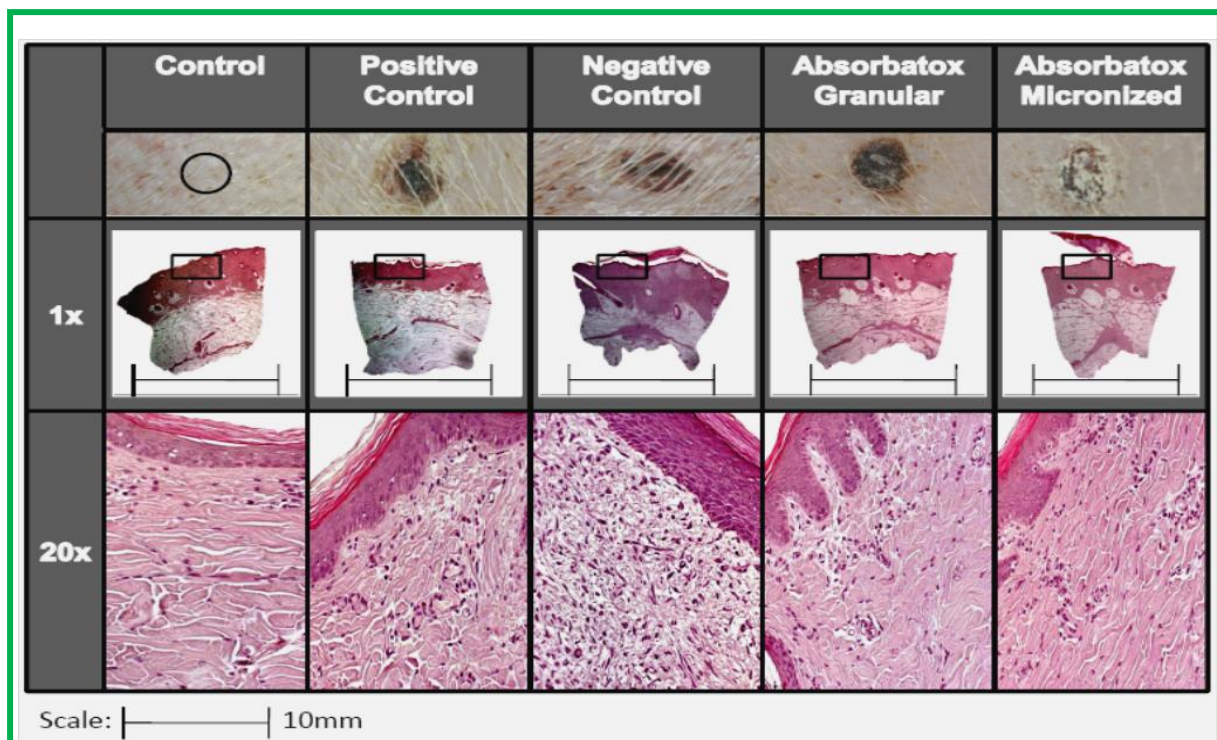


Figure 16: Histological comparison of wound tissue treated with Cerdak™ (positive control), negative control, and the two Absorbatox™-treatments used in the study by Oosthuizen *et al.* (2009).

In the Oosthuizen *et al.* (2009) study, the inflammatory cytokines found in the wound exudates retained within the wound dressings of the different treatment groups were

IL-1 β , IL-6, IL-12, and TNF- α . It was established that no significant differences or obvious trends relating to the concentration of inflammatory cytokines existed (Oosthuizen *et al.*, 2009). Concentrations of TGF- β were also assessed but no significant differences were observed in the wound exudates retained from the wound dressings of different treatments. Nonetheless, both studies showed improved wound healing in the Absorbatox™-treated groups than in the positive and negative controls. At the end of the wound exudates evaluations, the researchers hypothesised that the improved wound healing observed in the Absorbatox™ and Cerdak™ groups was probably because the cytokine-rich exudates – although absorbed by the treatments in the wound dressings - still remained in contact with the wound allowing them to continue their chemotactic functions.

The hypothesis proposed by this study is in line with literature which suggests that TGF- β is essential to wound healing due to its role in controlling cellular proliferation and differentiation (Ashraf *et al.*, 2009). In fact, a study cited by Ashraf *et al.* (2009) stated that topical application of TGF- β has been shown to increase tensile strength and reverse steroid-induced healing impairment in rats. Furthermore, according to a study conducted by Lin *et al.* (1989), the individual factor found in the wound that stimulated the greatest healing response was TGF- β , which promoted a significant increase in collagen synthesis and fibroblast proliferation. These effects were seen to be consistent with previous observations made in other wound healing models (Lin *et al.*, 1989).

The cytokines that were detected in the previous study's investigation of wound exudates have many different roles in the phase of inflammation. IL-1 is released by platelets that form the clot soon after a wound is sustained to prevent excessive bleeding. IL-1 also acts as a chemo-attractant for neutrophils, stimulating neutrophil adherence to the endothelial cells and thus represents the immune system's bacteria-destroying (Broughton *et al.*, 2006) and dead tissue-removing trigger. IL-12 is a T-cell stimulating factor and mediates the enhancement of the cytotoxic activity of the natural killer (NK) cells (Arno *et al.*, 2011). TNF- α in concert with IL-1 induces matrix-metalloproteinase transcription in macrophages and fibroblasts, while IL-6 is

released in response to IL-1 secretion and is responsible for recruiting macrophages in the proliferatory phase of healing (Broughton *et al.*, 2006).

The differences observed between the Absorbatox™-treated and the negative and positive control groups showed statistical significance in the differences between wound healing rates. The graphs, as well as the physical observations, exhibit improved and more rapid healing (however slight) in the Absorbatox™ groups compared to the other groups. The wound healing properties of the Absorbatox™-treated groups, although comparable to that of the Cerdak™ (positive control) group did show superiority to those of the negative control group. Despite this similarity between the Absorbatox™ and positive control (Cerdak™) groups, it should be noted the particle sizes and internal pore sizes of Cerdak™ are larger than those of Absorbatox™ which give Absorbatox™ an advantage as the more comfortable wound-healing device. In addition to this, perhaps in the case of comparing wound dressings, biological significance is an aspect that should also be considered: the Absorbatox™ wounds filled out then scarred sooner than the Cerdak™ and negative-control treatments which indicates improved wound healing and promises a result of a strong wound once healed.

In conclusion, pig skin wounds were found to be a good model for the study of excisional wound healing due to its similarity to human skin in many respects. Results from use of this animal model may be easily translated to the human condition to compare different treatment options and for testing different approaches in wound management. The results observed during this study indicate that Absorbatox™ could be used as a promising wound healing agent that results in strong wounds once healed.

CHAPTER 4: MALDI-MSI

INTRODUCTION

Mass spectrometry is a powerful analytical technique that has both qualitative and quantitative applications (El-Aneed *et al.*, 2009). The first mass spectrometer was constructed in 1912 by Sir Joseph John Thomson of Cambridge University. By 1913, Sir Thomson had demonstrated the value of this technique in the field of analytical chemistry. Since then, mass spectrometry has developed from analysing only inorganic molecules to biological macromolecules (El-Aneed *et al.*, 2009).

Mass spectrometry depends on the formation of gas-phase ions that are separated according to their mass-to-charge ratio (m/z) (El-Aneed *et al.*, 2009). Complex biological compounds such as proteins, however, cannot be converted to the gas phase without extensive degradation and significant destruction. Thus the advent of soft ionisation techniques that induced ionisation with limited fragmentation led to the progression of proteomic studies. MALDI MS – matrix-assisted laser desorption/ionisation mass spectrometry – is such a technique that resulted from many years of investigation into the use of lasers for the ionisation of biomolecules such as proteins (Tarran *et al.*, 2007; Caldwell *et al.*, 2008). The majority of the energy from the laser is used to volatilise an added ionisable matrix instead of degrading the proteins and other biomolecules within the sample (Jagtap and Ambre, 2005). MALDI MS has since gained massive popularity in modern proteomics due to its versatility in numerous applications and has been used in various extensive studies of biological processes and samples by the systematic analysis of proteins expressed in a cell or tissue (Caprioli *et al.*, 1997; Yates, 1998; El-Aneed *et al.*, 2009).

MALDI-TOF-MS was first introduced between 1987 and 1988 by Karas and Tanaka who reported UV-laser desorption of bio-organic compounds with masses above 10 kDa (Karas *et al.*, 1987; Karas *et al.*, 1988; Tanaka *et al.*, 1988). It made possible the sensitive detection and quantitation of proteins from tissue sections and even

serum samples as they fluctuate during the various biological processes and also during the stages of wound healing (Jemal and Xia, 2006; Zhao *et al.*, 2006).

In addition to being able to measure the protein fluctuations in tissue, MALDI MSI (mass spectrometry imaging), as pioneered by Caprioli *et al.* (1997) is a sensitive and robust technique that allows researchers to image tissue by the spatial quantitation of proteins present in histological sections. MALDI MSI and MALDI-TOF allow analysis of thin tissue sections including assessing relative concentration, location, composition, and spatial orientation of small molecules, lipids, proteins and peptides in biological structures (Yates, 1998; Aebersold and Goodlett, 2001; Jagtap and Ambre, 2005; Chaurand *et al.*, 2005; Marshall *et al.*, 2010). This makes following the changes occurring during physiological changes at molecular level possible, making it an ideal tool to investigate the biological effects that Absorbatox™ has on wound tissue with respect to its ability to provide an environment that results in improved wound healing.

The basic components of the MALDI mass spectrometer are the ion source, mass analyser, and detector. The ion source is the compartment in which charged species are produced from sample molecules. The mass analyser part of the instrument is where the ions are separated based on their mass-to-charge (m/z) ratio. This isolation of ions is driven by an electric field across a flight tube that accelerates ions with equivalent kinetic energy resulting in larger ions moving slower. The detector determines the abundance of each ion present and the mass depending on the order in which the ions strike it (El-Aneed *et al.*, 2009; Murayama *et al.*, 2009).

MALDI MSI separates the ionised particles ejected from an intact tissue sample treated with matrix according to differences in their m/z ratios. The data is then merged from the multi-channel (m/z) measurements of mass with a sample surface position allowing for rapid mapping of the ionisable content of tissues (Caldwell *et al.*, 2008; Murayama *et al.*, 2009). The technique depends on an ultraviolet absorbing matrix that easily ionises and transfers charge to the sample molecules. MALDI matrix is typically a small, acidic, aromatic compound selected for its ability to absorb

wavelength of the irradiating laser and to transfer energy to closely associated molecules (Aebersold and Goodlett, 2001; Chaurand *et al.*, 2005). The matrix is applied evenly to the tissue section on a conductive target plate and then irradiated in the source using a laser to induce ionisation of the sample molecules which are then analysed by MS to result in the spectral arrangement being plotted (Aebersold and Goodlett, 2001; Chaurand *et al.*, 2004; Chaurand *et al.*, 2005; Walch *et al.*, 2008; Goodwin *et al.*, 2008). The drying of the matrix-analyte combination results in the formation of crystals which are subjected to a UV laser beam tuned to an appropriate frequency which strikes the matrix-analyte combination. The matrix absorbs the UV laser impulse and since there is a high matrix to analyte ratio, the majority of the energy is absorbed by the matrix resulting in less direct irradiation of the analyte. The absorbed light energy results in the ejection of ions from the tissue samples which are then accelerated down an evacuated flight tube of known dimensions by a constant electrical field (Chaurand *et al.*, 2003). The lighter ions arrive at the detector faster than the heavier ions and the times-of-flight are recorded by a detector that produces a signal dependant on the number of impacts of each ion group (Chaurand *et al.*, 2003; Jagtap and Ambre, 2005). The data is generated from successive laser shots to yield a TOF mass spectrum as a function of time and translated into multiple mass spectra from the irradiated spot (Aebersold and Goodlett, 2001; Chaurand *et al.*, 2005; Jagtap and Ambre, 2005; Zhao *et al.*, 2006). The analysis of the ions gives insight into the composition of the tissue (El-Aneed *et al.*, 2009). Scanning across a tissue section at defined geometrical co-ordinates (Aebersold and Goodlett, 2001; Zhao *et al.*, 2006) results in mass spectra which can be compiled into a format in which the ions produce a map of the approximate quantities of biomolecule of each mass detected (Chaurand *et al.*, 2005) which can be shown on a colour-intensity scale at each sample co-ordinate location (Naono *et al.*, 1997). The resultant MALDI image is, to quote Leinweber *et al.* (2009), a ‘three-dimensional (3D) array of data with the plane of the tissue section representing the XY dimensions, with thousands of mass spectra acquired across the surface of the tissue representing the Z-dimension.’ This entire process can be summarised into a graphical representation as seen in Figure 17.

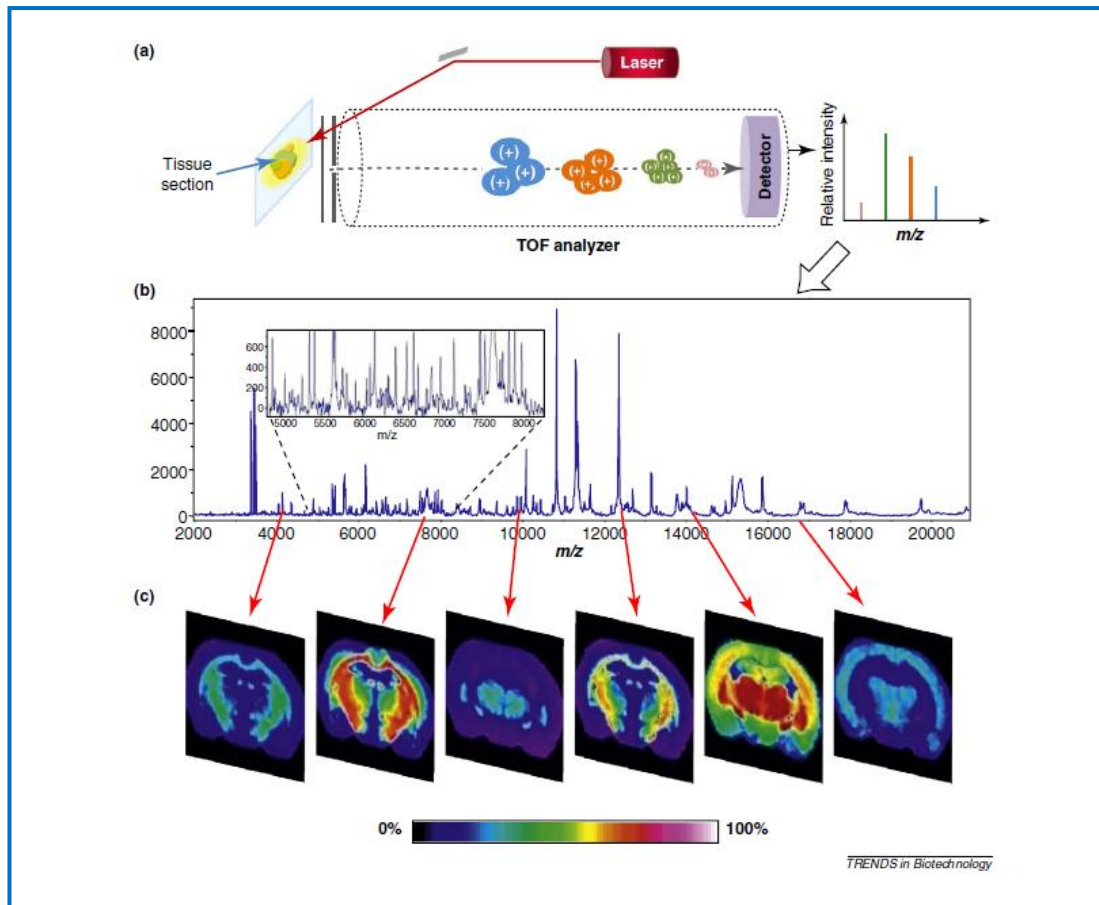


Figure 17: Graphical description of the process of the generation of ions and their subsequent translation into ion-density distribution images (Seeley and Caprioli, 2011).

Protein profiling and imaging from thin tissue sections are fairly new MALDI techniques (Chaurand *et al.*, 2005). These techniques involve the application of matrix onto the tissue either as a uniform layer (as in imaging) or in specific areas (as in profiling) shown in Figure 18 taken from Chaurand *et al.* (2005). Figure 18 shows the general method followed to obtain mass spectra and ion density distribution images.

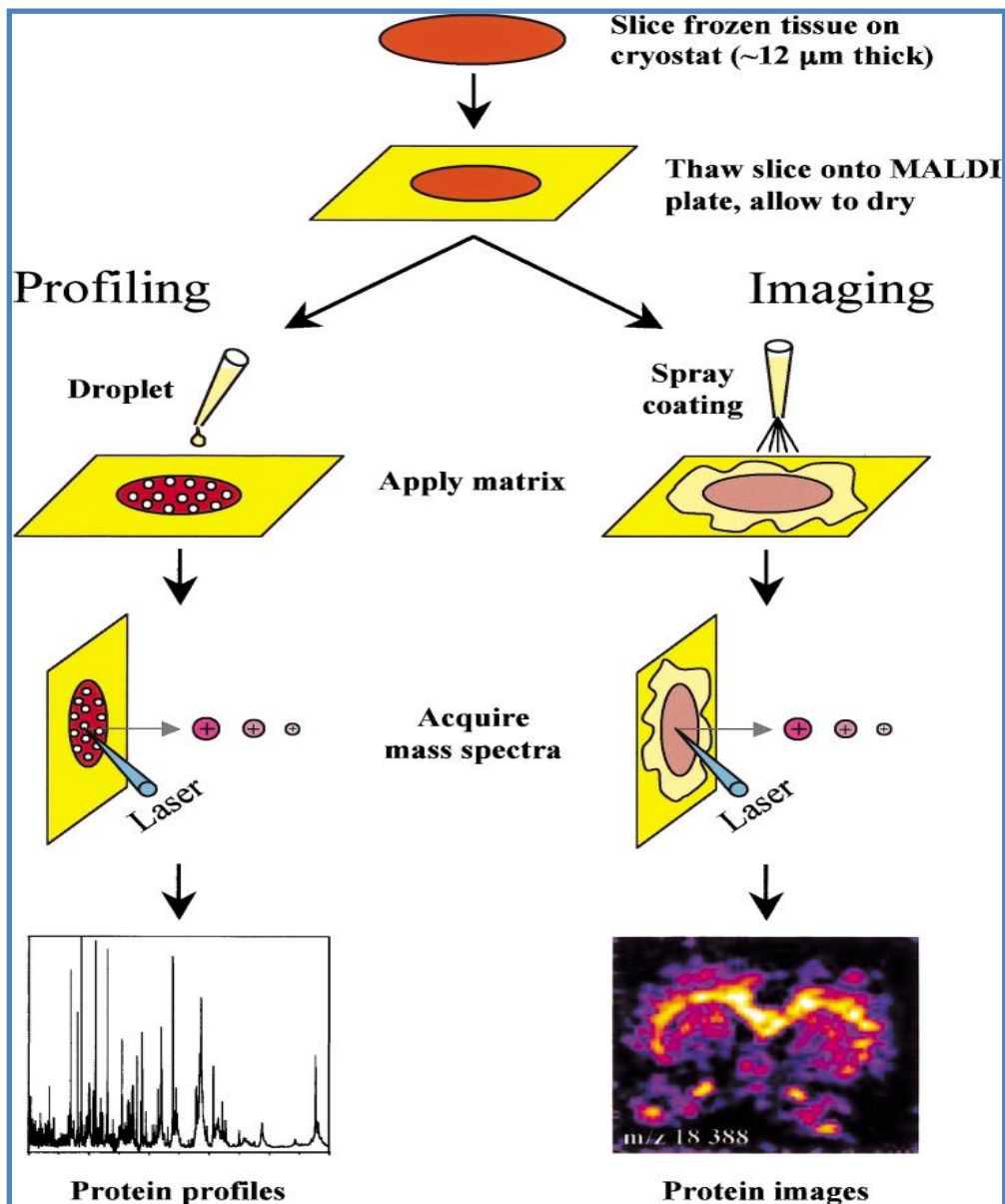


Figure 18: Difference in matrix application for both protein profiling and imaging (Chaurand *et al.*, 2005).

When applying matrix, care must always be taken to minimise analyte migration (Chaurand *et al.*, 2005; Caldwell *et al.*, 2008). Thus the application of matrix is a strong determinant of both spatial resolution and the number of unique ions detected per laser shot. Cheaper methods of applying the matrix include using TLC sprayers, airbrushes and even dipping the sample into the matrix, but these have the distinct disadvantage of being poorly reproducible. While it is possible, with careful manual application to deliver a homogenous layer, there is a greater possibility of over-

spraying a sample resulting in horizontal analyte migration and thus inaccurate results. Automated sprayers reduce the likelihood of such problems and have the added advantage of increased reproducibility (Aebersold and Goodlett, 2001; Caldwell *et al.*, 2008). The choice of matrix must also be optimal for the different molecular classes being analysed (Walch *et al.*, 2008). It has been reported that sinapinic acid provided the best signal for higher molecular weight proteins, while α -cyano-4-hydroxycinnamic acid is better suited to lower molecular weight peptides when analysing tissue sections (Aebersold and Goodlett, 2001).

To date, the majority of proteomic tissue analysis with MALDI MSI involves the use of snap-frozen tissue. However, since the standard method of tissue and organ preservation employed by many pathology laboratories is formalin fixation, researchers have developed methods to analyse formalin-fixed paraffin-embedded (FFPE) tissue. The ability to analyse FFPE tissue is of great value since these samples open the door to examine the clinical course of diseases and to use repository stored tissue sections to identify specific protein abundance (Chaurand *et al.*, 2006; Lemaire *et al.*, 2007; Groseclose *et al.*, 2008; Ronci *et al.*, 2008).

Formalin fixation causes cross-links between closely associated proteins in tissue thus forming a meshwork that stabilizes the tissue mass and maintains morphology. While triglycerides are not affected, formalin fixation could occur in the protein portion of lipoproteins. Formalin acts mainly on the amino groups, more specifically the lysyl residues, of the proteins to form intra-and inter-molecular cross-links. This cross-linking results in the formation of aminomethylol groups that condense with other functional groups to form (hydroxy)methylene bridges. It is this aspect of formalin fixation that results in the variably reversible damage to some antibody binding sites (Werner *et al.*, 2000; Ronci *et al.*, 2008; Namimatsu *et al.*, 2005).

In the case of formalin fixation, enzyme digestion or heat-induced epitope retrieval may unmask masked sites. The use of an antigen retrieval reagent such as citrate buffer can be used for this purpose and has been shown to produce specific immunostaining and epitope sensitivity equivalent to that attained in frozen (unfixed)

tissue with more specific antigen localisation (Namimatsu *et al.*, 2005). Namimatsu *et al.* (2005) explains a possible mechanism of antigen retrieval (epitope retrieval): formalin cross-links start off as imines that can react with citraconic anhydride to give reversibly modified amines. Hydrolysis of the adducts of citraconic anhydride and amines occurring at pH 7.4 in hot water, liberates the originally fixed amines.

Below are the chemical explanations of the processes of formalin-fixation and antigen retrieval, respectively.

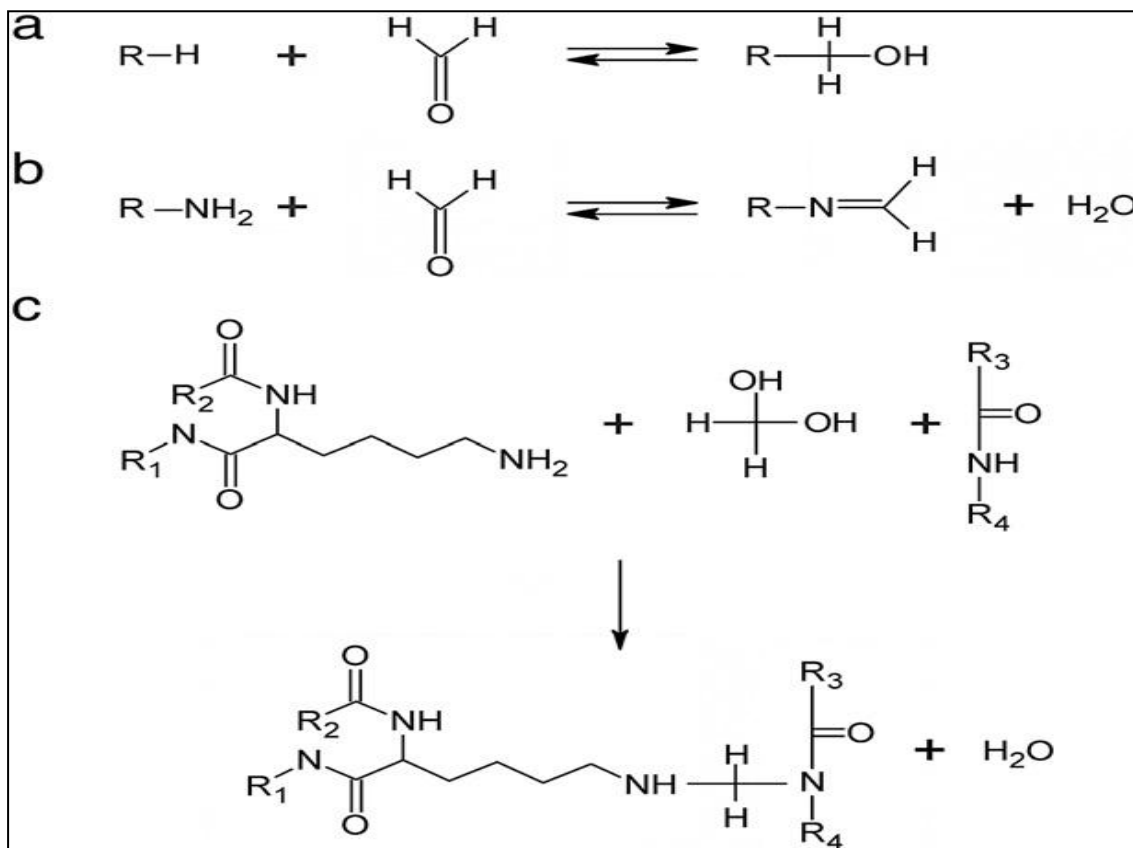


Figure 19: Simplified scheme of formaldehyde reaction with proteins. (a) Formaldehyde is added to a protein with the formation of a reactive hydroxymethyl molecule. (b) Formation of an imine group (Schiff's base). (c) Methylene bridge formation between a lysine residue (lysyl group) and nitrogen of a peptide linkage. Formaldehyde is depicted as methylene glycol, formed by reaction with water (D'Amico *et al.*, 2009).

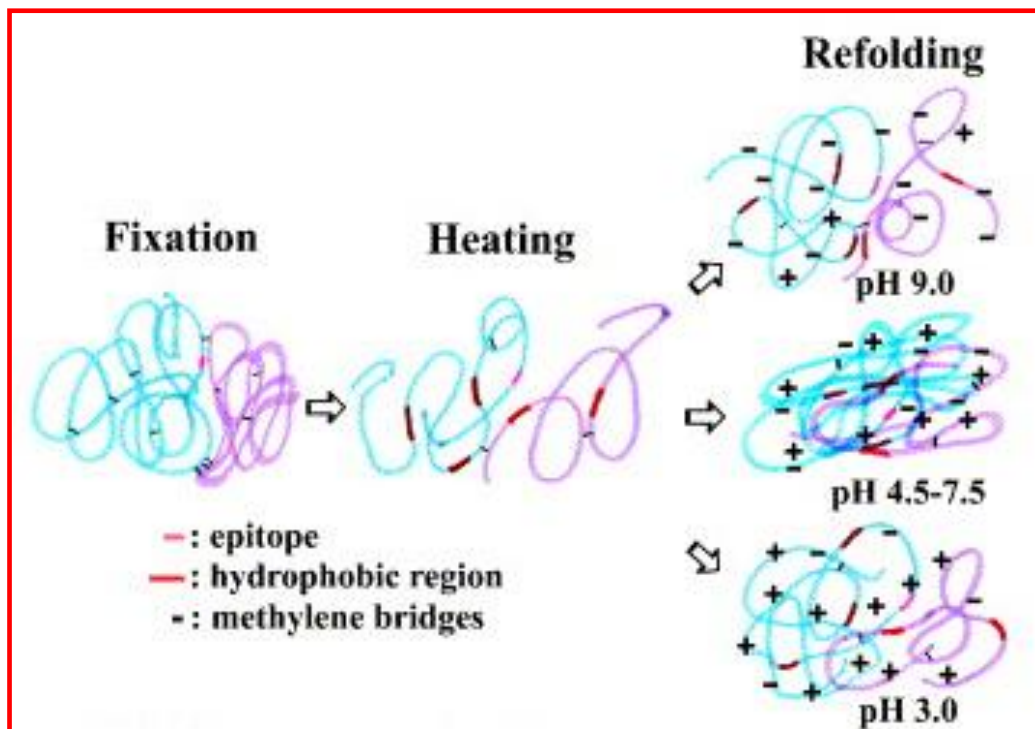


Figure 20: The above diagram shows the protein effects of formalin fixation and that of antigen retrieval (Yamashita, 2007).

MATERIALS AND METHODS

Formalin-Fixation Paraffin-Embedding (FFPE)

Instrumentation

Tissue processing was performed using a Thermo Scientific Excelsior ES Tissue Processor. Tissue sections were made using a Leica RM 2265 microtome and mounted onto histological glass slides.

Tissue preparation

The complete full thickness wounds and at least 3 mm of surrounding skin were surgically excised from the backs of the pigs at selected recovery times while under anaesthesia and placed individually in marked specimen containers filled with 10% buffered formalin solution. The new wound was stitched closed, treated with topical antibiotic and a gauze pad and secured with OpSite breathable membrane. The excised samples were kept in the formalin solution until they were processed appropriately for wax embedding.

The tissue biopsies were transferred from their individual formalin-filled containers to labelled histology cassettes and processed using a sequence of formalin, solutions of various percentages of ethanol, and xylene in a Thermo Scientific Excelsior ES Tissue Processor in preparation for wax-embedding. The formalin fixing maintains the tissue morphology, the graded ethanol solutions dehydrated the tissue and the xylene was used to serve as a clearing agent (Werner *et al.*, 2000). This tissue preparation process was fully automated.

Wax embedding

Each wound biopsy was placed into individual wax-embedding moulds and orientated to provide the correct histological cut of the wound tissue. A small quantity of molten paraffin wax was poured into each mould. The mould was briefly placed on a cold plate to allow the lowest level of wax to partially set to “hold” the biopsy. The biopsy was then carefully orientated and positioned in the almost “sticky” wax in the mould. The mould was then further filled around the biopsy section with molten wax while the biopsy was held by the first layer of sticky wax. Each sample was labelled immediately after placing the cassette on the mould. Care was taken to not over cool the first layer of wax as this would cause cracking when more hot wax was poured into the mould and result in broken or torn tissue sections. When the wax had set, the moulds were carefully removed and the wax blocks were stored at room temperature.

Sectioning

The wax blocks were placed on a cold plate at approximately -18°C . This is because cold wax is easier to section and does not fold over itself the way warmer wax does. Serial tissue sections were cut at a thickness of $10\ \mu\text{m}$ using a Leica RM 2265 microtome using the manual hand wheel and mounted on histological glass slides. The slides were kept overnight in an oven at 37°C to allow them to dry and to ensure better adherence to the glass slides.

Mass Spectrometry

Sample preparation

To date, the majority of proteomic tissue analysis and imaging by MALDI MSI involves the use of snap-frozen tissue (Chaurand *et al.*, 2006; Lemaire *et al.*, 2007). The use of FFPE tissue in MALDI MSI requires more sample preparation than does frozen tissue. Two processes are needed to be able to use FFPE for MALDI MSI. The first is to remove all the wax surrounding the tissue as wax can also ionise and give a strong background signal in a MALDI spectrum. The second process is that of antigen retrieval to try reverse the protein cross-linkage before the sample can be analysed. A number of approaches were used to optimise sample preparation methods as well as slide conductivity. Some challenges arose and they, along with their solutions, are presented.

Challenge one: Conductivity of slides

A conductive target plate must be used for MALDI-TOF-MS analysis of both proteins and peptides from precipitated samples or tissue sections. In most cases, a special indium tin oxide (ITO) coated slide is used to give high quality mass spectra. Since such slides were not available, standard histological glass slides were used. The slides were rinsed with acetone then distilled water and allowed to dry before being coated with gold using a gold sputter coater used for

SEM sample preparation. Histological glass slides (three at a time) were placed in a gold sputter coater. Argon gas was used to provide a source of ions for the gold bombardment. Gold deposition lasted for 30 seconds at 300 mA. A study conducted by Chaurand *et al.* (2004) investigated the signal quality resulting from the use of an ITO-coated slide versus a gold-coated slide. The study demonstrated no significant difference in signal intensity or resolution (Chaurand *et al.*, 2004; Murayama *et al.*, 2009; Marshall *et al.*, 2010).

Outcome: The histological tissue sections were immediately mounted onto the gold-coated slides after sectioning which meant that these slides were also put through the sample preparation procedures. During the de-waxing procedures, small sections of the gold coating started lifting at the corners where the slides were being handled. Since the gold that peeled off immediately floated to the surface and did not adhere to the tissue, it was decided that the use of the slides could continue. During the process of antigen retrieval however, the gold coating came off as a sheet along with the tissue sample. This caused damage to the tissue sample in terms of folding over itself and breakage.

A possible reason for this is that commercial gold-coated slides have an adhesion layer of chromium (Cr) or titanium (Ti) under the gold layer. If this layer of adhesion is absent, the gold delaminates from the glass during processes such as sonication. While the gold-coated slides used in this study were not exposed to sonication, the process of antigen retrieval delaminated the gold even without considerable turbulence (Sigma-Aldrich®, n.d). A possible reason for this is: vapour-deposited gold results in a weak bond between the gold film and glass slide since the gold film adheres to the glass by mechanical means only and this film is damaged by significant water exposure (Mosier-Boss and Lieberman, 1999; Roth, 1994) such as during antigen retrieval.

Solution: The challenge of conductivity was overcome by using conductive copper tape (Hua *et al.*, 2007). Tissue sections were mounted on uncoated slides and put through the sample preparation as described above. A sample holder was

custom made to allow a glass slide to be placed into it in such a way that the slide would not protrude above the holder's border as this would also raise issues of the incident angle of the laser not falling where it should and ions being "lost". The glass slides were cut to a size suitable for the custom-made holder using a glass cutter and mounted onto the holder using 3M™ Copper Conductive Tape. One end of the tape was placed on the glass slide while the other end was stuck onto the slide holder. This was repeated on the opposite edge of the glass slide. This solution allowed for the required sample preparation treatments of the tissue without the loss of tissue samples but also provided the necessary conductivity to generate high quality spectra.

Challenge two: Trypsin digestion

Digestion of the sample with trypsin results in relatively short peptides that have predictable C-terminal amino acids and for which mass data can be accurately determined. The resultant peptide fragments are usually in a specific pattern (peptide map) which is used as a fingerprint of a known protein sequence (Caprioli *et al.*, 1997; Murayama *et al.*, 2009; Önnarfjord, n.d).

Method 1: A trypsin (Mass spectrometry grade Trypsin Gold (Promega)) solution at a concentration of 0.05 µg/mL was made up in 20 mM NH₄CO₃. The trypsin solution was gently and evenly sprayed onto the entire tissue segment using an airbrush (pneumatic nebuliser). The slide was then placed in a limited volume incubation chamber which had a central platform upon which the slide could be placed and surrounded by a small volume of water to create a humid environment. This was then placed in an oven at 37°C for a period of 2 hours.

Outcome 1: At the end of the 2 hour period, it was noticed that the tissue samples were completely dry. The slides were put through MSI analysis after the tissue was sprayed with matrix. Only matrix peaks could be observed. This suggested that the trypsin dried out on the tissue long before the 2 hour period was over and thus no digestion had occurred.

This hypothesis was tested by repeating the “incubation” step using a bovine serum albumin (BSA) standard that was spotted onto the plate and allowed to dry. After digestion using the same procedure, the slide came out dry. Matrix was again sprayed onto the slide and the sample was analysed. Again, the matrix peaks were observed. No BSA peptides or trypsin peaks could be observed in the MS results. This confirmed that the trypsin digestion was not working and probably due to rapid dehydration of the applied enzyme solution.

Solution 1: Both a tissue sample and a BSA spotted slide were used in this part of the trypsin digestion. After the tissue and BSA were sprayed with trypsin, the samples were incubated in a CO₂ incubator at 37°C and 90% relative humidity with 5% CO₂ for a period of 2 hours. These conditions are also the optimal physiological conditions of trypsin. The samples were incubated in the same incubation chamber as before to ensure humidity was maintained. At the end of incubation, the samples were still moist. MS analysis showed matrix, some trypsin, as well as a few BSA peptide peaks. However, no significant peaks were observed for the wound biopsy tissue.

The modification of Djidja *et al.* (2010) was then used. This method used a very high trypsin concentration of 20 µg/mL since the previous concentration used was too dilute for on-tissue digestion; the previous concentration is used mainly for detecting proteins already in solution. This time, the trypsin was made up in 40 mM NH₄CO₃.

Outcome 2: The trypsin digestion according to the method of Djidja *et al.* (2010) resulted in peptide peaks for both the BSA spots and the wound biopsy tissue samples without requiring further optimisation.

Once these challenges were overcome, the sample preparations continued as necessary.

De-waxing (Deparaffinisation)

The tissue sections mounted onto the slides were put through a de-waxing process following the in-house protocol of the Mass Spectrometry Research Centre of Vanderbilt University (Tennessee, USA). This process was not effective in clearing the wax from the tissue and slides most likely because the tissue processing methods and the type of tissue used in this study were different from those used at Vanderbilt University. The in-house protocol of Novartis Institutes for BioMedical Research (Basel, Switzerland) was then used. The procedure was as follows: the de-waxing procedure was a sequence of two 15 minute washes in clean xylene, followed by a series of 5 minutes washes in 100% ethanol, 85% ethanol, and finally 70% ethanol. Each solution was placed in a 7.6 cm x 5.7 cm x 3 cm staining dish which was filled to cover the slides. Four slides were treated at a time.

Antigen retrieval

The purpose of this step is to reverse, as best as possible, the cross-links formed during formalin fixation. This was done using a method based largely on the in-house protocol of the Mass Spectrometry Research Centre of Vanderbilt University (Tennessee, USA).

The slides were placed into a 10 mM Tris buffer solution at pH 9 for antigen retrieval directly after the process of de-waxing. The Vanderbilt protocol used a decloaking chamber, however, waterbaths and microwaves have also been used for this procedure (Namimatsu *et al.*, 2005). The antigen retrieval was performed in an equivalent of a waterbath. The slides were carefully placed upright in a 900 mL beaker containing 900 mL Tris buffer at 60°C and the beaker was returned to an oven set at 60°C for a period of 35 minutes to maintain the antigen retrieval solution at a constant temperature. At the end of the 35 minute period, the beaker was set on the bench to cool for about 5 minutes. The slides were then washed five times using a buffer exchange sequence where half the liquid is removed and replaced with distilled water each time. The final wash was 100% distilled water.

In cases where trypsin digestion did not immediately follow antigen retrieval, the slides were kept vertical to allow them to dry and placed in an uncharged desiccator until they were used in the next procedure. The dry slides were rehydrated by placing them into distilled water for two minutes before continuing with trypsin digestion.

Trypsin digestion

Mass spectrometry grade Trypsin Gold (Promega) trypsin was used for the digestion step of this component of the study. The enzyme was purchased frozen and already aliquoted into Eppendorf tubes. They were stored at -20°C and only brought out when needed. The enzyme was resuspended in 20 mM NH_4CO_3 buffer before being used for the digestion processes. The application of the enzyme was done by airbrushing which allowed a generous but even enzyme application. After the tissue samples were sprayed with trypsin, they were placed in a limited volume incubation chamber which contained a central platform upon which the slides were mounted. The platform was surrounded by a small volume of water to create a humid environment during the 2 hour incubation. The incubator conditions were 37°C with 5% CO_2 at 90% relative humidity.

Trypsin hydrolyses the protein on the C-terminal side of lysine and arginine, unless the following amino acid is a proline. The advantage of this is that potentially at least two protonation sites are created per peptide resulting in peptides that are easily ionised. These are detected as positive ions.

Matrix application

Following the *in situ* digestion, a solution of 10 mg/mL of CHCA (α -Cyano-4-hydroxycinnamic acid) in a mixture of 50:50:0.1 acetonitrile:water:trifluoroacetic acid by volume was sprayed directly onto the tissue using a pneumatic nebuliser. A volume of 16 mL of matrix was used for four slides. The edges of the glass slides

were taped to a metal plate which was held upright by a magnetised board. To prevent making the sections too wet and thus cause molecular migration, the matrix was sprayed from top to bottom, left to right. This gave the matrix at the top of the plate time to dry a bit while the glass slides near the bottom were sprayed. The same was true for the bottom slides when the top slides were being sprayed.

Histological staining

For the interpretation of the MALDI-MS image, correlating it to the histological data obtained from a stained section gives valuable information and in some cases is essential (Walch *et al.*, 2008). This is termed histological directed analysis (Cornett *et al.*, 2007). This technique is applied to sequentially adjacent histological tissue sections where one tissue section is stained with haematoxylin and eosin (H&E) (purchased from Sigma-Aldrich) while the adjacent section is analysed using MALDI MSI ((Cornett *et al.*, 2007; Walch *et al.*, 2008). The concept is that the limited thickness of the tissue sections allows for the analysis of certain protein morphology whose distribution spans up to about four sections allowing for a good comparison between the stained tissue and the MALDI MSI analysed tissue section.

A 1% stock solution of Eosin Y was made up in a 1:4 dilution of distilled water to 95% EtOH. From this, a working solution of 0.25% Eosin in 0.005% glacial acetic acid was made up. Both solutions were stored at room temperature. A volume of 50 g of Haematoxylin was dissolved in 1 L solution of 25% EtOH.

The staining protocol was as follows: 10 minutes in xylene (twice); rehydrate the sections in two changes of 100% EtOH for 5 minutes each followed by 2 minutes in 95% EtOH then 2 minutes in 70% EtOH and a brief wash in distilled water. The sections were then stained by placing them in Haematoxylin for 8 minutes. The slides were then washed in water for a period of 10 minutes and then rinsed in distilled water. This was followed by a rinse (10 dips) in 95% EtOH and 1 minute in Eosin Y to counterstain. The sections were then dehydrated using the following procedure: 5 minutes in 95% EtOH and 5 minutes in 100% EtOH (twice); and

cleared using two 5 minute rinses in xylene. H&E stains the nuclei blue and the cytoplasm pink. A drop of xylene-based mounting medium was placed on the tissue section and the coverslip was placed on the slide at an angle so as to prevent the formation of air bubbles. Care was also taken to not slide the coverslip along the tissue to try straighten it since this would damage the tissue. Once the slides were properly dried, the tissues were scanned at highest resolution (typically 1200 dpi) on a flatbed scanner to provide histological images against which the ion-intensity distribution images could be compared.

Mass spectrometry analysis

In situ peptide analysis was performed on an AB SCIEX QSTAR[®] equipped with Analyst QS 2.0 Software. MALDI-MSI data were acquired in positive mode operating with a Nd:YAG laser collecting full scan mass spectra from 100 to 2 000 Da. Images were generated and reconstructed using TissueView 1.0 Software. MALDI-TOF mass calibration was performed using spots of BSA and cytochrome *c* prior to MALDI-MSI analysis. Peptide images were acquired at a spatial resolution set at 250 μm with a laser repetition rate of 1.8 seconds per data point in a dynamic pixel which allows for the ionisation of more material per laser activated spot. The laser power level was set at 40%.

RESULTS AND DISCUSSION

The ability to image the protein species in the wound tissue using mass spectrometry techniques has the potential to identify possible targets to improve current wound healing technologies. With regards to this study, the potential to manipulate the cationic selectivity of Absorbatox™ to remove mediators possibly compromising wound healing, or proteins to expedite wound healing now exists. In this study, full-thickness wounds were created on the psoas ridge of the backs of pigs, then excised at different recovery times, fixed and analysed using MALDI-MSI. The wounds were created by punch biopsy and then excised on different days during the wound healing process, with each day marking a 'milestone' of the healing process. Tissue samples were excised during the inflammatory, proliferatory, and remodelling phases. Serial sections of 10 µm thick were made of the top, middle, and bottom of the wound as in Figure 21.

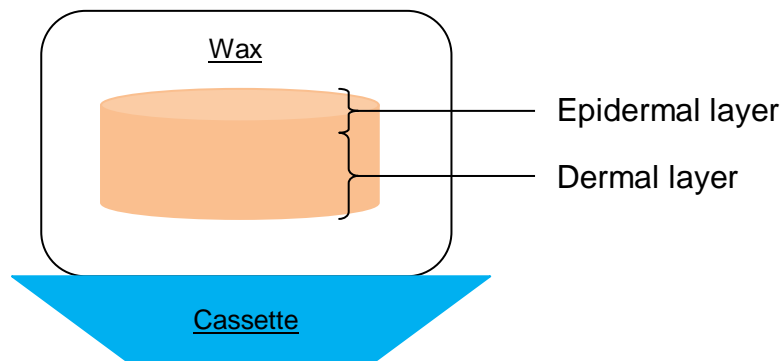


Figure 21: Diagram of the embedded tissue and the approximate areas at which sections were made for MALDI-MS analysis.

Since matrix application was by pneumatic nebuliser, peptide mass and matrix - signals were observed throughout each tissue section. Despite this, certain peptide masses were observed solely in the wound or in the healthy tissue at certain days allowing for the progression of wound healing to be monitored.

Histology–directed MALDI imaging was performed. Two adjacent sections of the sample tissue are used: one for H&E staining and one for MALDI analysis. This allows for the combined mass spectral signal to be localised on the tissue.

Because FFPE tissue, as opposed to the conventional use of snap-frozen tissue was analysed during this study, the analyte masses observed at any point on the tissue were derived from a peptide resulting from the tryptic digestion and not an entire identified protein. Thus for the remainder of this chapter, the analyte masses will be referred to by their m/z number.

The analyte masses were selected by drawing regions of interest (ROIs) on the composite MSI scan of the tissue to indicate the wound, the healthy tissue, and the matrix on the slide, and then analysing them. By stacking the y-axis of the intensities of individual analyte masses, the analyte masses specific to wounds and/or the healthy tissue were selected for ion-intensity distribution images. An example of this is shown in Figure 22.

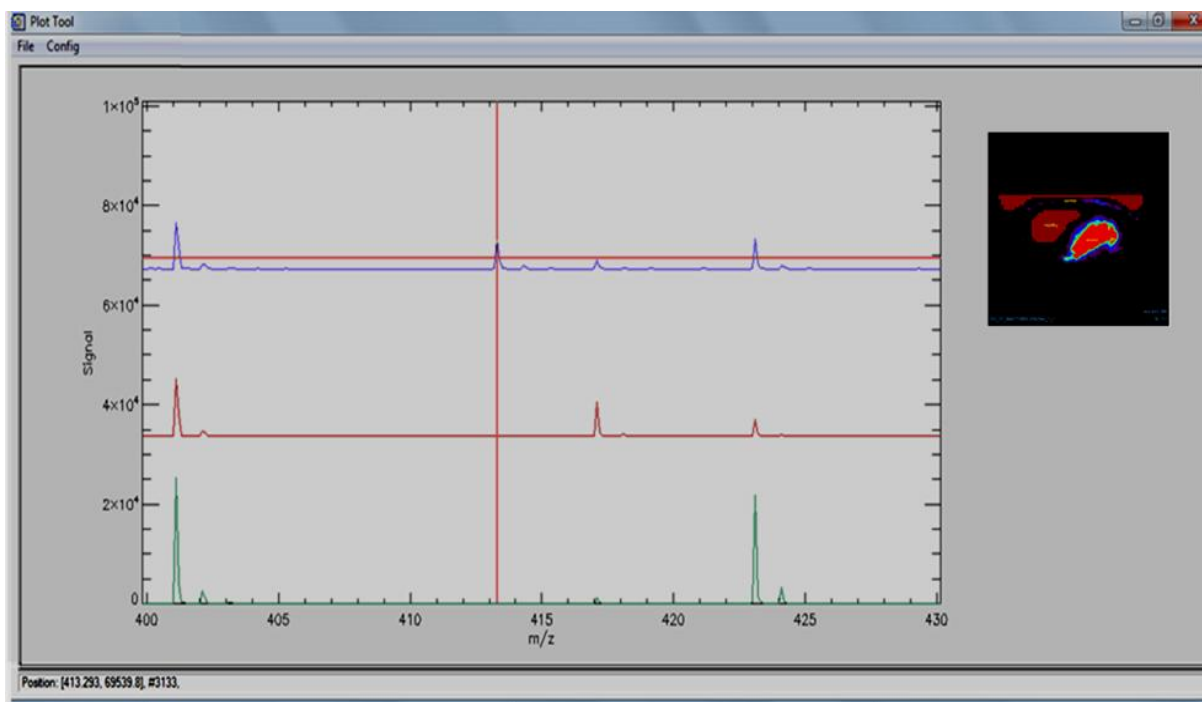


Figure 22: Screen shot of the stacked mass spectra of the wound (blue), healthy (red), and the CHCA matrix (green) as seen in TissueView 1.0.

With the aim of ensuring that tissue section images could be accurately compared, each tissue section was corrected by subtracting the matrix background and normalising for signal intensities to give an accurate representation of the protein and non-protein species present in each tissue section.

Each phase of wound healing is characterised by fluctuations of certain protein species and the synthesis of new blood vessels, nerve cells, and epithelial cells, in addition to growth mediators for the tissue (Diegelmann and Evans, 2004; Broughton *et al.*, 2006; Boateng *et al.*, 2008; Sibbald and Woo, 2008).

The inflammatory phase begins almost as soon as the wound is sustained and lasts four to six days. The proliferatory phase begins between the fourth and sixth day and lasts until the thirteenth or fourteenth day. The remodelling phase begins around the thirteenth day after the wound is sustained and can last a few days, months, and even years depending on the size and depth of the wound (Broughton *et al.*, 2006; Boateng *et al.*, 2008). This phase also results in the development of scar tissue, the nature of which is determined by the strength of the new epithelia (Hunt *et al.*, 2000; Boateng *et al.*, 2008). Full thickness wounds, such as those induced in the animals used in this study, could remain in the remodelling phase for a month or longer. From the description of the wound healing sequence given above, it is clear that the phases of wound healing also overlap extensively.

In Figure 23 below, the wounds in the pink boxes are those wounds in the inflammatory phase. The wounds in the green boxes are in the proliferatory phase and the blue boxes are those wounds predominantly in the remodelling phase.

The wound sections were cut from approximately the same depth of the dermal layer and were all from the micronised Absorbatox™ treatment group. In each image, the signal intensities were normalised to show the most intense to the least intense signals after subtracting the matrix signal background from within and around the wound. Many molecules detected during MALDI MSI had a selective distribution matching to the geometry of the healing wound.

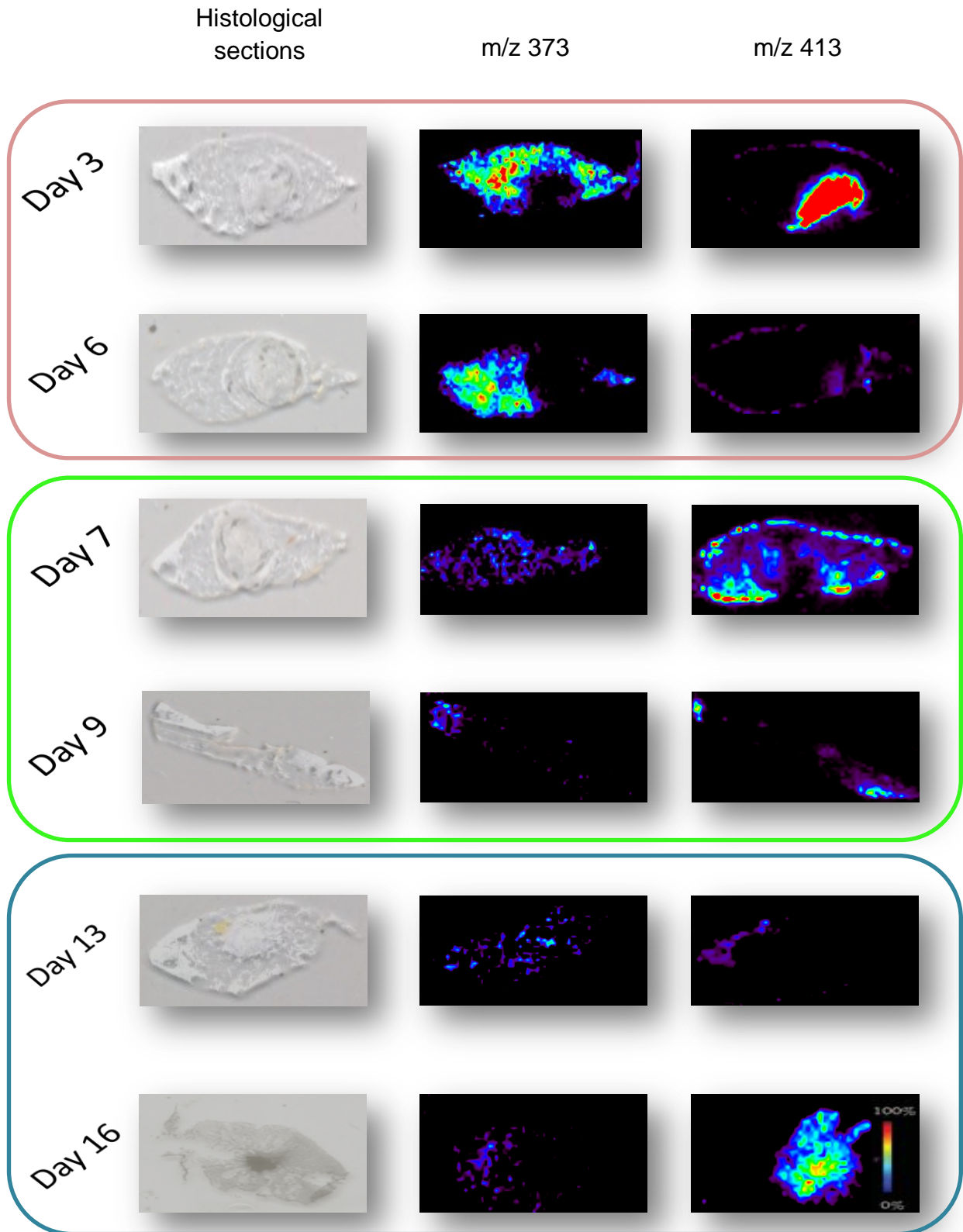


Figure 23: Histology-directed MALDI-MS images of full-thickness wounds showing the progression of wound healing following the intensity of selected peptides with m/z 373 and m/z 413.

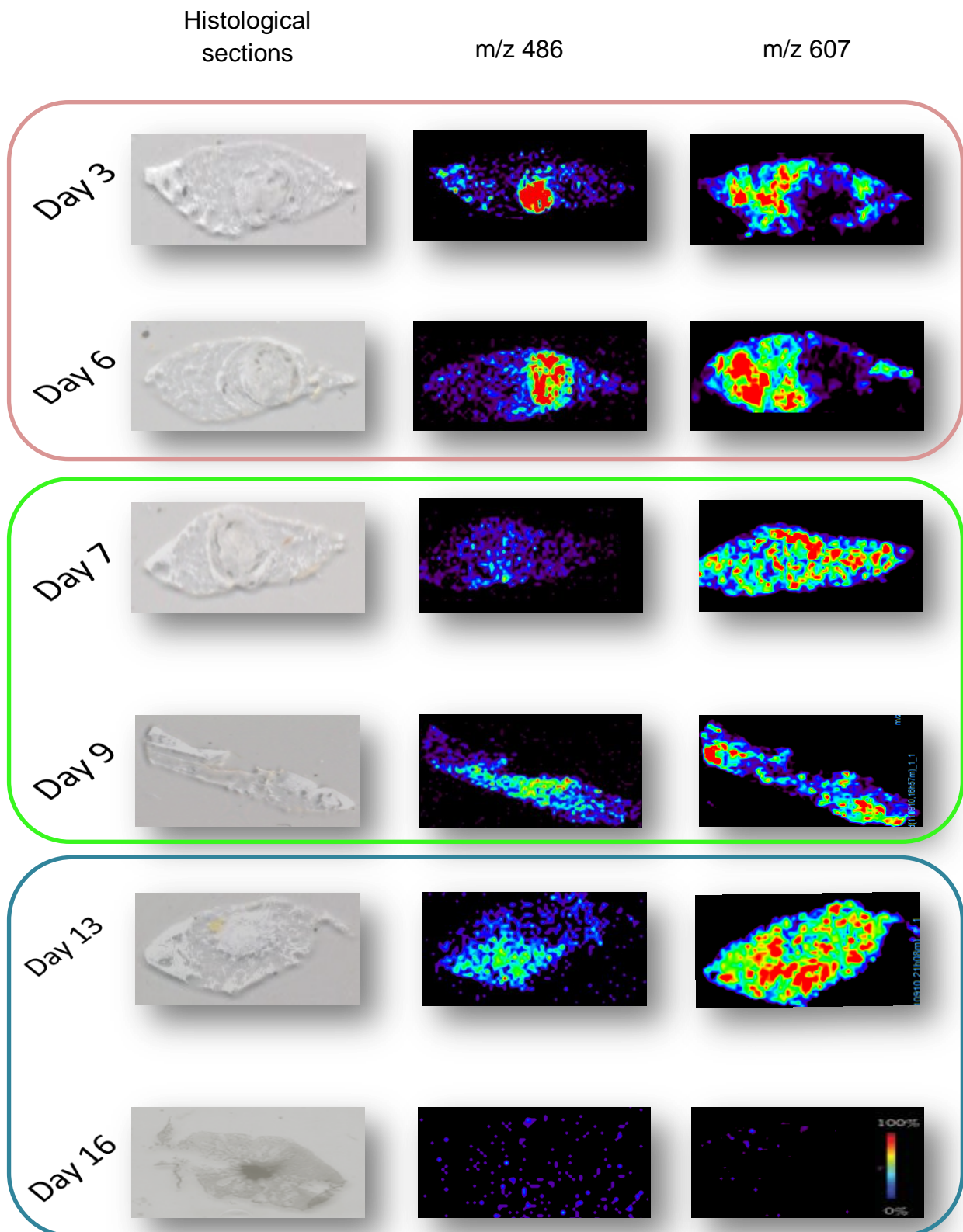


Figure 24: Histology-directed MALDI-MS images of full-thickness wounds showing the progression of wound healing following the intensity of selected peptides with m/z 486 and m/z 607.

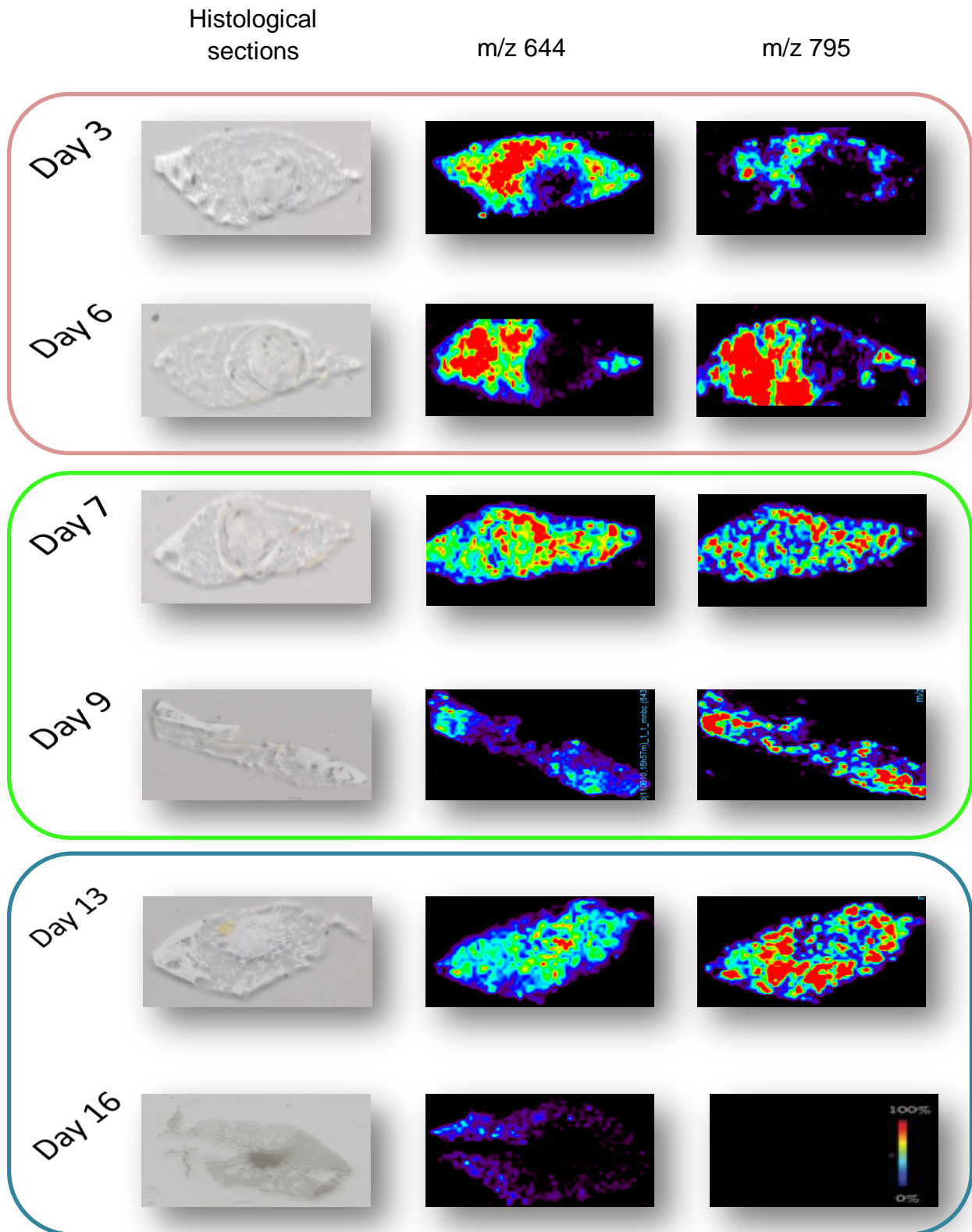


Figure 25: Histology-directed MALDI-MS images of full-thickness wounds showing the progression of wound healing following the intensity of selected peptides with m/z 644 and m/z 795.

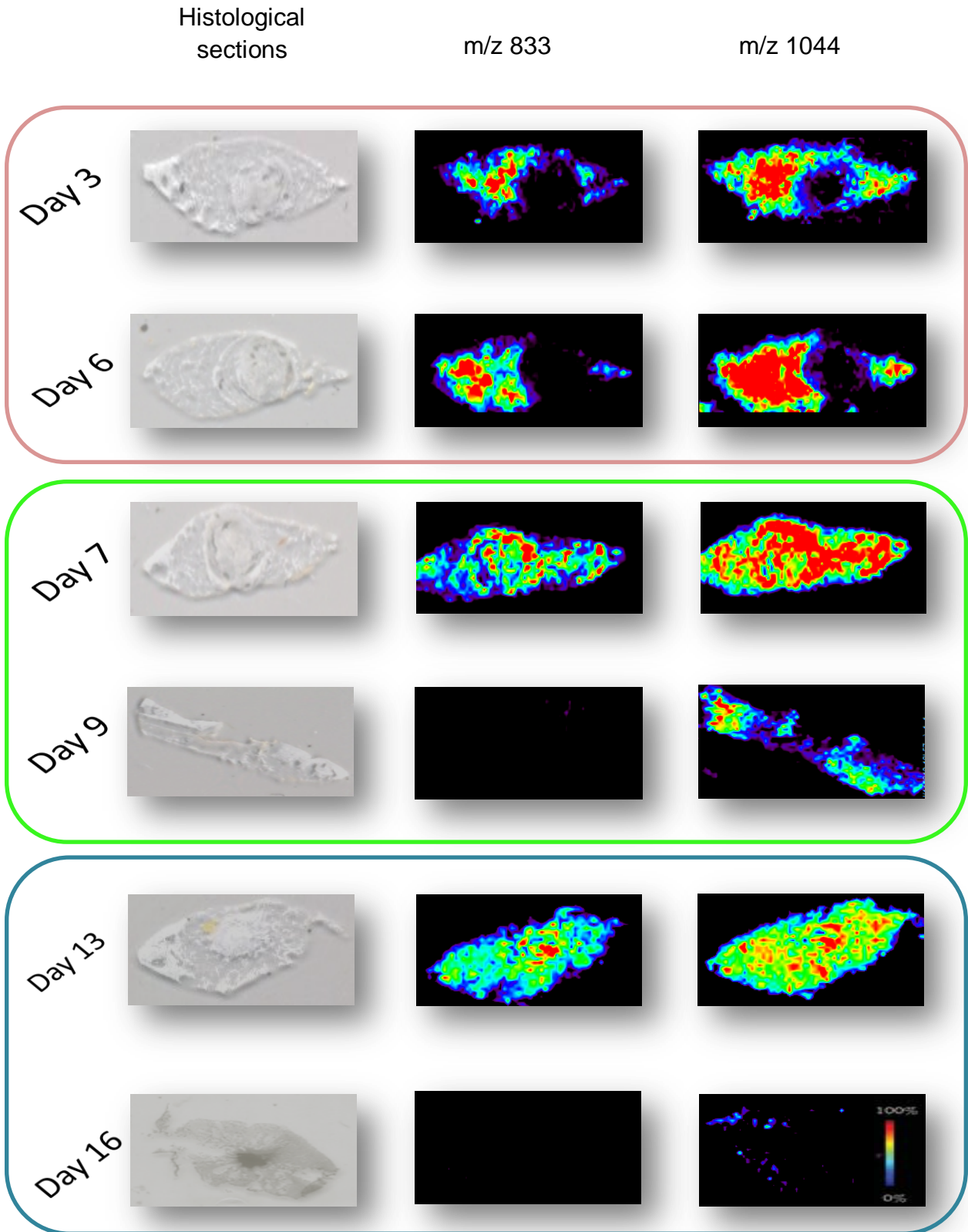


Figure 26: Histology-directed MALDI-MS images of full-thickness wounds showing the progression of wound healing following the intensity of selected peptides with m/z 833 and m/z 1044.

The method used for analysing the wound tissue involved trypsin digestion resulting in peptides, the spectra of which were run through protein databases to identify to which proteins each peptide belonged. Since few peptides were identified with this technique, no certain protein identifications could be made at this point therefore the healing phases discussed in this chapter will be in relation to what is known from literature about protein presence and function.

Peptide of m/z 373

The mass of this peptide would imply a peptide of only 3 amino acids if the terminal amino acid is either lysine or arginine which can be assumed if it is a tryptic digest product. An alternative would be residues of about 8 amino acids; making the same assumption with respect to the terminal AA if the peptide is a doubly charged peptide. Normally, MALDI ionisation gives singly charged ions only but, it is known that the smaller ions can be doubly charged. A further question could be whether this is an experimental artefact as the interference of low mass ions by the matrix is a problem when using MALDI ionisation. On Day 3, the wound is in the phase of inflammation. At this time, a great deal of cellular and extracellular activity is expected within and just around the wound. The signs of inflammation (redness, very warm skin, and pain) were seen in the same area and this peptide seems to follow this same pattern. Regions of high and moderate intensity of this peptide were observed almost exclusively in the healthy surrounding tissue on Day 3 showing a steady decline but still clearly visible on Day 6.

On Day 7, the wound would be in the proliferatory phase. From Day 7 all the way through to Day 16, very low intensity of this peptide was observed in the tissue. Day 7 seems to show an even distribution of low-intensity peptide throughout the tissue. The peptide wanes on Day 9 when the wound is in the transition phase between proliferation and remodelling. The same intensity of the signal is observed during the remodelling phase (Days 13 and 16) however the distribution of the peptide is not as concentrated as during the inflammatory phase. Thus, it is very possible that this peptide is involved mainly in the early stages of inflammation.

The inflammatory phase is largely characterised by vasodilation which also gives the wound area the red appearance and warm-to-the-touch feeling. Protein-rich exudate enters the wound inducing vasodilation under the influence of histamine and serotonin (Broughton *et al.*, 2006; Boateng *et al.*, 2008). The dilated blood vessels facilitate the infiltration of pro-inflammatory cytokines such as interleukin-1 (IL-1), tumour necrosis factor alpha (TNF- α), platelet factor (PF4), and transforming growth factor beta (TGF- β) all of which contribute to attracting neutrophils which have a major role in eliminating invading material and cell debris by phagocytosis.

Peptide of m/z 413

During the first few days of inflammation (Day 3), high-intensity of a peptide with m/z of 413 is observed within the area of the wound. The peptide becomes considerably less intense, then completely disappears from the wound by Day 6 and is concentrated only on the edges of the wound. At this stage the wound is entering the proliferatory phase. The intensity of this peptide increases to about low-to-moderate on Day 7 when the wound is expected to be in the proliferatory phase. More intense peptide signal is seen on the edges of the tissue. The same intensity of peptide is also detected on the right edge of the tissue on Day 9. The peptide then diminishes at the beginning of the remodelling phase (Day 13) only to reappear much stronger on Day 16 with the highest intensity appearing in the centre of the wound. The peptide, now, although more concentrated within the wound, extends beyond the border of the wound but does not exhibit a “tissue-wide” distribution.

The location of this peptide coincides with the activity of and roles played by TNF- α and TGF- β .

TNF- α and TGF- β are present in the inflammatory phase as chemoattractants for neutrophils, but also play an important role in the remodelling phase by releasing anti-inflammatory cytokines (Broughton *et al.*, 2006; Boateng *et al.*, 2008). Both factors upregulate the inhibitory activity of TIMPs which in turn decreases the extracellular matrix degradation by MMPs (Broughton *et al.*, 2006; Muller *et al.*, 2008).

Peptide of m/z 486

The intensity of a peptide with m/z of 486 is high and most concentrated in the wound on Day 3. The same intensity of peptide along with some moderate peptide intensity with a wider distribution is observed in and just around the wound on Day 6 when the wound is approaching the end of the inflammatory phase. On Day 7, a weaker, “tissue-wide” distribution of this peptide is seen. A vertical side-view of the same tissue in the late proliferatory phase, Day 9, shows increased peptide in the healthy tissue “cupping” the wound as it nears the end of the proliferatory phase. At the initiation of the remodelling phase, a “tissue-wide” distribution of a moderate concentration of peptide is seen. As the remodelling phase advances (Day 16), the peptide concentration decreases further and takes on a relatively random “tissue-wide” distribution.

The timing and the location of this peptide in the inflammatory and proliferatory phases can be related to the function or presence of many other elements involved in this transition phase of the wound healing process including: macrophages, TGF- β , TNF- α , and IL-1 in both phases.

Both interleukin-1 (IL-1) and tumour necrosis factor alpha (TNF- α) are initially released by the platelets and later by neutrophils and monocytes/macrophages. Both these cytokines are chemo-attractants for neutrophils and stimulate the adherence of the neutrophils to the endothelial cells. The neutrophils play a phagocytic role in the wound, engulfing cell debris, bacteria and other contaminants that may have entered the wound when injury was sustained (Diegelmann and Evans, 2004; Broughton *et al.* 2006; Boateng *et al.*, 2008; Sibbald and Woo, 2008). Macrophages are observed towards the end of the inflammatory phase and are necessary for the wound to progress into the proliferation phase. The macrophages release a form of platelet-derived growth factor (PDGF), vascular endothelial growth factor (VEGF), and transforming growth factor beta (TGF- β) to facilitate angiogenesis which occurs during the proliferation phase (Diegelmann and Evans, 2004; Broughton *et al.*, 2006; Sibbald and Woo, 2008; Kyriakides *et al.*, 2009). The macrophages - through phagocytosis - are also involved in clearing the combination

of excessive or damaged extracellular matrix and debris that could alter the proteome in and around these cells (Broughton *et al.*, 2006).

Peptide of m/z 607

This peptide was found to be present in high intensity throughout the wound healing timeline except for the last day measured; the peptide was completely absent in the late remodelling phase. During the earlier phases of wound healing, the peptide was present mainly in the healthy tissue. On Days 7 and 13, when the tissue is transitioning from the inflammatory to the proliferatory and from the proliferatory to the remodelling phase, respectively, the peptide maintained its intensity but was more widely distributed throughout the tissue.

While the peptide is present in the tissue up until the early phase of remodelling, the areas at which it concentrates differ from phase to phase which can be related to the presence and role of the components involved at the different phases.

During the inflammatory phase – Days 3 and 6 – the peptide is concentrated in the healthy tissue. This could be a result of the vasodilation in the areas immediately surrounding the wound which facilitates the infiltration of numerous growth factors due to the increased vascular permeability. Another possibility is the movement of neutrophils to other sites in the tissue through the extracellular matrix (Diegelmann and Evans, 2004; Broughton *et al.*, 2006).

During the proliferation phase, the matrix is being laid down on macrophage initiation through PDGF and TNF- α expression. Macrophages also initiate epithelialisation by inducing fibroblasts and keratinocytes proliferation with IL-1 and KGF-2, respectively. The fibroblasts cause keratinocytes proliferation and migration but these fibroblasts also migrate into the wound and initiate the deposition of extracellular matrix. The keratinocytes at this stage express VEGF to direct angiogenesis towards the edge of the wound (Singer and Clark, 1999) while TGF- β stimulates the proliferation of

fibroblasts of the tissue around the wounded area (Diegelmann and Evans, 2004; Blakytyn and Jude, 2006; Broughton *et al.*, 2006). It is thus possible that the intensity of the peptide in this area can be related to the presence and functions of the discussed growth factors, cytokines, and cells.

Peptide of m/z 644

This peptide exhibited high-intensity in select areas of the healthy tissue during both the inflammatory (Day 3 and 6) and early proliferatory phases (Day 7). In both cases, the peptide was more strongly present in the healthy tissue around the actual wound, although a wider distribution of the peptide was observed throughout the tissue on Day 7. A vertical side-view of the tissue on Day 9, showed low peptide abundance throughout the tissue with peptide only visible in healthy tissue away from the edges of the wound. On Day 13, a really small spot of high peptide intensity was present within the wound. This high peptide concentration was, however, absent during the remodelling phase (Day 16). A low intensity of peptide was observed in the healthy tissue and no peptide was observed in the wound area.

The behaviour of this peptide can be related to the presence and activity of the growth factors, VEGF and PDGF; cytokine IL-1; and macrophage cells which appear and are active in the inflammatory and proliferatory phases. IL-1 is released by platelets and stimulates neutrophil adherence during inflammation. The IL-1 also attracts macrophages which release various chemoattractants which, in turn, recruit additional macrophages. The macrophages initiate provisional matrix through the expression of PDGF in the later stages of inflammation as the wound transitions into proliferation. The VEGF is expressed by the keratinocytes which are stimulated by the macrophages during angiogenesis, towards the end of the proliferatory phase (Broughton *et al.*, 2006).

Peptide of m/z 795

A peptide with m/z of 795 was detected with a generally weak intensity during the early phase of inflammation (Day 3) with two small areas of the healthy tissue exhibiting the highest intensity. The peptide increases greatly in intensity and concentrated in the healthy tissue surrounding the wound during the inflammatory/proliferatory transitional phase of the healing process (Day 6). The distribution of the peptide at high intensity was more evenly spread throughout both healthy as well as wound tissue during the proliferatory phase (Days 7 and 9) and then again concentrated more around the wound during the early remodelling phase (Day 13) although there appeared to less peptide present than on Day 6.

Considering that this peptide was observed from the point of transition between the inflammation and proliferation phases, right up until early in the remodelling phase (Days 6 to 13), as well as the location of peptide activity, the distribution patterns of the ions could be related to the presence, function, and effects of TGF- β . TGF- β is observed throughout these phases and thus the peptide activity observed here could be as a result of TGF- β influence (Broughton *et al.*, 2006).

During the inflammatory phase, TGF- β acts as a chemoattractant for monocytes which infiltrate the tissue and become activated macrophages which will play a dual role as phagocytes but also as secretors of growth factors PDGF and VEGF (Singer and Clark, 1999). TGF- β , in conjunction with PDGF and the extracellular matrix, stimulates the fibroblasts of the tissue in the region of the wound to proliferate. The provisional extracellular matrix is gradually replaced with a collagenous matrix, presumably as a result of TGF- β stimulation (Singer and Clark, 1999; Broughton *et al.*, 2006). This growth factor is also responsible for the up-regulation of TIMP and the synthesis of collagen I. TIMPs inhibit MMPs thus increasing tissue adhesion proteins. Finally, to ensure increased wound contractility, TGF- β influences the differentiation of fibroblasts into myofibroblasts (Singer and Clark, 1999).

Peptide of m/z 833

The peptide with m/z of 833 showed peculiar behaviour. While the peptide was present in different amounts but relatively equal intensities (moderate to high) in the healthy regions of the tissue on most of the days in the of the wound healing process, it was completely absent on Days 9 and 16. The peptide was present in healthy tissue adjacent to the wound area during the inflammatory phase (Day 3) but seemed to migrate closer to the wound's edge on Day 6. The amount of peptide present seemed to decrease on Day 7 and was present across the healthy and wounded tissue at this time. The peptide disappeared completely on Day 9 but reappeared with a general distribution with the highest intensity in the centre of the wound on Day 13. Moderate peptide intensity was present throughout the healthy tissue surrounding the wound. The peptide was again not detected on Day 16.

The fact that the peptide appeared to no longer be present on certain days could be due to experimental phenomenon or due to some kind of protein modification taking place within the section representing the peptide of m/z 833. In both cases, it would be expected that at least some background signal would be detectable yet the background remained completely blank. As the samples did show other peptides from the same experimental runs it is unlikely to be due to a matrix related or digestion related problem. The same is true for experimental Day 16 for the peptide of m/z 795.

Peptide of m/z 1044

The peptide with m/z of 1044 was present in high intensity in the healthy tissue around the wound during early inflammation. The peptide intensity increased in the healthy tissue by Day 6. The distribution pattern changed on Day 7 when the peptide, remaining almost as intense as on the previous days, spread throughout all the tissue including the wound. Towards the end of the proliferatory phase (Day 9), the peptide had begun decreasing to a low-to-moderate intensity and was still distributed across the entire tissue section on Day 13 with some small, random areas

of higher intensity with most areas of moderate intensity by early in the remodelling phase. Almost no peptide was observed in the tissue on Day 16, although a low background could be seen remote from the wound in the healthy tissue.

Peptides with m/z 833 and 1044 show overlapping occurrence throughout the wound healing process and will be discussed together. However, since the processes of inflammation, proliferation, and remodelling have been discussed in the previous discussions of peptide behaviour, only the differences between the two images will be considered in terms of the functions and presence of elements that can be related to wound healing.

On Day 9 – when the wound is going through proliferation – m/z peptide 833 is absent but some m/z 1044 peptide is observed throughout the tissue with some areas of intense peptide observed at the edge of the tissue. A possible reason for this is that this phase of healing sees the proliferation of endothelial cells and fibroblasts as well as the migration of fibroblasts from the healthy tissue into the wound to set in motion the deposition of the extracellular matrix (Broughton *et al.*, 2006). In addition to this, epithelial cells on the edge of the wound begin to proliferate to create a protective barrier against fluid loss and potential infection (Singer and Clark, 1999; Broughton *et al.*, 2006). A more intense (m/z 1044) peptide is observed throughout the tissue on Day 13 – the early days of the remodelling phase – with regions of intense peptide being observed in disperse regions of the healthy tissue and wound area. A similar intensity of the peptide with m/z 833 is noticeable on this day too. In both cases, the species involved here could have a role to play in the replacement of collagen III with the mature collagen I to ensure a wound that is resistant to reopening under force, or even the activity of TGF- β which up-regulates TIMP so as to decrease MMP activity (Diegelmann and Evans, 2004; Broughton *et al.*, 2006; Sibbald and Woo, 2008). Equally likely, in the case of m/z 833, the concentration of intense peptide observed at the wound area could be protein components of the scab that had formed by this day of the study in the Absorbatox™ groups since this phase results in the formation of scar tissue (Hunt *et al.*, 2000; Boateng *et al.*, 2008).

In later stages of remodelling, Day 16, TIMP activity is expected to be enhanced under the direction of TGF- β . A weak peptide of m/z 1044 is noted and is a possible indication of this (Broughton *et al.*, 2006).

CONCLUSION

Wound healing starts immediately after an injury is sustained and proceeds with complex but well-organized interactions among various types of growth factors, cytokines, tissues and cells in sequential, overlapping phases that aim to restore physiological and anatomical integrity (Lin *et al.*, 2003; Diegelmann and Evans, 2004; Blaytny and Jude, 2006; Boateng *et al.*, 2008; Gibson and Schultz, 2009).

The object of MSI is to obtain information from tissue sections concerning the localisation and identification of the proteins (and lipids) (Kaletaş *et al.*, 2009). MALDI MS tissue imaging can generate data rich spectra, however, the ability to successfully identify and pinpoint wound elements using this label-free imaging technique is largely dependent on the methods and reagents used during sample preparation (Kaletaş *et al.*, 2009; Van Remoortee *et al.*, 2010). For example, if the method used to apply the matrix is poor, resulting in excessive matrix being applied to the tissue, the chance of tissue analyte migration increases significantly (Aebersold and Goodlett, 2001; Caldwell *et al.*, 2008). Equally important, are the wash steps put in place, especially in the case of FFPE tissue, to ensure that the quality of the peptide signal obtained is not disturbed by that given by the wax surrounding the tissue (Kaletaş *et al.*, 2009).

Aside from the need to incorporate effective wash steps, the use of quality trypsin to give representative tryptic peptides is necessary to give the added advantage of increasing sensitivity of detection considering that a large number of the growth factors are involved in the wound healing process but are present in very low concentrations. Also many of the highly abundant proteins have extremely high

molecular mass (fibronectin has a mass of approximately 400 kDa) and some, like collagen, do not cleave effectively with trypsin due to the sparse distribution of both lysine and arginine residues. In general, low abundance proteins are difficult to analyse using MALDI-TOF when there are proteins with abundance of greater than 100 times. The digestion of high molecular weight proteins directly on tissues, and the subsequent image analysis of the resultant unique peptides, enables visualisation of their distribution throughout the tissue section (Kaletaş *et al.*, 2009) but does require unique peptide masses to be able to confidently identify the protein from which the peptide was released. False positive results can easily be inferred by incomplete data.

Some complications in using this technique were highlighted when some time points did not reveal peptides that were seen at all other time points and the reasons cannot be easily pinpointed.

The identification of proteins directly from tissue using MALDI-MSI following *in situ* enzymatic digestion, is a fairly new proteomic approach that has the potential to bring about localisation and identification of potential wound protein targets (Djidja *et al.*, 2009) such as over-active MMPs, TIMPs, or even inappropriately active or inactive TGF- β . Examination of the healing wound at multiple recovery intervals after *in situ* enzyme digestion allowed for the observation of proteomic differences and similarities. These differences in protein distributions also showed in some cases, the difference between the wound area as well as the healthy tissue (Caldwell *et al.*, 2008; Djidja *et al.*, 2010). The use of MALDI-MSI for this study not only allowed for the monitoring of the wound healing processes, but further cemented what is currently known about the process: the phases of wound healing most certainly do overlap (Diegelmann and Evans, 2004; Blaytny and Jude, 2006; Boateng *et al.*, 2008; Gibson and Schultz, 2009).

On the whole, direct tissue analysis using MALDI-MSI is a powerful and valuable tool for assessing protein (and non-protein) molecule location. The correlation of this information to the anatomical structures in tissue as seen in histology-directed

analysis, offers a great promise for better understanding of the biological processes of wound healing (Cornett *et al.*, 2007; Walch *et al.*, 2008). And while more sample preparation is required for the successful identification of proteins in FFPE tissue, with part of this preparation eliminating important lipid molecules that then cannot be imaged, this study opened the door to gain insight into the proteins at work within a healing wound.

CHAPTER 5: PROTEIN IDENTIFICATION

INTRODUCTION

Proteomics is the study of the expressed protein complement of the genome of an organism including the quantitation, identification, and characterisation of proteins isolated from biological systems (O'Malley, 2002; Mallick and Kuster, 2010). Two strategies exist for protein identification: “top-down” proteomics, in which intact proteins are analysed using mass spectrometry, and “bottom-up” proteomics in which the peptides in proteolytic digests of proteins are analysed (Resing and Ahn, 2005). The analysis of intact proteins requires the acquisition of tandem mass spectra which are matched against predicted fragments of all peptides present in a sequence database and which correspond to the measured molecular masses (Baldwin, 2004; Resing and Ahn, 2005). The measured masses used in this method are obtained from internally-fragmented peptides which result in “informative” C- and N-terminal peptide fragments (Nielsen *et al.*, 2005; Resing and Ahn, 2005). “Bottom-up” (shotgun) proteomics was first publicized in a study that identified over 1400 proteins including several low abundance proteins from *Saccharomyces cerevisiae* (Baldwin, 2004; Habermann *et al.*, 2004; Olsen *et al.*, 2004; Resing and Ahn, 2005). “Bottom-up” proteomics, which includes peptide mass fingerprinting, is the simplest method of protein identification using MALDI-MS analysis. The matrix-assisted laser desorption/ionisation time-of-flight mass spectrometry (MALDI-TOF-MS) based peptide fingerprinting method entails proteolytic digestion of a sample with the acquisition of one MS spectrum containing all the masses of the detected peptides resulting from singly charged ions ($[M+H]^+$). The combination of all these masses is used as a fingerprint to search a database of theoretical protein cleavages (O'Malley, 2002; Baldwin, 2004). Protein mass fingerprinting by MALDI-MS often fails to identify low molecular mass proteins and protein fragments due to the limited number of detectable unique peptides in these smaller proteins (Thiede *et al.*, 2005).

With the progression of proteomics and the improvement of the communication network in biological research, the importance of databases has proven itself

remarkable. The current quest of many research groups is to sequence all genes and to make the information available on publically accessible databases (Rastogi *et al.*, 2006). These databases are constructed by bioinformatics groups around the world and are accessible at all times to add information or to perform searches.

Bioinformatics is defined as “the mathematical, statistical and computing methods that aim to solve biological problems using DNA and amino acid sequences and related information” (Rastogi *et al.*, 2006).

There are a number of databases of different types that currently exist. The database types are the primary databases, the composite databases, and the structural databases (Rastogi *et al.*, 2006). Primary databases contain over 300 000 protein sequences and serve as a repository for the raw data. Composite databases compile and filter sequence data from various primary databases to create combined and non-redundant sets that are more comprehensive than the individual databases. They also include data on protein sequences from translated coding regions in DNA sequence databases. Structural databases pertain to 2D and 3D macromolecular structures (Rastogi *et al.*, 2006).

MASCOT and BLAST are databases that can be used for peptide mass fragment searches by correlating mass spectra of peptides in sequence databases to return a positive identification and to identify homology between proteins, respectively.

The acronym MASCOT stands for modular approach to software construction operation and test (Simpson and Jackson, 1979; Simpson, 1986). MASCOT is a probability-based search engine for peptide identification and peptide sequence assignment (Olsen *et al.*, 2004; Weatherly *et al.*, 2005). Every submitted tandem mass spectrum is assigned a list of matching peptide sequences found in the database accompanied by a score that indicates the statistical significance of the match of the peptide to the submitted spectra. The score is calculated as $10 \times$ the negative logarithm of the probability that the peptide identification is a chance event. The algorithm then determines a threshold ion score under which there is less than

95% confidence in each individual peptide match (Nielsen *et al.*, 2005; Weatherly *et al.*, 2005; Xu and Ma, 2006).

BLAST – basic local alignment search tool – is one of the most commonly used sequence analysis tools available in the public domain to identify unknown proteins by sequence similarity to homologous proteins that are available in the database (Habermann *et al.*, 2004; McGinnis and Madden, 2004; Johnson *et al.*, 2005). The database was developed by the National Centre for Biotechnology Information (NCBI) in the USA. BLAST is a sequence similarity search program designed for speed with minimal sacrifice of sensitivity to distant sequence relationships. BLAST is capable of comparing nucleotide or protein queries to a database of nucleotide or protein sequences (McGinnis and Madden, 2004; Rastogi *et al.*, 2006). This search engine is based on the Karlin-Altschul statistical theory which states that all scoring schemes for which a positive score is possible, and the expected score is negative, have implicit target frequencies (Olsen *et al.*, 2004). In addition to this, BLAST can perform alignments and provide information on the statistical significance of the matches it reports. This significance value is termed the “e-value”. The e-value, or expect value, is a parameter that describes the number of hits that could be expected by chance when searching a database of a certain size (McGinnis and Madden, 2004; Johnson *et al.*, 2008). The higher the e-value, the lower the number of significant hits; in the case of a comparison, a high e-value may give a large number of possible proteins very few of which may be relevant to wound healing.

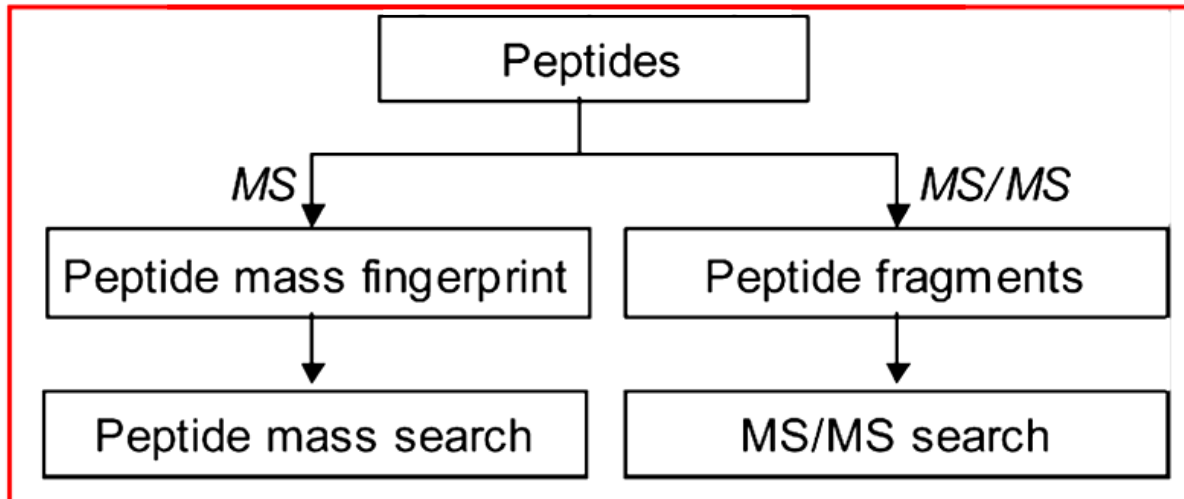


Figure 27: The figure above shows the “top-down” (right) and “bottom-up” (left) methods that can be used to identify and characterise proteins (Thiede *et al.*, 2005).

MATERIALS AND METHODS

Protein identification was performed using MASCOT (Matrix Science Inc. website: <http://www.matrixscience.com>) by submitting the peptide fingerprint data collected from MALDI imaging of trypsinised histological wound slices in a query search. Within the MASCOT search engine, the criteria were set up to include two possible missed cleavages and the modifications allowed were: histidine/tryptophan oxidation, methionine oxidation and methionine deoxidation, sodiation (C-terminal, aspartic acid, and glutamic acid), as well as deamidation at the N-terminus and at glutamine. The following settings were also selected: database – NCBI non-redundant; taxonomy – mammals; peptide mass tolerance was set to 1.2 Da. Only trypsin digests were considered. Setting the number of missed cleavages gives an indication of how well the trypsin digestion is expected to have been and tests more possibilities. In other words, setting the missed cleavages to zero simulates a limit digest suggesting a perfect digestion in which all possible cleavages have taken place leaving no uncleaved fragments. The variable modifications refer to those modifications that may or may not be present in the analysed sample including

artefacts of sample handling, such as oxidation, as well as other modifications such as the addition of cyanate from the alkaline decomposition of urea. The presence or absence of these modifications is usually not known to the researcher at the time of the database submission. The MASCOT default threshold values were used for the search criteria. In all the analyses, the values were below the threshold and therefore positive identification of the proteins within the tissue was not possible using this search engine. Since the MASCOT score was statistically unreliable, all acquired peptide sequences were further interpreted by the BLAST database to see if a likely homology based match could be found.

The acquired peptide sequences used in the MASCOT search were pasted into BLAST. The e-value was adjusted to 30 however most of the proteins identified fell below an e-value of 10. The query was filtered for the taxonomy i.e: *Sus scrofa*. All other BLAST parameters were left at their default settings. The spectra were then matched to peptide sequences which either identified the protein or confirmed a hit already identified using the MASCOT search.

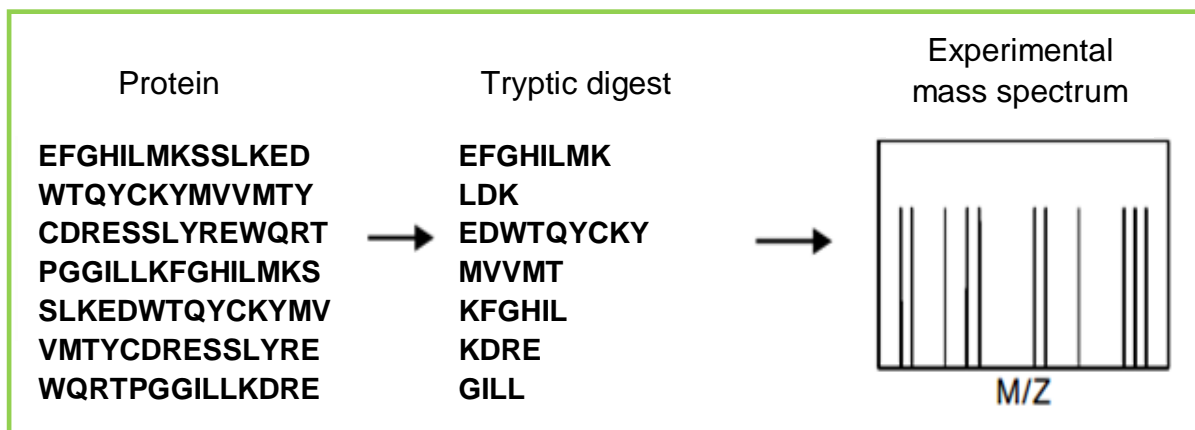


Figure 28: Graphical description of the workflow for collecting “bottom up” proteomic data. On-tissue trypsin digestion resulted in tryptic digests which gave spectra that were fed into databases to give positive identification of the proteins detected in the wound tissue (adapted from Fenyö, 2000).

RESULTS AND DISCUSSION

The idea of the protein identification part of the study was to identify target proteins that were to be monitored for their changing concentrations, the change in the active enzymes, and that of the extracellular matrix proteins with an optimistic hope of being able to find unique peptides that were specifically associated with cytokines, growth factors and select proteins. During wound healing it would be expected that extracellular matrix proteins would be the most abundant proteins along with collagen, elastin, laminin, keratin, fibronectin as well as intracellular proteins, especially actin to be found. Other proteins that were expected to have been found in fairly large concentrations were the matrix metalloproteinases which are reported to be active in wounds during the initial inflammatory phase and during the remodelling phase. Intracellular proteins from the cells that are involved in the different phases of wound healing would also be expected to be found in the different areas of the wound tissue due to the high concentration of the cells involved. This would include the cells like platelets, neutrophils, macrophages, fibroblasts, keratinocytes and specific cells found in the layers of dermis such as fat cells. Due to the fact that the tissue analysed was subjected to cross linking by formalin exposure, it was expected that several unusual protein or peptide calls would be made when comparing the data to databases containing only unchanged protein information. Identification of proteins from several different animal species was reported when the species was not limited to *Sus scrofa* in the FFPE tissue after trypsinisation. As this was seen during initial database submissions, all of the peptides identified between Days 3 to 16 of the wound healing process were limited to *Sus scrofa*. Despite this, details of some of the porcine proteins could not be found. This is partially because the Swine Genome Sequencing Consortium involved in sequencing the pig genome, have not yet completed the pig genome sequence analysis (Archibald *et al.*, 2010). For this reason, some information for the transcription factors, etc., found in the pig was related back to their human equivalent proteins.

Figure 29 is an example of the output of a BLAST search of a particular set of data submitted for protein identification:

gi|229558899|gb|ACQ76903.1|: homeodomain transcription factor Nanog-like protein [Sus scrofa]

gi|154622684|gb|ABS83566.1|: NANOG [Sus scrofa]

gi|194018700|ref|NP_001123443.1|;gi|90820134|gb|ABD98822.1|: homeodomain transcription factor Nanog [Sus scrofa]

gi|350586518|ref|XP_003356650.2|: PREDICTED: hypothetical protein LOC100623549 [Sus scrofa]

gi|311253626|ref|XP_003125614.1|: PREDICTED: RNA-binding protein 12B [Sus scrofa]

gi|350589828|ref|XP_003131000.2|: PREDICTED: coiled-coil domain-containing protein 70-like isoform 1 [Sus scrofa]

gi|311268009|ref|XP_003131832.1|: PREDICTED: nuclear speckle splicing regulatory protein 1-like [Sus scrofa]

Figure 29: An output table of possible proteins identified from the data submitted to the BLAST database.

Several high intensity peptides with their MS spectra were submitted to MASCOT and BLAST databases for possible identification. These peptides were selected from the peptides with the highest signal intensities in an attempt to improve the quality of the submitted MS data and to limit the effects of the background noise. This technique of using the most abundant signal intensities introduces a subjective bias for the most abundant peptide which is not necessarily the most abundant protein in the area of the sample being investigated. Proteins identified were not

subjected to false positive assessment, but rather assessed from the point of their potential function and whether this could fit the observation of these proteins in the wound biopsies relative to the healing time. The results of this are dealt with in the chronological order of healing and a brief description of the functional characteristics of each identified protein is given.

Proteins identified on tissue from wound repair DAY THREE

Homeodomain transcription factor Nanog-like protein

A homeodomain is a protein structural domain that encodes for a homeobox consisting of approximately 60 amino acid residues that make up a structure in which three alpha-helices are connected. This structure interacts with specific DNA sequences in genes regulated by the homeotic gene (Gehring, 1992; Billeter *et al.*, 1993).

The transcription factors (TFs) are proteins that bind to the promoter region of a gene to regulate its rate of transcription (Barnes and Adcock, 1998).

The homeodomain transcription factor for Nanog-like protein is a protein that is involved in the regulation of gene expression of the protein NANOG.

NANOG

NANOG is a multidomain protein with a conserved NK-2 type homeodomain. It is thought to have a role in controlling pluripotency and the differentiation of stem cells. These stem cells go through extensive proliferation but continue to remain prepared for multilineage differentiation (Chambers *et al.*, 2003; Pan and Pei, 2005; Camp *et al.*, 2009). Pluripotency refers to the potential of a stem cell to differentiate into any of the three germ layers: endoderm, mesoderm, or the ectoderm (such as epidermal

cells) (Arno *et al.*, 2011). NANOG has been proposed to play a key role in maintaining stem cell pluripotency presumably by regulating the expression of genes critical to stem cell renewal and differentiation (Chambers *et al.*, 2003; Pan and Pei, 2005; Camp *et al.*, 2009; Zhu *et al.*, 2011). This presumption, however, is based on *in vitro* studies (Camp *et al.*, 2009) and thus remains controversial.

A study conducted by Camp *et al.* (2009) identified the homologous genes of mammalian NANOG in various teleost fish species. They concluded that the primary role of NANOG was in the regulation of embryonic stem cell proliferation (Chambers *et al.*, 2003; Mitsui *et al.*, 2003; Camp *et al.*, 2009).

The presence of NANOG in the wound at such an early stage of repair shows that despite all the processes of inflammation occurring at the time, the tissue is preparing to enter the proliferatory phase by employing this protein to regulate the differentiation and proliferation of stem cells (and possibly other cell types) that will be needed further down the line of the wound healing process. NANOG is also responsible for significantly up-regulating genes involved in the cell cycle, DNA replication, as well as DNA damage repair (Han *et al.*, 2012).

Hypothetical protein LOC100623549

These are proteins that have been predicted from DNA sequence data but for which no experimental evidence of their *in vivo* expression exists. A hypothetical protein is a consequence of a large open reading frame not having an analogue in the protein database and thus cannot be related to proteins of known function or structure (Zambarenski *et al.*, 1998; Eisenstein *et al.*, 2000).

The function of such a protein can be determined by comparing the amino acid sequence of the open reading frame against all functionally assigned sequences in a protein sequence database (Zambarenski *et al.*, 1998). If an extensive similarity exists between the open reading frame and a functionally assigned sequence, it is assumed that the coded proteins share the same function. This, unfortunately, is not

true for as many as 62% of compared sequences (Zambarenski *et al.*, 1998). A more sensitive and reliable method of defining the function of the hypothetical protein is to employ structural genomics although its applicability has been brought into question (Zambarenski *et al.*, 1998; Eisenstein *et al.*, 2000).

RNA-binding protein 12B

These proteins play key roles in the post-transcriptional control of RNAs. The RNA, along with the RNA-binding proteins (RBPs), regulates the pattern of gene expression during development. Many of the RNA-binding proteins are essential factors in the maintenance of the viability of germlines (Lee and Schedl, 2006; Zhu *et al.*, 2011) and early embryonic cells during their development. They also have essential functions in the development of tissues such as neuron, muscle, hypodermis, and excretory cells. An additional role is played in the timing of development. The RBPs involved in somatic development have also been shown to localise to nuclear speckles in the hypodermis and nervous system (Lee and Schedl, 2006).

Coiled-coil domain-containing protein 70-like isoform 1

The coiled-coil domains are the motifs most commonly used by proteins for oligomerisation. They consist of amphipathic helices that are usually made up of a 4-3 pattern of hydrophobic and hydrophilic residues repeated in heptads (Leskov *et al.*, 2003).

Nuclear speckle splicing regulatory protein 1-like

This protein regulates the splicing of nuclear speckles. The nuclear speckles are small, sub-nuclear, membraneless organelles, also called the splicing factor (SF) compartments or interchromatin granule clusters. They are located in the interchromatin regions of mammalian nucleoplasm and play a role in mitosis

(Lamond and Spector, 2003; Spector and Lamond, 2011). While speckles are present in all cells, their levels are increased during cell division as compared to when the cell is resting (Álvarez *et al.*, 2003). It could thus be possible that speckles in this stage are signalling the early progression from inflammation into proliferation.

Proteins identified on tissue from wound repair DAY SIX

Two of the proteins identified within the wound tissue six days after initiation were also present on Day 3 of the repair sequence. Considering the functions of the RNA-binding proteins and the coiled-coil domain-containing protein, it is understandable why they would still be present after six days.

Protein SCAF11

This is a scaffold protein. These proteins are molecules that bind to at least two other signalling proteins. They have an additional ability to regulate signal transduction and sometimes, to pinpoint signalling molecules associated with the plasma membrane, nucleus, Golgi, endosomes and mitochondria to specific areas of a cell (Shaw and Filbert *et al.*, 2009). A number of golgin subfamily proteins were also identified in the present study and may be closely associated with SCAF11 to regulate the translocation of fibroblast-synthesised proteoglycans to the Golgi apparatus for use in the proliferatory and remodelling phases (Blakytyn and Jude, 2006; Broughton *et al.*, 2006). The scaffold proteins could also serve to enhance kinase specificity. Modelling studies conducted by Shaw and Filbert. (2009) confirmed that a scaffold protein can bind mitogen-activated protein kinase (MAPK). The activation of MAPKs resulted from membrane tears that occur during fibroblast-collagen matrix remodelling (Broughton *et al.*, 2006) and, together with other kinases, plays a role in cell migration that is initiated in response to extracellular signals such as growth factors (many of which are present in the inflammatory phase) (Enomoto *et al.*, 2005).

Serine/threonine-protein kinase MRCK alpha-like

At Day six, the wound is expected to be transitioning between the inflammation and proliferation stages (Blakytyn and Jude, 2006). The proliferatory phase is characterised by the migration of cells (such as fibroblasts) through the newly formed extracellular matrix and into the wound where they lay down new extracellular matrix, develop new tissue, and initiate angiogenesis (Blakytyn and Jude, 2006; Broughton *et al.*, 2006; Boateng *et al.*, 2008; Arno *et al.*, 2011).

Cytoplasmic serine/threonine protein kinases appear to be activated by signal transduction from a variety of cell-surface receptors (Sözeri *et al.*, 1992). The serine/threonine kinase, Akt, is a well-known regulator of cell survival, proliferation, and growth as well as angiogenesis and signal transduction (even at various stages of muscle development) (Song *et al.*, 1993; Enomoto *et al.*, 2005). It has also been shown to be vital for cell migration (Enomoto *et al.*, 2005).

The detection of this protein in wound tissue on Day 6, matches the changes in cell function that are expected at this phase of wound healing; in agreement with literature (Enomoto *et al.*, 2005; Blakytyn and Jude, 2006; Broughton *et al.*, 2006; Boateng *et al.*, 2008; Arno *et al.*, 2011).

Myosin-Va

Myosin-Va is an actin-based motor molecule (Libby *et al.*, 2004; Desnos *et al.*, 2007; Wagner *et al.*, 2010) that transports from the endoplasmic reticulum into the dendritic spines of Purkinje neurons (Wagner *et al.*, 2010). Myosin-Va may promote the recruitment of secretory granules - which store hormones and neuropeptides - at the release sites by driving the trafficking of these granules toward the plasma membrane (Libby *et al.*, 2004; Desnos *et al.*, 2007). Neuropeptides stimulate cell proliferation and also prompt growth factor production (Sibbald and Woo, 2008).

Proteins identified on tissue from wound repair DAY SEVEN

Data from Day seven did not show an overlap of protein identities observed on previous days.

Periaxin

Periaxin is required for the maintenance of myelin in the peripheral nervous system. It is expressed exclusively by myelinating Schwann cells. Myelin is a multi-lamellar structure that surrounds axons and increases axonal conduction velocity (Scherer *et al.*, 1995; Gillespie *et al.*, 2000). It is possible that nerve regeneration in the wound tissue was initiated by Day 7.

B-cell linker protein (BLNK)

BLNK is an adaptor protein expressed in B cells and macrophages. This protein represents a central linker protein that links the B cell receptor-associated kinases with a multitude of signalling pathways and may regulate B cell function and development (Fu *et al.*, 1998; Wienands *et al.*, 2008). Research has shown that B cells, which produce antibodies against damaged tissue, play a role in wound healing (Boyce *et al.*, 2000; Nishio *et al.*, 2009). Nishio *et al.* (2009) observed that nude mice that had undergone splenectomy experienced delayed wound healing but that transfer of enriched B cells resulted in accelerated wound healing in these mice. Boyce *et al.* (2000) also observed a link between increased B lymphocytes and healing in human wounds however, the role of the cells in either case was not defined.

Leucine-rich repeats and immunoglobulin-like domains 3 (LRIG)

LRIG behaves like a suppressor of receptor tyrosine kinases, such as epidermal growth factor receptor (EGFR) (Yi, *et al.*, 2009). Epidermal growth factor (EGF) is chemotactic and a potent mitogenic stimulant for epithelial cells, endothelial cells, and fibroblasts (Blakytyn and Jude, 2006, Broughton *et al.*, 2006). LRIG has a direct effect on cell growth and proliferation by inhibiting the continuation of both these processes. At this time (Day 7), the wound is expected to be in the proliferatory phase. The suppression of the effect of EGF could be a way of preventing further migration of the epithelial cells and fibroblasts into the wound.

Angiomotin like 2

Angiomotin is a protein of 675 amino acid residues that is expressed in human endothelium. The function of this protein is to regulate and increase the random migration and directed migration of endothelial cells toward growth factors (Trojanovsky *et al.*, 2001; Bratt *et al.*, 2005; Aase *et al.*, 2007).

It appears that while fibroblast and epithelial proliferation is being slowed or stopped by the presence of LRIG, the process of angiogenesis - the formation of new blood vessels either through sprouting or intussusceptive growth (Bratt *et al.*, 2005) - is just beginning. This is an expected event during the proliferation phase of wound healing (Blakytyn and Jude, 2006; Broughton *et al.*, 2006).

Testis-specific Y-encoded-like protein 2-like (TSPYL-2)

TSPYL-2, also known as differentially expressed nucleolar TGF- β_1 target (DENTT), is expressed in various tissues including normal human lung (Kandalaf *et al.*, 2008). As a member of the super-family, TSPYL, TSPYL-2 plays a role in the regulation of cell proliferation and meiotic differentiation (Martínez *et al.*, 2002).

Conserved oligomeric Golgi (COG) complex subunit 7

The COG complex is thought to operate in a pathway essential for the proper structure and function of the Golgi apparatus. The Golgi apparatus is central to the modification, sorting, and packaging of newly synthesized protein (Presley *et al.*, 1998) including new proteins for cell secretion or use inside the cell (Presley *et al.*, 1998; Ungar *et al.*, 2005). The Golgi apparatus plays a role in proteoglycan synthesis which is present in the extracellular matrix of animals (Cuberts *et al.*, 1994; Campbell, 1996). The extracellular matrix is vital for proper wound healing as it serves as the scaffold for mature collagen deposition (Broughton *et al.*, 2006).

FAS-associated factor 1

FAS-associated factor-1 (FAF1) is a FAS-binding, pro-apoptotic protein that is involved in down-regulating NF- κ B activation and promoting apoptosis. NF- κ B is activated by diverse stimuli, including the pro-inflammatory cytokines: TNF- α and IL-1 (Park *et al.*, 2004; Blakytyn and Jude, 2006). The presence of this regulatory protein at this stage of wound healing could indicate how a normal wound ensures proper healing by arresting the inflammatory process when the invading material or cell debris has been eliminated by down-regulating the NF- κ B resulting from the inflammatory cytokines.

Protein phosphatase 1 (PP1)

Protein phosphatase 1 is a eukaryotic serine/threonine phosphatase responsible for the regulation of a wide variety of cellular functions (Cohen, 2002). PP1 is highly enriched in dendritic spines and plays a role in both the regulation of ionic conductance and long-term synaptic plasticity (Allen *et al.*, 1997). While no dendritic spine proteins had been detected prior to Day 7, it is not to say that those proteins were not present. The BLAST searches were conducted at an e-value of 30 meaning that chance-hits were drastically decreased. While this adjustment most likely gives the most healing-relevant proteins, there is a possibility that other

relevant proteins were not identified. Aside from this, the presence of periaxin could explain how PP1 fits into this stage of wound healing.

TPM 3

TPM 3 is an entire gene. This gene transcribes the tropomyosin alpha-3 chain. A tropomyosin beta chain was also identified on this day. The tropomyosins are a family of actin filament binding proteins. The tropomyosins provide stability to the filaments and regulate access of other actin-binding proteins (Lees-Miller and Helfman, 2005).

Proteins identified on tissue from wound repair DAY NINE

WD repeat-containing protein 87

The WD repeats are a conserved sequence motif that typically end in tryptophan and aspartic acid (WD) and are usually found in all eukaryotes. They have been linked to gene expression, RNA processing, signal transduction, and cell division (Yoon *et al.*, 2004). Their function in cell cycle regulation is to serve as a mitotic checkpoint responsible for ensuring accurate chromosome segregation (Yoon *et al.*, 2004; Smith, 2008). The occurrence of the WD repeat-containing protein during the proliferatory phase is necessary, not just for division, but to ensure that the cells do not enter anaphase if a misaligned chromosome is present (Yoon *et al.*, 2004). This is probably important for the stem cells that later differentiate into epidermal cells (Arno *et al.*, 2011).

Girdin

Girdin is a novel actin-binding Akt substrate that plays an important role in actin organization and Akt-dependent cell motility in fibroblasts (Jiang *et al.*, 2008). Girdin

is expressed ubiquitously and is vital in the formation of stress fibres and lamellipodia (the cytoskeletal actin projections on the mobile edge of a motile cell) and is essential for cell migration (Enomoto *et al.*, 2005; Jiang *et al.*, 2008).

Kinesin family member 16B

Members of this super-family are microtubule-associated motor proteins. The motors bind to microtubules and convert chemical energy supplied by ATP hydrolysis into kinetic energy allowing these motors to move along the microtubules (Hirokawa *et al.*, 1998). The kinesins play a part in cell division (Goshima and Vale, 2005) particularly during pro-metaphase and metaphase. During these cell division phases, the kinesins maintain the spindle length and slide the microtubules apart within the spindles (Jiang *et al.*, 2008).

The detection of so many proteins involved in cell division on Day 9 is confirmation that, as literature explains (Jiang *et al.*, 2008), the wound is in the proliferatory phase.

Rho-associated protein kinase 2

Rho family members are regulators of actin re-arrangement and cell growth (Serra-Pagès *et al.*, 1998). These small GTPases have been implicated in cytoskeletal reorganisation to form stress fibres. They have also been shown to function in the mediation and co-ordination of cell migration and morphology, in response to initiation by growth factors and other extracellular signals (Matsui *et al.*, 1996; Enomoto *et al.*, 2005). Rho exerts a variety of actions in the cell, including transcriptional regulation by serum-response factor (Uehata *et al.*, 1997).

ERC protein 2-like

This protein has been studied in humans; however, the BLAST search indicated that this protein is found in *Sus scrofa*. In humans, the protein was thought to organise the cytomatrix at the nerve terminals active zone (CAZ). The CAZ has been implicated in defining the site of Ca²⁺-dependent exocytosis of neurotransmitter molecules. The ERC protein may also recruit liprin-alpha proteins to the CAZ (Ohtsuka *et al.*, 2002).

The presence of this protein implies that neuronal activity is occurring in the wound at this time. This is possible since sensory nerves that innervate the skin are found in contact with dermal and epidermal cells, and can play a role in the wound healing process by releasing a variety of neuropeptides (NP) such as substance P (Blakytyn and Jude, 2006). Although the nerves in the full-thickness wound have obviously sustained damage, it should be kept in mind that a characteristic of the proliferatory phase is the *migration* of epidermal cells (which, according to Blakytyn *et al.* (2005), may be in contact with these sensory nerves) into the wound area.

Neurofilament heavy polypeptide was also detected in the wound on Day 9 and may be related to the ERC protein.

Proteins identified on tissue from wound repair DAY THIRTEEN

Once again, zinc fingers, proteins involved in RNA-binding, as well as coiled-coil domain-containing proteins and members of the kinesin family were identified in the wound tissue. This phase of the wound healing process has been referred to as transitional phase since the wound is not expected to have fully completed the proliferation phase, therefore detecting proteins with strong influences and important roles in both mitosis and cell migration are still expected.

Ankyrin repeat domain-containing protein 12-like

The ankyrin repeat is one of the most common, modular, protein–protein interaction motifs in nature and is also the most frequently observed amino acid motif in protein databases. This 33-amino acid residue motif has diverse functions including transcription initiation, cell cycle regulation, cytoskeletal integrity and ion transport amongst others. It was first identified as the yeast cell cycle regulator and the *Drosophila* signalling protein, Notch. Notch-family receptors mediate signals that control the selection between alternative cell differentiation and this signal in primary neurogenesis, directs cells to adopt an epidermal fate as opposed to the default state of neural differentiation (Royet *et al.*, 1998; Mosavi *et al.*, 2002; Mosavi *et al.*, 2004).

Proteins identified on tissue from wound repair DAY SIXTEEN

At this stage, the wound is expected to be in the remodelling phase (Boateng *et al.*, 2008) yet there is an overlap seen in some of the proteins detected during this and the inflammatory phases. Detecting these proteins in the inflammatory phase suggested that the wound was preparing to enter the proliferatory phase. Detecting these species during the remodelling phase is not unusual since the pro-collagen precursors and immature, but predominant, collagen III synthesized during the proliferatory phase, are replaced by a mature, organised collagen I network that ensures that a wound is strong and resistant to force and reopening (Diegelmann and Evans, 2004; Broughton *et al.*, 2006; Sibbald and Woo, 2008). The overlapping protein species were the RNA-binding proteins, hypothetical proteins, as well as the nuclear speckling splicing regulatory proteins.

RNA polymerase-associated protein LEO1

RNA-polymerase 1 transcribes the rRNA gene to produce the majority of the ribosome. Since no information on the function of protein LEO 1 is currently

available, the RNA polymerase-associated factor 1 complex (Paf1C) was used for functional comparison. The RNA polymerase-associated factor 1 complex is a transcription elongation factor with known roles in polymerase II transcription and has been shown to have a role in maintaining the identity of the few pluripotent embryonic stem cells present (Zhang *et al.*, 2010). Transcription factors and proteins involved in the maintenance of pluripotency in stem cells were first detected on Day 3 when the wound was preparing to enter the proliferatory phase. The presence of such proteins during the remodelling phase may be due to the continued processes of angiogenesis and the stimulation of fibroblast dendritic network swelling (Blakytyn and Jude, 2006). Wound contractility is also an aspect of healing that is further reinforced during the remodelling phase. To increase contractility, cells such as the fibroblasts must differentiate into myofibroblasts. While this takes place under the influence of TGF- β , the presence of a protein that plays a role in maintaining the pluripotency of stem cells suggests the possibility that perhaps some stem cells can also undergo such differentiation (Blakytyn and Jude, 2006; Zhang *et al.*, 2010).

Golgin subfamily A member 5-like

The members of the golgin family give identity and structure to the Golgi apparatus and form part of the complex protein network at the Golgi membrane (Striegl *et al.*, 2009). The presence of the golgin during the proliferatory phase seems to be in preparation for the remodelling phase to increase the overall thickness of the matrix for strong repair. The Golgi is involved in the production and packaging of the extracellular matrix and is increased in size and function during highly functional phases. The thicker, denser extracellular matrix expressed by fibroblasts results from stronger collagen fibrils since the proteoglycans within it are replaced by the more mature collagen type I. The end result is a strong, less pliant wound (Broughton *et al.*, 2006). This member of the golgin subfamily was also identified on Day 6. Fibroblasts present during the proliferatory phase (Day 6 is the expected time of transition from inflammatory to proliferation phases) (Boateng *et al.*, 2008), are also involved in the initial synthesis of proteoglycans to create the matrix.

CTTNBP2 N-terminal like

Cortactin-binding protein 2 is a neuron-specific, F-actin associated protein that is responsible for the regulation and maintenance of dendritic spinogenesis (Hsueh, 2012). The dendritic spines are neuron-specific, actin-rich, subcellular structures at the site of excitatory synapses (Nimchinsky *et al.*, 2002; Hsueh, 2012).

The presence of proteins responsible for dendritic spinogenesis suggests neuro-regeneration. This is the regrowth or repair of nerve tissue by mechanisms such as new neurons, axons, and synapses. While nerve recovery can still occur in the case of nerves being separated by a large gap, i.e.: punch biopsy, it is more difficult to achieve due to the muscle and skin damage. This however, does not exclude that nerve regeneration is possible or taking place.

Nucleoprotein TPR

The nucleoprotein TPR was identified on wound healing Day 16. A nucleoprotein is a protein that is structurally associated with nucleic acid. The TPR (translocated promoter region) is a component of the TPR-MET fusion protein. MET is a membrane receptor normally expressed by epithelial cells and is essential in wound healing (Grotegut, 2006; Chmielowiec *et al.*, 2007).

CONCLUSION

Wound healing is most certainly a complex continuum of overlapping events. After having identified many proteins and defining their functions, it is clear that the phases of wound healing do, in fact, overlap greatly. The overlap and continuum is well represented in Figure 30.

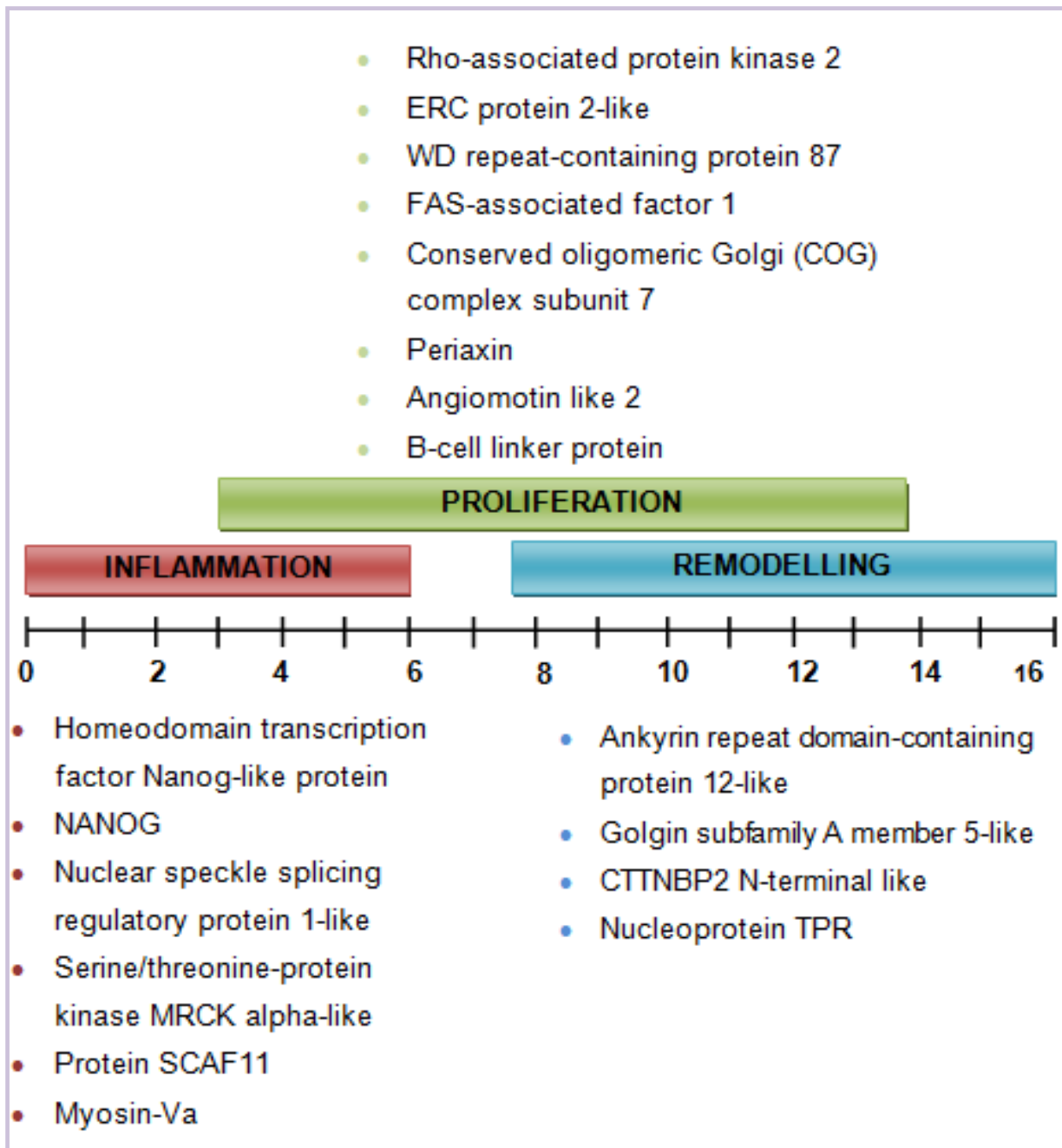


Figure 30: A graphical description illustrating the overlap seen in the wound healing process in terms of the proteins detected in the animal models used in this study.

The identification of these proteins in the porcine wound tissue involved the use of peptide mass fingerprinting (PMF) which compares the experimentally obtained spectrum to theoretical spectra using a score to measure the degree of similarity. A high score for the theoretical spectrum is considered the best representative of the experimental spectrum (McGinnis and Madden, 2004; Johnson *et al.*, 2008). The two databases used were MASCOT and BLAST. MASCOT, in many cases, identified the proteins as those belonging to other animal species completely unrelated to *Sus scrofa*. This was not completely unusual since the wound biopsies had been fixed in formalin which introduces the structural modification of methylene bridges (Lemaire *et al.*, 2007; Stauber *et al.*, 2008). The tryptic digests of the FFPE tissue could have yielded peptides very different from a tryptic digest of a fresh, frozen sample.

The use of proteomics allowed for the identification of the proteins detected in the porcine wound samples. While the proteins detected did not seem to play a direct role in wound healing, each had a function that can support an aspect of the wound healing process. That is, many of the proteins identified play roles in DNA replication, cell migration, and the transcription of genes that are necessary in the formation of collagen, nerve tissue, as well as contractile fibroblasts. All the proteins identified were of porcine origin, and while the most prominent growth factors in wound healing were not detected in these samples of porcine wound tissues, the proteins detected have been discussed and their roles in the wound healing process have been explained.

During inflammation – immediately upon injury to around Day 6 - inflammatory cytokines and immune cells come into play to mediate this process and to remove foreign particles so as to prevent infection (Broughton *et al.*, 2006, Blakytyn and Jude, 2006). While none of the literature referenced mention the proteins identified in the present study, when the characteristics of this phase are looked at more closely, the BLAST-identified proteins seem well-placed in this phase. During inflammation, a fibrin clot is formed and serves as a scaffold for the invading immune cells. This clot also generates cellular signals to induce neutrophil response. The

matrix metalloproteinases (MMPs) in this healing phase clear damaged extracellular matrix and facilitate cell migration (Blakytyn and Jude, 2006; Broughton *et al.*, 2006, Sibbald and Woo, 2008). With regards to the current study, it is the serine/threonine-protein kinase MRCK alpha-like protein and protein SCAF 11 identified in this phase that were shown to be the proteins involved in regulating cell growth and survival, cell migration, and signal transduction.

Proliferation begins around day four after the wound is sustained through to day 14. During this phase, the main cells undergoing proliferation are the fibroblasts, keratinocytes, and endothelial cells following signals initiated by growth factors. Angiogenesis in this phase is also directed by the keratinocytes (Broughton *et al.*, 2006, Boateng *et al.*, 2008). BLAST identified myosin-Va which recruits granules for neuropeptide storage. Neuropeptides prompt chemotaxis, growth factor production, and stimulate cell proliferation (Libby *et al.*, 2004, Desnos *et al.*, 2007, Sibbald and Woo, 2008). Other proteins involved in cell proliferation are: NANOG, Rho-associated protein kinase 2, WD repeat containing protein 87, and ankyrin repeat domain-containing protein which are up-regulated at DNA replication level (Han *et al.*, 2012); responsible for transcription regulation (Uehata *et al.*, 1997); involved in cell division as a mitotic checkpoint (Yoon *et al.*, 2004; Smith, 2008); and initiate transcription and cell cycle regulation (Mosavi *et al.*, 2002), respectively. NANOG was identified during the inflammatory phase, however, as previously reported (Blakytyn and Jude, 2006; Broughton *et al.*, 2006; Boateng *et al.*, 2008), and as was observed in the study, the wound healing phases overlap extensively. Angiogenesis is expected in this phase (Blakytyn and Jude, 2006; Broughton *et al.*, 2006; Boateng *et al.*, 2008). Angiomotin like 2 protein, identified in this phase and expressed by endothelial cells, regulates and increases endothelial migration (Trojanovsky *et al.*, 2001, Bratt *et al.*, 2005, Aase *et al.*, 2007).

The remodelling (maturation) phase is characterised by extracellular matrix construction by continued synthesis and degradation of the extracellular matrix constituents (Diegelmann and Evans, 20004, Broughton *et al.*, 2006). The strengthening of the new epithelium also occurs in this phase (Boateng *et al.*, 2008).

Nucleoprotein TPR which is expressed by epithelial cells has been described as being essential to wound healing (Grotegut, 2006; Chmielowiec *et al.*, 2007) and was identified during this phase. When the matrix stiffens, Rho-kinase dependent, myosin-light-chain phosphorylation mechanism of contraction is observed (Broughton *et al.*, 2006). Rho-associated protein kinase was identified during the proliferation phase which greatly overlapped with the remodelling phase. Ankyrin repeat domain-containing protein, identified by BLAST, plays a role in maintaining cytoskeletal integrity (Uehata *et al.*, 1997). The acid also couples to G-proteins to activate numerous signal transduction pathways initiated by GTPases such as Rho (Broughton *et al.*, 2006).

This chapter discussed the proteins detected in the porcine wound tissue by MALDI-MSI and this was achieved using the bottom-up proteomics approach and submitting only the most intense peptide signals for database comparisons. Despite the unconventional use of FFPE samples thus requiring further tissue sample preparation in this study, several proteins that play a supportive role in cell proliferation and wound healing were identified and did show a time based flux in their concentration which could be matched to the wound healing phase when they were identified.

Several proteins were expected to have been found such as collagen, fibronectin and elastin but in retrospect, these proteins although abundant, do not cleave easily with trypsin and this would account for the lack of peptides from these proteins in the extracted peptide signal intensities. There are a number of other proteins such as the matrix metalloproteinases and actin that would be expected to be present and found. Initially, this was seen as a failure in terms of the study, but the insight into the molecular events occurring during wound healing is valuable information and the limitations of the use of FFPE treated samples was noted.

A study conducted by Lemaire *et al.* (2007) presented two methods for the direct analysis of (dewaxed) FFPE tissue. The first method – which utilises reactive matrix

(2,4-dinitrophenylhydrazine) - is useful for tissues preserved in formalin for less than one year (ideally 6 months) while the other can be used for FFPE tissue irrespective of the length of fixation time. The latter relies on repeated spotting of 2 μ L of trypsin onto the tissue every 10 minutes. At the end of digestion, the tissue was rinsed with 80% ethanol and then sprayed with matrix before MALDI analysis. The use of reactive matrix provided improved signal due to its ability to neutralise formalin residues. The Lemaire *et al.* (2007) study concluded that after a year in formalin, it is impossible to obtain good signal by direct analysis. The tissues used in the present study were stored in formalin for approximately 10 months which could explain the challenges experienced in obtaining good signals from some of the proteins that were expected to be found.

The identification of wound proteins from formalin-fixed paraffin-embedded tissue analysed using MALDI-MSI was successfully done using probability-based search engines. Although the proteins that were expected to be observed were not identified, most likely due to the modifications leading to “faulty” trypsin digestion, the most intense signals identified proteins that can play a role in the wound healing process.

CONCLUDING REMARKS

The original aim of this study was to investigate Absorbatox™ as a wound healing agent to assess whether it can be used in effective treatment for chronic wounds. The study was divided into two branches: physical characterisation of Absorbatox™; which gave insight into the physical attributes as well as the characterisation of healing wounds where the effects of Absorbatox™ on wounds were measured and compared.

The physical characteristics of Absorbatox™ (granular and micronised) were determined to try understand its role as a wound healing agent prior to testing its influence on wound tissue protein profiles.

The physical characteristics of the surface areas and pore volumes were assessed using the BET nitrogen adsorption-desorption technique, and the particle size distribution assessed by laser particle sizing. The particle size differences of the granular and micronised Absorbatox™ is visible at the macroscopic level and the laser particle sizing results confirmed this in addition to determining the size distribution. Also, the BET nitrogen adsorption-desorption indicated that the surface area of the granular Absorbatox™ is significantly less than that of the micronised Absorbatox™. When considering the surface-area to volume ratio, it is clear that the two methods employed to physically characterise the Absorbatox™ indirectly confirmed each other's findings. The BET nitrogen adsorption-desorption showed Type IV isotherms with Type 3 hysteresis for both the granular and micronised Absorbatox™ samples which indicate that the particles are mesoporous (2 - 50 nm) and exhibit non-uniformity in particle size within each sample. The laser particle sizer showed a micronised Absorbatox™ particle range of 0.8 to 300 µm which is large enough to accommodate the average pore volume of 28 nm as determined by BET nitrogen adsorption-desorption. The granular Absorbatox™ had a particle size range of 2 – 875 µm which could easily accommodate the average pore volume of 45 nm.

Since the main functionality of the Absorbatox™ lies in its ability to draw up wound exudate by strong capillary forces, a very important physical characteristic of the Absorbatox™ is in fact the pore size. A smaller pore size results in stronger capillary action which allows removal of excess wound exudate to provide an optimal wound environment and to promote healing. Granular and micronised Absorbatox™ were used as the test treatments in the animal study and compared against a negative control (a normal wound dressing) and a positive control (Cerdak™ - commercially available ceramic particle based adsorbent dressing).

The animal study was performed to use a wound healing model from which the wounds would be analysed for rates of healing in terms of wound contraction and re-epithelialisation indicated by wound dimensions including depth measurements. The use of a porcine wound healing model was based on the fact that the skin of the pig closely resembles that of humans in anatomy and function with the only major difference being the absence of sweat glands in porcine skin. Wound healing in pigs occurs primarily by re-epithelialisation which is the same process as in human skin wounds.

The difference between wound healing rates of the Absorbatox™-treated and Cerdak™-treated groups were statistically significant and it is important to note that the histological evaluations of the wounds treated with Absorbatox™ showed wound closures that are associated with the establishment of new epithelium with well-defined basal layers, normal collagen arrangement and neovascularisation that more closely resembled normal, healthy tissue than the Cerdak™-treated wounds. Measurements of the wound dimensions in the different treatment groups showed signs of better wound healing in the Absorbatox™ treatment group. For example, treatment with Absorbatox™ resulted in quicker decrease in wound depth with less and slower wound contraction and reached scarring in a shorter period compared to both negative as well as positive control groups. A wound that heals primarily by wound contraction is not as resistant to tensile force and re-opening as one that heals mainly by re-epithelialisation. Thus Absorbatox™ and the Cerdak™ (positive control) both improve the strength of a healed wound. However, unlike the

micronised Absorbatox™, Cerdak™ wound dressings are filled with ceramic spheres with an average particle size of 2.2 mm, pore widths ranging 0.3 – 5 µm, and a surface area of 6 m²/g (Cerdak™, n.d). This suggests that Cerdak™ has a weaker capillary force than micronised Absorbatox™.

The positive results exhibited by Absorbatox™ are easily translatable to human skin due to the similarity of human skin to the porcine skin model making it a promising wound healing agent that can result in a stronger wound once completely healed. In light of the apparent improved wound healing based on the wound measurements and histological assessment, wound tissue from wounds treated with Absorbatox™ were analysed using MALDI-MSI in an attempt to assess the presence of the selected cytokines as observed in previous studies.

MALDI-MSI was used to determine the presence of proteins in histological sections of excised wound tissue biopsies at different stages of the wound healing process to establish which proteins and non-protein species are present during the different stages of wound healing. This technique also allowed for the relative quantitation of protein fluctuations in the tissue as the wound heals.

Fresh-frozen tissue samples are typically used for MALDI-MS analysis however, the snap-frozen tissue samples for this study were lost due to shipping delays and consequently, the thawing and tissue decay which resulted in attempting the analysis of formalin preserved tissue by MALDI-MSI. This proved to be a challenging, but not impossible task to analyse formalin-fixed paraffin-embedded (FFPE) tissue and required several added sample preparation steps than analysis of fresh, snap-frozen tissue. The sample preparation required for successful imaging of FFPE tissue unfortunately washes away almost all lipids during the dewaxing steps and thus only the protein derived peptides could be imaged using this preserved tissue. The most important aspects to take into account when conducting MALDI analysis is to ensure that target plate conductivity is maintained and that the proteins to be analysed are within the range of instrument detection. Both goals were achieved by using

conductive copper tape and introducing an optimised trypsin digestion step to the dewaxed samples during sample preparation. Trypsin digestion cleaves the proteins to produce peptides that range between 8-15 amino acids and approximately 1600 Da. This peptide size is ideally suited for MALDI analysis as singly charged ions are formed. The first aspect of wound healing that was confirmed is that wound healing does indeed begin immediately after a wound is sustained with the most intense activity occurring in and immediately around the wound during the initial phase of inflammation. Some proteins involved in wound healing were successfully imaged with respect to location and relative concentrations by means of ion intensity distributions, indicating the locations of the most activity in the wound. These were in agreement with literature about the sites of protein activity in the wound during the various stages of healing and allowed monitoring of the healing process. Using this technology in conjunction with microscopy of the histological sections, allowed for the ions to be visually correlated to the anatomical structures in tissue located to specific positions or areas in the tissue.

Despite the loss of lipid molecules during the sample preparation, achieving the objective of detecting proteins in the wound confirmed the possibility of using formalin-preserved tissue for visualising peptide fluctuations in healing wounds.

The final objective was to identify the proteins of origin for selected high intensity signal peptides identified by MALDI-MSI. The approach used to achieve this was “bottom-up” proteomics which uses the proteolytic digests of proteins to identify complete proteins based on peptide fragment fingerprinting and amino acid sequence data. The MASCOT and BLAST protein databases were used for this assessment. These databases compare the experimentally obtained spectra to theoretical spectra for similarity of possible peptide masses and give a score as to whether or not a protein can be identified. BLAST was used to confirm the results obtained by MASCOT since many of the MASCOT-identified proteins in the wound tissue samples did not belong to *Sus scrofa* (the domestic pig). This is most likely due to the tissue having undergone formalin fixation which formed cross-links between the proteins. Although the tissue samples were subjected to antigen

retrieval, formalin-fixation introduces methylene bridges between the amino groups of the lysine chains which are not always reversible; and since trypsin cleaves at both arginine and lysine, the tryptic digests could have yielded peptides very different from a tryptic digest of a fresh, frozen sample with no post-translational modifications.

BLAST identified the proteins as being of porcine origin. The proteins identified, however, did not seem to play a direct role in wound healing; that is, no collagen or extracellular matrix proteins were identified (a possible side-effect of the formalin preservation and subsequent trypsin digestion); however, the function of the proteins identified appear to play a role to various aspects of the wound healing process especially cell proliferation and control.

During inflammation, inflammatory cytokines, immune cells, and metalloproteinases come into play to mediate this process, facilitate cell migration, and remove foreign particles so as to prevent infection. A literature search found that the functions of the serine/threonine-protein kinase MRCK alpha-like protein and protein SCAF 11 identified in this phase regulate cell growth and survival, cell migration, and signal transduction.

The NANOG, Rho-associated protein kinase 2, WD repeat containing protein 87, and ankyrin repeat domain-containing protein identified are involved in up-regulating DNA replication and mitosis while the angiominin like 2 protein plays a role in regulating endothelial cell migration. Myosin-Va recruits granules for neuropeptide storage and these neuropeptides stimulate cell proliferation. During the proliferatory phase, fibroblast and endothelial cell proliferation is predominant. Angiogenesis also starts during this phase. While the major proteins normally involved in these phases were not identified, it seems that the less acknowledged proteins also contribute to the final status of a “healed” wound.

The same situation was found in the remodelling phase where collagen synthesis continues and the epithelial cells are strengthened. Nucleoprotein TPR – also identified in this phase - contributes towards strengthening the new epithelial cells (Grotegut, 2006; Chmielowiec *et al.*, 2007).

This study shows that Absorbatox™ with its unique physical characteristics is a promising wound healing agent that appears to accelerate wound healing by encouraging cell proliferation and re-epithelialisation at a time when untreated full-thickness wounds are still apparently caught in the inflammatory phase. This was confirmed by the proteins that were identified in the wounds. In addition to this, the wounds, although formalin-fixed, could be successfully imaged using MALDI-MSI and the wound healing process was easily monitored.

During the planning of this study, the ultimate achievement was envisioned as being able to use MALDI-MSI to visualise and indentify the proteins most cited in literature in the wound tissues obtained in this study. The vision was to gain new insight into wound healing. The wound healing proteins most cited in literature were, unfortunately, not identified. What did happen, however, led to the enlightenment of the physical aspects of Absorbatox™ which may have been responsible for the remarkable wound healing observed in the pilot study conducted in 2009 by Oosthuizen *et al.* when Absorbatox™ was first tested as a wound healing agent. This study confirmed that pigs make a good model for the study of excisional wound healing because of the similarities between porcine and human skin and because of this, the results from this animal model may be easily translated to the human condition making Absorbatox™ a promising wound healing agent that will result in strong wounds once healed. Proteins that were never on the radar of intended discovery were identified and this manifested the vision: new insight into wound healing was gained. This study exposed some changes that occur in the wound on the sub-cellular and to some extent, the molecular level. As Cooper *et al.* (1999) conveyed in an article about gaining new understanding into wound healing, there is a need to approach wound healing at both the cellular and molecular levels to help

better wound management. This research may have contributed towards moving in that direction.

IMPROVEMENTS TO CURRENT STUDY

While all the objectives in the study were achieved, there are some areas in which improvements to the study could be made.

- To better evaluate how Absorbatox™ affects the wound healing process for chronic wounds, diabetic pig models could have been used. Of course, the number of pigs would need to be increased accordingly. Thus the animal study design would have been:

Diabetic pigs

Two pigs

20 wounds

Both pigs should have wounds treated with Absorbatox™, positive control, and negative control

Healthy pigs

Two pigs

20 wounds

- MALDI MSI should have been conducted on the Absorbatox™, negative and positive control wounds of exactly the same day post initiation. Although this was the original plan, the destruction of the frozen tissue which contained the above-mentioned treatments resulted in only Absorbatox™ treatments in formalin being usable.
- Adding a technique such as liquid extraction surface analysis (LESA) coupled to ESI tandem mass spectrometry to identify peptide amino acid sequences in specific wound areas and healthy tissue areas would have improved the research impact by giving more complete data including CID fragmentation confirming the peptide sequences.

Despite there being room for improvement in the research, all the objectives were met. Laser particle sizing was added to the physical characterisation to gain knowledge of the particle size distribution of the Absorbatox™ samples. This, in turn, worked to indirectly confirm the nitrogen adsorption findings.

The aim of this study was to assess changes in wound tissue and possibly identify a mechanism by which Absorbatox™ improves wound healing. This was achieved.

MALDI-MSI was used to successfully image chronological changes occurring in the tissue during wound healing process despite formalin-fixed tissue being used.

Absorbatox™ was shown to seemingly accelerate wound healing by encouraging cell proliferation and re-epithelialisation at a time when untreated full-thickness wounds were still apparently caught in the inflammatory phase. The proteins identified and the times at which they were present confirmed this.

Thus, Absorbatox™ has been characterised as a wound healing agent both physically and biologically.

REFERENCES

- Aase, K., Ernkvist, M., Ebarasi, L., Jakobsson, L., Majumdar, A., Yi, C., Birot, O., Ming, Y., Kvanta, A. and Edholm, D. (2007). Angiotensin regulates endothelial cell migration during embryonic angiogenesis. *Genes and Development*, 21(16), 2055-2068.
- Abbas, Z. and Archibald, L. (2007). The diabetic foot in sub-saharan africa: A new management paradigm. *Diabetic Foot*, 10(3), 128.
- Absorbatox™ (n.p.) *Absorbatox™ - Executive Summary*. [report] Pretoria: p.1-12.
- Aebersold, R., and Goodlett, D. R. (2001). Mass spectrometry in proteomics. *Chemical Reviews*, 101(2), 269-295.
- Allen, P. B., Ouimet, C. C., and Greengard, P. (1997). Spinophilin, a novel protein phosphatase 1 binding protein localized to dendritic spines. *Proceedings of the National Academy of Sciences*, 94(18), 9956-9961.
- Allen, T. (1997). *Particle size measurement* (Fifth Ed. ed.). London: Chapman and Hall.
- Álvarez, M., Estivill, X., and de la Luna, S. (2003). DYRK1A accumulates in splicing speckles through a novel targeting signal and induces speckle disassembly. *Journal of Cell Science*, 116(15), 3099-3107.
- Archibald, A.L., Bolund, L., Churcher, C., Fredholm, M., Groenen, M.A.M., Harlizius, B., Lee, K.T., Milan, D., Rogers, J. and Rothschild, M.F. (2010). Pig genome sequence-analysis and publication strategy. *BMC Genomics*, 11(1), 438.
- Arno, A., Smith, A. H., Blit, P. H., Al Shehab , M., Gauglitz, G. G., and Jeschke, M. G. (2011). Stem cell therapy: A new treatment for burns? *Pharmaceuticals*, 4(10), 1355-1380.

Ashraf, A., Lee, P.H., Kim, K., Zaporozhan, V., Bonassar, L., Valentini, R., Spangenberg, A. and Weinzweig, J. (2009). Effect of sustained-release PDGF and TGF-beta on cyclophosphamide-induced impaired wound healing. *Plastic and Reconstructive Surgery*, 124(4), 1118-1124.

Bae, Y. S., Yazaydin, A. O., and Snurr, R. Q. (2010). Evaluation of the BET method for determining surface areas of MOFs and zeolites that contain ultra-micropores *Langmuir : The ACS Journal of Surfaces and Colloids*, doi:10.1021/la100449z

Baldwin, M. A. (2004). Protein identification by mass spectrometry issues to be considered. *Molecular and Cellular Proteomics*, 3(1), 1-9.

Barnes, P and Adcock, I. (1998). Transcription factors and asthma. *European Respiratory Journal*, 12(1), 221-234.

Barrett, E., Joyner, LG and Halenda, PP. (1951). The determination of pore volume and area distributions in porous substances. I. computations from nitrogen isotherms. *J. Am. Chem. Soc.*, 73(1)

Barth, H. G. and Flippen, R. B. (1995). Particle size analysis *Analytical Chemistry*, 67(12), 257 <last_page> 272.

Barton, T.J., Bull, L.M., Klemperer, W.G., Loy, D.A., McEnaney, B., Misono, M., Monson, P.A., Pez, G., Scherer, G.W. and Vartuli, J.C. (1999). Tailored porous materials. *Chemistry of Materials*, 11(10), 2633-2656.

Bérend, I., Cases, J., Francois, M., Uriot, J., Michot, L., Masion, A. and Thomas, F. (1995). Mechanism of adsorption and desorption of water vapor by homoionic montmorillonites; 2, the Li⁺, Na⁺, K⁺, Rb⁺ and Cs⁺-exchanged forms. *Clays and Clay Minerals*, 43(3), 324-336.

Billeter, M., Qian, Y. Q., Otting, G., Müller, M., Gehring, W. and Wüthrich, K. (1993). Determination of the nuclear magnetic resonance solution structure of an antennapedia homeodomain-DNA complex. *Journal of Molecular Biology*, 234(4), 1084-1097.

- Blakytyn, R., and Jude, E. (2006). The molecular biology of chronic wounds and delayed healing in diabetes. *Diabetic Medicine : A Journal of the British Diabetic Association*, 23(6), 594-608.
- Boateng, J. S., Matthews, K. H., Stevens, H. N., and Eccleston, G. M. (2008). Wound healing dressings and drug delivery systems: A review. *Journal of Pharmaceutical Sciences*, 97(8), 2892-2923.
- Bowen, P. (2002). Particle size distribution measurement from millimeters to nanometers and from rods to platelets *Journal of Dispersion Science and Technology*, 23(5), 631 -662.
- Boyce, D., Jones, W., Ruge, F., Harding, K., and Moore, K. (2000). The role of lymphocytes in human dermal wound healing. *British Journal of Dermatology*, 143(1), 59-65.
- Bratt, A., Birot, O., Sinha, I., Veitonmäki, N., Aase, K., Ernkvist, M. and Holmgren, L. (2005). Angiomotin regulates endothelial cell-cell junctions and cell motility. *Journal of Biological Chemistry*, 280(41), 34859-34869.
- Breck, D. (1964). Crystalline molecular sieves. *Journal of Chemical Education*, 41(12), 678.
- Broekhoff, J., and de Boer, J. (1968). Studies on pore systems in catalysts: XIII. pore distributions from the desorption branch of a nitrogen sorption isotherm in the case of cylindrical pores B. applications. *Journal of Catalysis*, 10(4), 377-390.
- Broughton, G., 2nd, Janis, J. E., and Attinger, C. E. (2006). The basic science of wound healing. *Plastic and Reconstructive Surgery*, 117(7 Suppl), 12S-34S.
- Brunauer, S., Emmett, P. H. and Teller, Edward. (1938). Adsorption of gases in multimolecular layers. *J. Am. Chem. Soc.*, 60(2), 309.
- Burevski, D., and Poceva, J. (1994). Adsorption of nitrogen on nax, canax and nay zeolites. *Bulletin of the Chemists and Technologists of Macedonia*, 13(1), 15-18.

Caldwell, R. L., Opalenik, S. R., Davidson, J. M., Caprioli, R. M., and Nanney, L. B. (2008). Tissue profiling MALDI mass spectrometry reveals prominent calcium-binding proteins in the proteome of regenerative MRL mouse wounds. *Wound Repair and Regeneration*, 16(3), 442-449.

Camp, E., Sánchez-Sánchez, A.V., García-España, A., DeSalle, R., Odqvist, L., Enrique O'Connor, J. and Mullor, J.L. (2009). Nanog regulates proliferation during early fish development. *Stem Cells*, 27(9), 2081-2091.

Campbell, N. A. (1996). *Biology* (4th Edition ed.). Menlo Park, CA: The Benjamin/Cummings Publishing Company.

Caprioli, R. M., Farmer, T. B., and Gile, J. (1997). Molecular imaging of biological samples: Localization of peptides and proteins using MALDI-TOF MS. *Analytical Chemistry*, 69(23), 4751-4760.

Cerdak - the next dimension in wound care (n.d.) *Technical Information*. [online] Available at: <http://www.cerdak.co.za/techinfo.asp> [Accessed: 15 Apr 2012].

Chambers, I., Colby, D., Robertson, M., Nichols, J., Lee, S., Tweedie, S. and Smith, A. (2003). Functional expression cloning of nanog, a pluripotency sustaining factor in embryonic stem cells. *Cell*, 113(5), 643-655.

Chaurand, P., Schwartz, S. A., Billheimer, D., Xu, B. J., Crecelius, A., and Caprioli, R. M. (2004). Integrating histology and imaging mass spectrometry. *Analytical Chemistry*, 76(4), 1145-1155.

Chaurand, P., Schwartz, S. A., Reyzer, M. L., and Caprioli, R. M. (2005). Imaging mass spectrometry: Principles and potentials. *Toxicologic Pathology*, 33(1), 92-101.

Chaurand, P., Norris, J. L., Cornett, D. S., Mobley, J. A., and Caprioli, R. M. (2006). New developments in profiling and imaging of proteins from tissue sections by MALDI mass spectrometry. *Journal of Proteome Research*, 5(11), 2889-2900.

Chmielowiec, Jolanta; Borowiak, Malgorzata; Morkel, Markus; Stradal, Theresia; Munz, Barbara; Werner, Sabine; Wehland, Jürgen; Birchmeier, Carmen; and

Birchmeier, Walter. (2007). c-met is essential for wound healing in the skin. *The Journal of Cell Biology*, 177(1), 151-162.

Choma, J., Jaroniec, M., Burakiewicz-Mortka, W., and Kloske, M. (2002). Critical appraisal of classical methods for determination of mesopore size distributions of MCM-41 materials. *Applied Surface Science*, 196(1–4), 216-223.

Cohen, P. T. (2002). Protein phosphatase 1–targeted in many directions. *Journal of Cell Science*, 115(2), 241-256.

Cooper, D. M. (1999). Wound healing: New understandings. *Nurse Practitioner Forum*, 10(2), 74-86.

Cornett, D. S., Reyzer, M. L., Chaurand, P., and Caprioli, R. M. (2007). MALDI imaging mass spectrometry: Molecular snapshots of biochemical systems. *Nature Methods*, 4(10), 828-833.

Cuberts, B., Bray, D., Lewis, J., Raff, M., Roberts, K., and and Watson, J. (1994). *Molecular biology of the cell*. New York: Garland Science.

D'Amico, F., Skarmoutsou, E., and Stivala, F. (2009). State of the art in antigen retrieval for immunohistochemistry. *Journal of Immunological Methods*, 341(1-2), 1-18.

De Clercq, B., Lant, P. A., and Vanrolleghem, P. A. (2004). Focused beam reflectance technique for in situ particle sizing in wastewater treatment settling tanks. *Journal of Chemical Technology and Biotechnology*, 79(6), 610-618.

De Ridder, F., Deriemaeker, L., Coppens, P., and Finsy, R. (2000). Shape and size determination by laser diffraction: Feasibility of data analysis by physical modeling. *Particle and Particle Systems Characterization*, 17(5-6), 195-205.

Desnos, C., Huet, S., Fanget, I., Chapuis, C., Böttiger, C., Racine, V., Sibarita, J.B., Henry, J.P. and Darchen, F. (2007). Myosin va mediates docking of secretory granules at the plasma membrane. *The Journal of Neuroscience*, 27(39), 10636-10645.

Diegelmann, R. F and Evans, M. C. (2004). Wound healing: An overview of acute, fibrotic and delayed healing. *Frontiers in Bioscience*, 9, 283-289.

Djidja, M.C., Claude, E., Snel, M.F., Francese, S., Scriven, P., Carolan, V. and Clench, M.R. (2010). Novel molecular tumour classification using MALDI–mass spectrometry imaging of tissue micro-array. *Analytical and Bioanalytical Chemistry*, 397(2), 587-601.

Djidja, M., Francese, S., Loadman, P.M., Sutton, C.W., Scriven, P., Claude, E., Snel, M.F., Franck, J., Salzet, M. and Clench, M.R. (2009). Detergent addition to tryptic digests and ion mobility separation prior to MS/MS improves peptide yield and protein identification for in situ proteomic investigation of frozen and formalin - fixed paraffin - embedded adenocarcinoma tissue sections. *Proteomics*, 9(10), 2750-2763.

Donohue, M. and Aranovich, G. (1998). Classification of gibbs adsorption isotherms. *Advances in Colloid and Interface Science*, 76, 137-152.

Dufresne-Martin, G., Lemay, J. F., Lavigne, P., and Klarskov, K. (2005). Peptide mass fingerprinting by matrix-assisted laser desorption ionization mass spectrometry of proteins detected by immunostaining on nitrocellulose. *Proteomics*, 5(1), 55-66.

Dutta, D., Chatterjee, S., Ganguly, B. N., and Pillai, K. T. (2005). Structural aspects of synthetic zeolite: A comparative assay through positron annihilation and gas adsorption methods. *Journal of Applied Physics*, 98(3), 1-7.

Eisenstein, E., Gilliland, G.L., Herzberg, O., Moulton, J., Orban, J., Poljak, R.J., Banerjee, L., Richardson, D. and Howard, A.J. (2000). Biological function made crystal clear-annotation of hypothetical proteins via structural genomics. *Current Opinion in Biotechnology*, 11(1), 25-30.

El-Aneel, A., Cohen, A., and Banoub, J. (2009). Mass spectrometry, review of the basics: Electrospray, MALDI, and commonly used mass analyzers. *Applied Spectroscopy Reviews*, 44, 210.

Enomoto, A., Murakami, H., Asai, N., Morone, N., Watanabe, T., Kawai, K., Murakumo, Y., Usukura, J., Kaibuchi, K. and Takahashi, M. (2005). Akt/PKB regulates actin organization and cell motility via Girdin/APE. *Developmental Cell*, 9(3), 389-402.

Fenyő, D. (2000). Identifying the proteome: Software tools. *Current Opinion in Biotechnology*, 11(4), 391-395.

Ferraris, C. F., Hackley, V. A., and Avilés, A. I. (2004). Measurement of particle size distribution in portland cement powder: Analysis of ASTM round robin studies. *Cement, Concrete and Aggregates*, 26(2), 1-11.

Floquet, N., Coulomb, J., Weber, G., Bertrand, O., and Bellat, J. (2003). Structural signatures of type IV isotherm steps: Sorption of trichloroethene, tetrachloroethene, and benzene in silicalite-I. *The Journal of Physical Chemistry B*, 107(3), 685-693.

Fowler, C. B., Evers, D. L., O'Leary, T. J., and Mason, J. T. (2011). Antigen retrieval causes protein unfolding evidence for a linear epitope model of recovered immunoreactivity. *Journal of Histochemistry and Cytochemistry*, 59(4), 366-381.

Fremout, W., Dhaenens, M., Saverwyns, S., Sanyova, J., Vandenabeele, P., Deforce, D. and Moens, L. (2010). Tryptic peptide analysis of protein binders in works of art by liquid chromatography-tandem mass spectrometry. *Analytica Chimica Acta*, 658(2), 156-162.

Fu, C., Turck, C. W., Kurosaki, T., and Chan, A. C. (1998). BLNK: A central linker protein in B cell activation. *Immunity*, 9(1), 93-103.

Gehring, W. J. (1992). The homeobox in perspective. *Trends in Biochemical Sciences*, 17(8), 277-280.

George, B. (1986). Mascot 3: An informal introductory tutorial. *Software Engineering Journal*, 1(3), 95.

Gibson, D., and Schultz, G. (2009). Chronic wound diagnostic for matrix metalloproteinase. *Wound Healing Southern Africa*, 2(2), 68.

Gillespie, C.S., Sherman, D.L., Fleetwood-Walker, S.M., Cottrell, D.F., Tait, S., Garry, E.M., Wallace, V.C.J., Ure, J., Griffiths, I.R. and Smith, A. (2000). Peripheral demyelination and neuropathic pain behavior in periaxin-deficient mice. *Neuron*, 26(2), 523-531.

Goodwin, R. J. A., Pennington, S. R., and Pitt, A. R. (2008). Protein and peptides in pictures: Imaging with MALDI mass spectrometry. *Proteomics*, 8(18), 3785-3800.

Goshima, G., and Vale, R. D. (2005). Cell cycle-dependent dynamics and regulation of mitotic kinesins in drosophila S2 cells. *Molecular Biology of the Cell*, 16(8), 3896-3907.

Groseclose, M. R., Massion, P. P., Chaurand, P., and Caprioli, R. M. (2008). High-throughput proteomic analysis of formalin-fixed paraffin-embedded tissue microarrays using MALDI imaging mass spectrometry. *Proteomics*, 8(18), 3715-3724.

Grotegut, S. (2006). *The role of Hepatocyte Growth Factor/Scatter Factor in Hepatoblastoma and Hepatocellular Carcinoma Progression*. PhD. Universität Basel.

Guo, S., and Dipietro, L. A. (2010). Factors affecting wound healing. *Journal of Dental Research*, 89(3), 219-229.

Habermann, B., Oegema, J., Sunyaev, S., and Shevchenko, A. (2004). The power and the limitations of cross-species protein identification by mass spectrometry-driven sequence similarity searches. *Molecular and Cellular Proteomics*, 3(3), 238-249.

Han, J., Mistriotis, P., Lei, P., Wang, D., Liu, S., and Andreadis, S. T. (2012). Nanog reverses the effects of organismal aging on mesenchymal stem cell proliferation and myogenic differentiation potential. *Stem Cells (Dayton, Ohio)*, 30(12), 2746-2759.

Hirokawa, N., Noda, Y., and Okada, Y. (1998). Kinesin and dynein superfamily proteins in organelle transport and cell division. *Current Opinion in Cell Biology*, 10(1), 60-73.

Hirsch, T., Spielmann, M., Zuhaili, B., Koehler, T., Fossum, M., Steinau, H., Yao, F., Steinstraesser, L., Onderdonk, A. and Eriksson, E. (2008). Enhanced susceptibility to infections in a diabetic wound healing model. *BMC Surgery*, 8(1), 5.

Hsueh, Y. P. (2012). Neuron-specific regulation on F-actin cytoskeletons: The role of CTTNBP2 in dendritic spinogenesis and maintenance. *Communicative and Integrative Biology*, 5(4), 334-336.

Hua, L., Low, T. Y., Meng, W., Chan-Park, M. B., and Sze, S. K. (2007). Novel polymer composite to eliminate background matrix ions in matrix assisted laser desorption/ionization-mass spectrometry. *Analyst*, 132(12), 1223-1230.

Hunt, T. K., Hopf, H. and Hussain, Z. (2000). Physiology of wound healing. *Advances in Skin and Wound Care*, 13(2 Suppl), 6-11.

Jagtap, R. and Ambre, A. (2005). Overview literature on matrix assisted laser desorption ionization mass spectroscopy (MALDI MS): Basics and its applications in characterizing polymeric materials. *Bulletin of Materials Science*, 28(6), 515-528.

Jaroniec, M. and Kaneko, K. (1997). Physicochemical foundations for characterization of adsorbents by using high-resolution comparative plots. *Langmuir*, 13(24), 6589-6596.

Jemal, M. and Xia, Y. Q. (2006). LC-MS development strategies for quantitative bioanalysis. *Current Drug Metabolism*, 7(5), 491-502.

Jiang, P., Enomoto, A., Jijiwa, M., Kato, T., Hasegawa, T., Ishida, M., Sato, T., Asai, N., Murakumo, Y. and Takahashi, M. (2008). An actin-binding protein girdin regulates the motility of breast cancer cells. *Cancer Research*, 68(5), 1310-1318.

Jimmy, C. Y., Zhang, L., and Yu, J. (2002). Rapid synthesis of mesoporous TiO₂ with high photocatalytic activity by ultrasound-induced agglomeration. *New Journal of Chemistry*, 26(4), 416-420.

Johnson, M., Zaretskaya, I., Raytselis, Y., Merezhuk, Y., McGinnis, S., and Madden, T. L. (2008). NCBI BLAST: A better web interface. *Nucleic Acids Research*, 36(suppl 2), W5-W9.

Johnson, R. S., Davis, M. T., Taylor, J. A., and Patterson, S. D. (2005). Informatics for protein identification by mass spectrometry. *Methods*, 35(3), 223-236.

Kaletaş, B.K., van der Wiel, Ingrid M, Stauber, J., Dekker, L.J., Güzel, C., Kros, J.M., Luider, T.M. and Heeren, R. (2009). Sample preparation issues for tissue imaging by imaging MS. *Proteomics*, 9(10), 2622-2633.

Kandalaft, L. E., Zudaire, E., Portal-Núñez, S., Cuttitta, F., and Jakowlew, S. B. (2008). Differentially expressed nucleolar transforming growth factor- β 1 target (DENTT) exhibits an inhibitory role on tumorigenesis. *Carcinogenesis*, 29(6), 1282-1289.

Kaneko, K. (1994). Determination of pore size and pore size distribution: 1. adsorbents and catalysts. *Journal of Membrane Science*, 96(1-2), 59-89.

Karas, M., Bachmann, D., Bahr, U., and Hillenkamp, F. (1987). Matrix-assisted ultraviolet laser desorption of non-volatile compounds. *International Journal of Mass Spectrometry and Ion Processes*, 78, 53-68.

Karas, M. and Hillenkamp, F. (1988). Laser desorption ionization of proteins with molecular masses exceeding 10,000 daltons. *Analytical Chemistry*, 60(20), 2299-2301.

Kusumaningtyas, R. D. (2006). Effect of zeolite 4a on water concentration in the system of the esterification reaction of acetic acid with 1-butanol. *Indonesian Journal of Chemistry*, 6(2), 132-137.

Kyriakides, T.R., Wulsin, D., Skokos, E.A., Fleckman, P., Pirrone, A., Shipley, J.M., Senior, R.M. and Bornstein, P. (2009). Mice that lack matrix metalloproteinase-9 display delayed wound healing associated with delayed reepithelization and disordered collagen fibrillogenesis. *Matrix Biology*, 28(2), 65-73.

Lamond, A. I. and Spector, D. L. (2003). Nuclear speckles: A model for nuclear organelles. *Nature Reviews Molecular Cell Biology*, 4(8), 605-612.

Lee, M. and Schedl, T. (2006) *RNA-binding proteins: WormBook*, ed. [e-book] St. Louis, MO: The C. elegans Research Community, Wormbook.
http://www.wormbook.org/chapters/www_RNAbindingproteins/RNAbindingproteins.html [Accessed: 2012].

Lees - Miller, J. P. and Helfman, D. M. (2005). The molecular basis for tropomyosin isoform diversity. *Bioessays*, 13(9), 429-437.

Leinweber, B. D., Tsaprailis, G., Monks, T. J., and Lau, S. S. (2009). Improved MALDI-TOF imaging yields increased protein signals at high molecular mass. *Journal of the American Society for Mass Spectrometry*, 20(1), 89-95.

Lemaire, R., Desmons, A., Tabet, J. C., Day, R., Salzet, M., and Fournier, I. (2007). Direct analysis and MALDI imaging of formalin-fixed, paraffin-embedded tissue sections. *Journal of Proteome Research*, 6(4), 1295-1305.

Leofanti, G., Padovan, M., Tozzola, G., and Venturelli, B. (1998). Surface area and pore texture of catalysts. *Catalysis Today*, 41(1), 207-219.

Leskov, K. S., Klovov, D. Y., Li, J., Kinsella, T. J., and Boothman, D. A. (2003). Synthesis and functional analyses of nuclear clusterin, a cell death protein. *The Journal of Biological Chemistry*, 278(13), 11590-11600.

Libby, R. T., Lillo, C., Kitamoto, J., Williams, D. S., and Steel, K. P. (2004). Myosin va is required for normal photoreceptor synaptic activity. *Journal of Cell Science*, 117(19), 4509-4515.

Lin, Z. Q., Kondo, T., Ishida, Y., Takayasu, T., and Mukaida, N. (2003). Essential involvement of IL-6 in the skin wound-healing process as evidenced by delayed wound healing in IL-6-deficient mice. *Journal of Leukocyte Biology*, 73(6), 713-721.

Liu, X., Wen, F., Yang, J., Chen, L., and Wei, Y. (2010). A review of current applications of mass spectrometry for neuroproteomics in epilepsy. *Mass Spectrometry Reviews*, 29(2), 197-246.

Mallick, P. and Kuster, B. (2010). Proteomics: A pragmatic perspective. *Nature Biotechnology*, 28(7), 695-709.

Marshall, P., Toteu-Djomte, V., Bareille, P., Perry, H., Brown, G., Baumert, M. and Biggadike, K. (2010). Correlation of skin blanching and percutaneous absorption for glucocorticoid receptor agonists by matrix-assisted laser desorption ionization mass spectrometry imaging and liquid extraction surface analysis with nanoelectrospray ionization mass spectrometry. *Analytical Chemistry*, 82(18), 7787-7794.

Martínez, A., Ozbun, L. L., Angdisen, J., and Jakowlew, S. B. (2002). Expression of differentially expressed nucleolar transforming growth factor - β 1 target (DENTT) in adult mouse tissues. *Developmental Dynamics*, 224(2), 186-199.

Matsui, T; Amano, M; Yamamoto, T; Chihara, K; Nakafuku, M; Ito, M; Nakano, T; Okawa, K; Iwamatsu, A; and Kaibuchi, K. (1996). Rho-associated kinase, a novel serine/threonine kinase, as a putative target for small GTP binding protein rho. *The EMBO Journal*, 15(9), 2208.

McGinnis, S. and Madden, T. L. (2004). BLAST: At the core of a powerful and diverse set of sequence analysis tools. *Nucleic Acids Research*, 32(suppl 2), W20-W25.

Mendioroz, S., Pajares, J. A., Benito, I., Pesquera, C., González, F., and Blanco, C. (1987). Texture evolution of montmorillonite under progressive acid treatment: Change from H3 to H2 type of hysteresis. *Langmuir*, 3(5), 676-681.

Micromeritics® Instrument Corporation (n.d.) *Gas Adsorption Theory*. [report] Norcross, Georgia: Micromeritics® Instrument Corporation.

Micromeritics® Saturn DigiSizer® II (n.d.) *Saturn DigiSizer® II: High-Definition Digital Particle Size Analyzer*. [e-book] Saturn DigiSizer® II.

<http://www.instrument.com.cn/show/literature/c12218.pdf> [Accessed: November 2012].

Mitsui, K., Tokuzawa, Y., Itoh, H., Segawa, K., Murakami, M., Takahashi, K., Maruyama, M., Maeda, M. and Yamanaka, S. (2003). The homeoprotein nanog is required for maintenance of pluripotency in mouse epiblast and ES cells. *Cell*, 113(5), 631-642.

Moritz, A. R. and Henriques, F. C. (1947). Studies of thermal injury: II. the relative importance of time and surface temperature in the causation of cutaneous burns. *The American Journal of Pathology*, 23(5), 695-720.

Mosavi, L. K., Cammett, T. J., Desrosiers, D. C., and Peng, Z. (2004). The ankyrin repeat as molecular architecture for protein recognition. *Protein Science*, 13(6), 1435-1448.

Mosavi, L. K., Minor Jr, D. L., and Peng, Z. (2002). Consensus-derived structural determinants of the ankyrin repeat motif. *Proceedings of the National Academy of Sciences*, 99(25), 16029-16034.

Mosier-Boss, P. A. and Lieberman, S. H. (1999). Comparison of three methods to improve adherence of thin gold films to glass substrates and their effect on the SERS response. *Applied Spectroscopy*, 53(7), 862-873.

Muller, M., Trocme, C., Lardy, B., Morel, F., Halimi, S., and Benhamou, P. Y. (2008). Matrix metalloproteinases and diabetic foot ulcers: The ratio of MMP-1 to TIMP-1 is a predictor of wound healing. *Diabetic Medicine*, 25(4), 419-426.

Murayama, C., Kimura, Y., and Setou, M. (2009). Imaging mass spectrometry: Principle and application. *Biophysical Reviews*, 1(3), 131-139.

Namimatsu, S., Ghazizadeh, M., and Sugisaki, Y. (2005). Reversing the effects of formalin fixation with citraconic anhydride and heat: A universal antigen retrieval method. *Journal of Histochemistry and Cytochemistry*, 53(1), 3-11.

Nanney, L. B., Caldwell, R. L., Pollins, A. C., Cardwell, N. L., Opalenik, S. R., and Davidson, J. M. (2006). Novel approaches for understanding the mechanisms of wound repair. *Journal of Investigative Dermatology.Symposium Proceedings*, 11(1), 132-139.

Naono, H., Hakuman, M., and Shiono, T. (1997). Analysis of nitrogen adsorption isotherms for a series of porous silicas with uniform and cylindrical pores: A new method of calculating pore size distribution of pore radius 1-2 nm. *Journal of Colloid and Interface Science*, 186(2), 360-368.

Nielsen, M. L., Savitski, M. M., and Zubarev, R. A. (2005). Improving protein identification using complementary fragmentation techniques in fourier transform mass spectrometry. *Molecular and Cellular Proteomics*, 4(6), 835-845.

Nimchinsky, E. A., Sabatini, B. L., and Svoboda, K. (2002). Structure and function of dendritic spines. *Annual Review of Physiology*, 64(1), 313-353.

Nishio, N., Ito, S., Suzuki, H., and Isobe, K. (2009). Antibodies to wounded tissue enhance cutaneous wound healing. *Immunology*, 128(3), 369-380.

O'Malley, R. (2002). Life's (more than) a BLAST. *The Biochemist*, 24, 21-23.

Ohtsuka, T., Takao-Rikitsu, E., Inoue, E., Inoue, M., Takeuchi, M., Matsubara, K., Deguchi-Tawarada, M., Satoh, K., Morimoto, K. and Nakanishi, H. (2002). Cast a novel protein of the cytomatrix at the active zone of synapses that forms a ternary complex with RIM1 and munc13-1. *The Journal of Cell Biology*, 158(3), 577-590.

Olsen, J. V., Ong, S. E., and Mann, M. (2004). Trypsin cleaves exclusively C-terminal to arginine and lysine residues. *Molecular and Cellular Proteomics*, 3(6), 608-614.

Önnerfjord, P. (n.d.) *Mass identity of biomolecules by MALDI-TOF MS*. [e-book] Lund, Sweden: p.1-9. <http://www.docin.com/p-273219794.html> [Accessed: 12 October 2010].

Oosthuizen, M., Bouwer, W., and Cromarty, A. D. (2009). *Comparative histological and flow cytometric assay for wounds during healing*. Unpublished manuscript.

Osman O, Tortorella M, Londei M, and Quaratino S. (2002). Expression of matrix metalloproteinases and tissue inhibitors of metalloproteinases define the migratory characteristics of human monocyte-derived dendritic cells. *Immunology*, 105, 73.

Pan, G. and Pei, D. (2005). The stem cell pluripotency factor NANOG activates transcription with two unusually potent subdomains at its C terminus. *Journal of Biological Chemistry*, 280(2), 1401-1407.

Papazoglou, E. S., Zubkov, L., Mao, X., Neidrauer, M., Rannou, N., and Weingarten, M. S. (2010). Image analysis of chronic wounds for determining the surface area. *Wound Repair and Regeneration*, 18(4), 349-358.

Park, M. Y., Jang, H. D., Lee, S. Y., Lee, K. J., and Kim, E. (2004). Fas-associated factor-1 inhibits nuclear factor- κ B (NF- κ B) activity by interfering with nuclear translocation of the RelA (p65) subunit of NF- κ B. *Journal of Biological Chemistry*, 279(4), 2544-2549.

Pond, W., Yen, J., and Crouse, J. (1989). Tissue mineral element content in swine fed clinoptilolite. *Bulletin of Environmental Contamination and Toxicology*, 42(5), 735-742.

Presley, J.F., Smith, C., Hirschberg, K., Miller, C., Cole, N.B., Zaal, K.J.M. and Lippincott-Schwartz, J. (1998). Golgi membrane dynamics. *Molecular Biology of the Cell*, 9(7), 1617-1626.

Rastogi, S. C., Mendiratta, N., and Rastogi, P. (2006). *Bioinformatics: Methods and applications* (Second ed.). New Delhi: Prentice-Hall of India.

Record, C.J., Chaikuad, A., Rellos, P., Das, S., Pike, A.C.W., Fedorov, O., Marsden, B.D., Knapp, S. and Lee, W.H. (2010). Structural comparison of human mammalian ste20-like kinases. *PloS One*, 5(8), e11905.

Resing, K. A. and Ahn, N. G. (2005). Proteomics strategies for protein identification. *FEBS Letters*, 579(4), 885-889.

Roberts, B. (1967). A procedure for estimating pore volume and area distributions from sorption isotherms. *Journal of Colloid and Interface Science*, 23(2), 266-273.

Ronci, M., Bonanno, E., Colantoni, A., Pieroni, L., Di Ilio, C., Spagnoli, L.G., Federici, G. and Urbani, A. (2008). Protein unlocking procedures of formalin-fixed paraffin-embedded tissues: Application to MALDI-TOF imaging MS investigations. *Proteomics*, 8(18), 3702-3714.

Roth, A. (1994). *Vacuum sealing techniques*. New York: American Institute of Physics.

Royet, J., Bouwmeester, T., and Cohen, S. M. (1998). Notchless encodes a novel WD40-repeat-containing protein that modulates notch signaling activity. *The EMBO Journal*, 17(24), 7351-7360.

Sakintuna, B., Aktaş, Z., and Yürüm, Y. (2003). Synthesis of porous carbon materials by carbonization in natural zeolite nanochannels. *Prepr.Pap.-Am.Chem.Soc., Div.Fuel Chem*, 48(2), 614.

Salama, T. M., Ali, I. O., Hanafy, A. I., and Al-Meligy, W. M. (2009). A novel synthesis of NaA zeolite encapsulated iron (III) schiff base complex: Photocatalytic oxidation of direct blue-1 dye with hydrogen peroxide. *Materials Chemistry and Physics*, 113(1), 159-165.

Scherer, S. S., Xu, Y., Bannerman, P., Sherman, D. L., and Brophy, P. J. (1995). Periaxin expression in myelinating schwann cells: Modulation by axon-glia interactions and polarized localization during development. *Development*, 121(12), 4265-4273.

Schultz, G. S. and Wysocki, A. (2009). Interactions between extracellular matrix and growth factors in wound healing. *Wound Repair and Regeneration*, 17(2), 153-162.

Seeley, E. H., and Caprioli, R. M. (2011). MALDI imaging mass spectrometry of human tissue: Method challenges and clinical perspectives. *Trends in Biotechnology*, 29(3), 136-143.

Serra-Pagès, C., Medley, Q. G., Tang, M., Hart, A., and Streuli, M. (1998). Liprins, a family of LAR transmembrane protein-tyrosine phosphatase-interacting proteins. *Journal of Biological Chemistry*, 273(25), 15611-15620.

Shaw, A. S. and Filbert, E. L. (2009). Scaffold proteins and immune-cell signalling. *Nature Reviews Immunology*, 9(1), 47-56.

Shevchenko, A., Sunyaev, S., Loboda, A., Shevchenko, A., Bork, P., and Ens, W. (2001). Charting the proteomes of organisms with unsequenced genomes by MALDI-quadrupole time-of-flight mass spectrometry and BLAST homology searching. *Analytical Chemistry*, 73(9), 1917-1926.

Sibbald, R.G, and Woo, K. Y. (2008). The biology of chronic foot ulcers in persons with diabetes. *Diabetes/metabolism Research and Reviews*, 24(S1), S25-S30.

Sigma-Aldrich® (n.d.) *Preparing Self-Assembled Monolayers (SAMs) A Step-by-Step Guide for Solution-Based Self-Assembly*. Aldrich® Technical Bulletins. [report] Milwaukee, USA: Sigma-Aldrich®, p.1-3.

Silverthorn, D. U. (2003). *Human physiology: An integrated approach* (3rd edition ed.) Benjamin-Cummings Publishing Company.

Simpson, H. (1986). The MASCOT method. *Software Engineering Journal*, 1(3), 103-120.

Simpson, H. and Jackson, K. (1979). Process synchronisation in MASCOT. *The Computer Journal*, 22(4), 332-345.

Sing, K. S. W. (1998). Adsorption methods for the characterization of porous materials. *Advances in Colloid and Interface Science*, 76–77(0), 3-11.

Sing, K., Sing, K., Everett, D., Haul, R., Moscou, L., Pierotti, R., Rouquerol, J., and Siemieniewska, T. (1982). Reporting physisorption data for gas/solid systems. *Pure and Appl Chem*, 54(11), 2201.

Singer, A. J. and Clark, R. A. (1999). Cutaneous wound healing. *New England Journal of Medicine*, 341(10), 738-746.

Smith, J. (1984). Definition of a zeolite. *Zeolites*, 4(4), 309-310.

Smith, T. F. (2008). Diversity of WD-repeat proteins. *The Coronin Family of Proteins*, 20-30.

Song, W. K., Wang, W., Sato, H., Bielser, D. A., and Kaufman, S. J. (1993). Expression of alpha 7 integrin cytoplasmic domains during skeletal muscle development: Alternate forms, conformational change, and homologies with serine/threonine kinases and tyrosine phosphatases. *Journal of Cell Science*, 106(4), 1139-1152.

Sözeri, O., Vollmer, K., Liyanage, M., Frith, D., Kour, G., Mark 3rd, G. and Stabel, S. (1992). Activation of the c-raf protein kinase by protein kinase C phosphorylation. *Oncogene*, 7(11), 2259.

Spector, D. L. and Lamond, A. I. (2011). Nuclear speckles. *Cold Spring Harbor Perspectives in Biology*, 3(2)

Storck, S., Bretinger, H., and Maier, W. F. (1998). Characterization of micro-and mesoporous solids by physisorption methods and pore-size analysis. *Applied Catalysis A: General*, 174(1), 137-146.

Striegl, H., Roske, Y., Kümmel, D., and Heinemann, U. (2009). Unusual armadillo fold in the human general vesicular transport factor p115. *PLoS One*, 4(2), e4656.

Sullivan, T. P., Eaglstein, W. H., Davis, S. C., and Mertz, P. (2001). The pig as a model for human wound healing. *Wound Repair Regen*, 9(2), 66-76.

Tanaka, K., Waki, H., Ido, Y., Akita, S., Yoshida, Y., Yoshida, T. and Matsuo, T. (1988). Protein and polymer analyses up to m/z 100 000 by laser ionization time-of-

flight mass spectrometry. *Rapid Communications in Mass Spectrometry*, 2(8), 151-153.

Tarran, S.L., Craft, G.E., Valova, V., Robinson, P.J., Thomas, G., Markham, R., Langlois, N.E. and Vanezis, P. (2007). The use of proteomics to study wound healing: A preliminary study for forensic estimation of wound age. *Medicine, Science and the Law*, 47(2), 134-140.

Thiede, B., Hohenwarter, W., Krah, A., Mattow, J., Schmid, M., Schmidt, F. and Jungblut, P.R. (2005). Peptide mass fingerprinting. *Methods (Duluth)*, 35(3), 237-247.

Thommes, M. (2010). Physical adsorption characterization of nanoporous materials. *Chemie Ingenieur Technik*, 82(7), 1059-1073.

Tian, J., Wong, K. K., Ho, C., Lok, C., Yu, W., Che, C., Chiu, J., and Tam, P. K. (2007). Topical delivery of silver nanoparticles promotes wound healing. *Chemmedchem*, 2(1), 129-136.

Troyanovsky, B., Levchenko, T., Månsson, G., Matvijenko, O., and Holmgren, L. (2001). Angiomotin an angiostatin binding protein that regulates endothelial cell migration and tube formation. *The Journal of Cell Biology*, 152(6), 1247-1254.

Tsapatsis, M., Lovallo, M., Okubo, T., Davis, M. E., and Sadakata, M. (1995). Characterization of zeolite L nanoclusters. *Chemistry of Materials*, 7(9), 1734-1741.

Twomey, T., Mackay, M., Kuipers, H., and Thompson, R. (1994). In situ observation of silicalite nucleation and growth: A light-scattering study. *Zeolites*, 14(3), 162-168.

Uehata, M., Ishizaki, T., Satoh, H., Ono, T., Kawahara, T., Morishita, T., Tamakawa, H., Yamagami, K., Inui, J. and Maekawa, M. (1997). Calcium sensitization of smooth muscle mediated by a rho-associated protein kinase in hypertension. *Nature*, 389(6654), 990-993.

Ungar, D., Oka, T., Vasile, E., Krieger, M., and Hughson, F. M. (2005). Subunit architecture of the conserved oligomeric golgi complex. *Journal of Biological Chemistry*, 280(38), 32729-32735.

Van Remoortere, A., Van Zeijl, R.J.M., Van den Oever, N., Franck, J., Longuespée, R., Wisztorski, M., Salzet, M., Deelder, A.M., Fournier, I. and McDonnell, L.A. (2010). MALDI imaging and profiling MS of higher mass proteins from tissue. *Journal of the American Society for Mass Spectrometry*, 21(11), 1922-1929.

Vanderhallen, F., Deriemaeker, L., Manderick, B., and Finsy, R. (2002). Shape and size determination by laser diffraction: Parametric density estimation by neural networks. *Particle and Particle Systems Characterization*, 19(2), 65-72.

Vardaxis, N. J., Brans, T. A., Boon, M. E., Kreis, R. W., and Marres, L. M. (1997). Confocal laser scanning microscopy of porcine skin: Implications for human wound healing studies. *Journal of Anatomy*, 190(Pt 4), 601-611.

Veenstra, T., Veenstra, T., and Yates, J. (2006). Mass spectrometry: The foundation of proteomics. *Proteomics for Biological Discovery*. J Wiley and Sons, , 1-18.

Velander, P., Theopold, C., Hirsch, T., Bleiziffer, O., Zuhaili, B., Fossum, M., Hoeller, D., Gheerardyn, R., Chen, M., Visovatti, S., Svensson, H., Yao, F. and Eriksson, E. (2008). Impaired wound healing in an acute diabetic pig model and the effects of local hyperglycemia. *Wound Repair and Regeneration*, 16(2), 288-293.

Wagner, W., Brenowitz, S. D., and Hammer III, J. A. (2010). Myosin-va transports the endoplasmic reticulum into the dendritic spines of purkinje neurons. *Nature Cell Biology*, 13(1), 40-48.

Wagner, S., Coerper, S., Fricke, J., Hunt, T.K., Hussain, Z., Elmlinger, M.W., Mueller, J.E. and Becker, H.D. (2003). Comparison of inflammatory and systemic sources of growth factors in acute and chronic human wounds. *Wound Repair and Regeneration*, 11(4), 253-260.

Walch, A., Rauser, S., Deininger, S. O., and Hofler, H. (2008). MALDI imaging mass spectrometry for direct tissue analysis: A new frontier for molecular histology. *Histochemistry and Cell Biology*, 130(3), 421-434.

Wang, C., Li, J., Wang, L., and Sun, X. (2008). Influence of NaOH concentrations on synthesis of pure-form zeolite A from fly ash using two-stage method. *Journal of Hazardous Materials*, 155(1), 58-64.

Wang, J. F., Olson, M. E., Reno, C. R., Wright, J. B., and Hart, D. A. (2001). The pig as a model for excisional skin wound healing: Characterization of the molecular and cellular biology, and bacteriology of the healing process. *Comp Med*, 51(4), 341-348.

Wang, S., Zhu, Z. H., Coomes, A., Haghseresht, F., and Lu, G. Q. (2005). The physical and surface chemical characteristics of activated carbons and the adsorption of methylene blue from wastewater. *Journal of Colloid and Interface Science*, 284(2), 440-446.

Weatherly, D. B., Atwood, J. A., Minning, T. A., Cavola, C., Tarleton, R. L., and Orlando, R. (2005). A heuristic method for assigning a false-discovery rate for protein identifications from mascot database search results. *Molecular and Cellular Proteomics*, 4(6), 762-772.

Webb, P. (n.d.) *Interpretation of Particle Size Reported by Different Analytical Techniques*. [e-book] Micromeritics Instrument Corporation.

<http://www.micromeritics.com/pdf/mas/interpretation%20of%20particle%20size%20by%20different%20techniques.pdf> [Accessed: 2012].

Webb, P. A (2004) *Why Demand for the SediGraph Endures*. The microReport Vol 15 No 1. [report] Micromeritics® Instrument Corporation.

Werner, M., Chott, A., Fabiano, A., and Battifora, H. (2000). Effect of formalin tissue fixation and processing on immunohistochemistry. *The American Journal of Surgical Pathology*, 24(7), 1016.

Wienands, J., Schweikert, J., Wollscheid, B., Jumaa, H., Nielsen, P. J., and Reth, M. (1998). SLP-65: A new signaling component in B lymphocytes which requires

expression of the antigen receptor for phosphorylation. *The Journal of Experimental Medicine*, 188(4), 791-795.

Woodford, C. (2012) *Zeolites*. [image online] Available at:
<http://cdn4.explainthatstuff.com/zeolite-crystal-structure.jpg> [Accessed: April 2013].

Worley, K. C., Wiese, B. A., and Smith, R. F. (1995). BEAUTY: An enhanced BLAST-based search tool that integrates multiple biological information resources into sequence similarity search results. *Genome Research*, 5(2), 173-184.

Xu, C., and Ma, B. (2006). Software for computational peptide identification from MS-MS data. *Drug Discovery Today*, 11(13-14), 595-600.

Yağşı, N. (2004). *Production and Characterisation of Activated Carbon from Apricot Stones*. MSc. The Middle East Technical University.

Yamashita, S. (2007). Heat-induced antigen retrieval: Mechanisms and application to histochemistry. *Progress in Histochemistry and Cytochemistry*, 41(3), 141-200.

Yates, J. R., 3rd. (1998). Mass spectrometry and the age of the proteome. *Journal of Mass Spectrometry*, 33(1), 1-19.

Yi, W., Haapasalo, H., Holmlund, C., Jarvela, S., Raheem, O., Bergenheim, A.T., Hedman, H. and Henriksson, R. (2009). Expression of leucine-rich repeats and immunoglobulin-like domains (LRIG) proteins in human ependymoma relates to tumor location, WHO grade, and patient age. *Clinical Neuropathology*, 28(1), 21-27.

Yoon, Y.M., Baek, K.H., Jeong, S.J., Shin, H.J., Ha, G.H., Jeon, A.H., Hwang, S.G., Chun, J.S. and Lee, C.W. (2004). WD repeat-containing mitotic checkpoint proteins act as transcriptional repressors during interphase. *FEBS Letters*, 575(1), 23-29.

Young, S. (2005). *Method Development and Validation for Measuring the Particle Size Distribution of Pentaerythritol Tetranitrate (PETN) Powders*,

Yu, J. C., Xu, A., Zhang, L., Song, R., and Wu, L. (2004). Synthesis and characterization of porous magnesium hydroxide and oxide nanoplates. *The Journal of Physical Chemistry B*, 108(1), 64-70.

Zarembinski, T.I., Hung, L.W., Mueller-Dieckmann, H.J., Kim, K.K., Yokota, H., Kim, R. and Kim, S.H. (1998). Structure-based assignment of the biochemical function of a hypothetical protein: A test case of structural genomics. *Proceedings of the National Academy of Sciences*, 95(26), 15189-15193.

Zhang, Y., Smith, A.D., Renfrow, M.B., Schneider, D.A., Zhang, Y., Smith IV, A.D., Renfrow, M.B. and Schneider, D.A. (2010). The RNA polymerase-associated factor 1 complex (Paf1C) directly increases the elongation rate of RNA polymerase I and is required for efficient regulation of rRNA synthesis. *Journal of Biological Chemistry*, 285(19), 14152-14159.

Zhao, C., Jiang, H., Smith, D. R., Bruckenstein, S., and Wood, T. D. (2006). Integration of an on-line protein digestion microreactor to a nanoelectrospray emitter for peptide mapping. *Analytical Biochemistry*, 359(2), 167-175.

Zhu, R., Iacovino, M., Mahen, E., Kyba, M., and Matin, A. (2011). Transcripts that associate with the RNA binding protein, DEAD-END (DND1), in embryonic stem (ES) cells. *BMC Molecular Biology*, 12(1), 37.

APPENDIX: Letters of ethical approval and statistical analysis

AESC 3

UNIVERSITY OF THE WITWATERSRAND, JOHANNESBURG

STRICTLY CONFIDENTIAL

ANIMAL ETHICS SCREENING COMMITTEE (AESC)

CLEARANCE CERTIFICATE NO. 2008/47/04

APPLICANT: Ms W Potgieter

SCHOOL: Department of Pharmacology

DEPARTMENT:

LOCATION: University of Pretoria


PROJECT TITLE: The investigation of Absorbatox as a wound healing agent when applied as a wound dressing

Number and Species

6 30kg female white pigs

Approval was given for the use of animals for the project described above at an AESC meeting held on 30.09.2008. This approval remains valid until 30.09.2010

The use of these animals is subject to AESC guidelines for the use and care of animals, is limited to the procedures described in the application form and to the following additional conditions:

Signed:  _____ Date: 06/10/2008
(Chairperson, AESC)

I am satisfied that the persons listed in this application are competent to perform the procedures therein, in terms of Section 23 (1) (c) of the Veterinary and Para-Veterinary Professions Act (19 of 1982)

Signed:  _____ Date: 06/10/2008
(Registered Veterinarian)

cc: Supervisor:
Director: CAS

Works 2000/In0015/AESCcert.wps

100
1908 - 2008



UNIVERSITEIT VAN PRETORIA
UNIVERSITY OF PRETORIA
YUNIBESITHI YA PRETORIA

Ref: H027-08

10 December 2008

ANIMAL USE AND CARE COMMITTEE

Private Bag X04
Onderstepoort
0110

Tel: 012-529 8434
Fax: 012-529 8300


Prof JR Snyman
Department of Pharmacology
Faculty of Health Sciences
University of Pretoria
(jacques.snyman@up.ac.za)

Dear Prof Snyman

H027-08: The investigation of Absorbatox® as a wound healing agent when applied as a wound dressing (W Potgieter)

Your reply to the questions raised by the AUCC is accepted and the above protocol was approved by the Chairman of the Animal Use and Care Committee.

Best regards



Elmarie Mostert
AUCC Contact Person

Copy: Dr AD Cromarty
W Potgieter

100
1908 - 2008



UNIVERSITEIT VAN PRETORIA
UNIVERSITY OF PRETORIA
YUNIBESITHI YA PRETORIA

Ref: H027-08 (Amendment 1)

27 January 2009

Prof JR Snyman
Department of Pharmacology
Faculty of Health Sciences
(jacques.snyman@up.ac.za)

ANIMAL USE AND CARE COMMITTEE

Private Bag X04
Onderstepoort
0110

Tel: 012-529 8434
Fax: 012-529 8300

Dear Prof Snyman

H027-08 (Amendment 1): The investigation of Absorbatox[®] as a wound healing agent when applied as a wound dressing (W Potgieter)

The above protocol amendment was approved by the Animal Use and Care Committee at its meeting held on 26 January 2009.

Best regards

Elmarie Mostert
AUCC Contact Person

Copy: Dr AD Cromarty
W Potgieter

The Research Ethics Committee, Faculty Health Sciences, University of Pretoria complies with ICH-GCP guidelines and has US Federal wide Assurance.

- * **FWA** 00002567, Approved dd 22 May 2002 and Expires 20 Oct 2016.
- * **IRB** 0000 2235 IORG0001762 Approved dd 13/04/2011 and Expires 13/04/2014.



Universiteit van Pretoria
University of Pretoria

Faculty of Health Sciences Research Ethics Committee
Fakulteit Gesondheidswetenskappe Navorsingsetiekkomitee

DATE: 1/10/2012

NUMBER	184/2012 - Late submission : E-mail to all members
TITLE OF THE PROTOCOL	Characterisation of Absorbatox™ as a wound healing agent
PRINCIPAL INVESTIGATOR	Miss K Mncube Dept:Pharmacology;University of Pretoria. Cell:0724595352E-Mail: khulekani.mncube@gmail.com
SUB INVESTIGATOR	Not Applicable
STUDY COORDINATOR	Not Applicable
SUPERVISOR (ONLY when STUDENTS)	Dr Duncan A. Cromarty E-Mail: duncan.cromarty@up.ac.za
STUDY DEGREE	MSc
SPONSOR COMPANY	Not applicable
MEETING DATE	26/09/2012

The Protocol was approved on 26/09/2012 by a properly constituted meeting of the Ethics Committee subject to the following conditions:

1. The approval is valid for 3 years period [till the end of December 2015], and
2. The approval is conditional on the receipt of 6 monthly written Progress Reports, and
3. The approval is conditional on the research being conducted as stipulated by the details of the documents submitted to and approved by the Committee. In the event that a need arises to change who the investigators are, the methods or any other aspect, such changes must be submitted as an Amendment for approval by the Committee.

Members of the Research Ethics Committee:

Prof M J Bester	(female)BSc (Chemistry and Biochemistry); BSc (Hons)(Biochemistry); MSc(Biochemistry); PhD (Medical Biochemistry)
Prof R Delpont	(female)BA et Scien, B Curationis (Hons) (Intensive care Nursing), M Sc (Physiology), PhD (Medicine), M Ed Computer Assisted Education
Dr NK Likibi	MBB HM – Representing Gauteng Department of Health) MPH
Dr MP Mathebula	(female)Deputy CEO: Steve Biko Academic Hospital; MBChB, PDM, HM
Prof A Nienaber	(female) BA(Hons)(Wits); LLB; LLM; LLD(UP); PhD; Dipl.Datametrics(UNISA) – Legal advisor
Mrs MC Nzeku	(female) BSc(NUL); MSc(Biochem)(UCL, UK) – Community representative
Prof L M Ntlhe	MbChB (Natal) FCS (SA)
Snr Sr J Phatoli	(female) BCur(Eet.A); BTec(Oncology Nursing Science) – Nursing representative
Dr R Reynders	MBChB (Prêt), FCPaed (CMSA) MRCPCH (Lon) Cert Med. Onc (CMSA)
Dr T Rossouw	(female) MBChB (cum laude); M.Phil (Applied Ethics) (cum laude), MPH (Biostatistics and Epidemiology (cum laude), D.Phil
Dr L Schoeman	(female) B.Pharm, BA(Hons)(Psych), PhD – Chairperson: Subcommittee for students' research
Mr Y Sikweyiya	MPH; SARETI Fellowship in Research Ethics; SARETI ERCTP; BSc(Health Promotion)Postgraduate Dip (Health Promotion) – Community representative

Dr R Sommers (female) MBChB; MMed(Int); MPharmMed – **Deputy Chairperson**
Prof TJP Swart BChD, MSc (Odont), MChD (Oral Path), PGCHE – School of Dentistry representative
Prof C W van Staden MBChB; MMed (Psych); MD; FCPsych; FTCL; UPLM - **Chairperson**



DR R SOMMERS; MBChB; MMed(Int); MPharmMed.
Deputy Chairperson of the Faculty of Health Sciences Research Ethics Committee, University of Pretoria

◆ Tel: 012-3541330 ◆ Fax: 012-3541367 / 0866515924 ◆ E-Mail: manda@med.up.ac.za
◆ Web: //www.healthethics-up.co.za ◆ H W Snyman Bld (South) Level 2-34 ◆ Private Bag x 323, Arcadia, Pta, S.A., 0007



UNIVERSITEIT VAN PRETORIA
UNIVERSITY OF PRETORIA
YUNIBESITHI YA PRETORIA
Denkilekis • Leading Minds • Dikgopolo tsa Dihlotefi

DEPARTMENT OF STATISTICS

LETTER OF STATISTICAL SUPPORT

Date: 11 April 2012

This letter is to confirm that **K Mncube**, studying at the University of Pretoria, discussed the project with the title **Characterisation of ABSORBATOX™ as a wound healing agent** with me.

I hereby confirm that I am aware of the project and also undertake to assist with the statistical analysis of the data generated from the project.

The data analysis consists of two-way analyses of variance (ANOVA) to compare the effects of treatments.

The sample consists of the outcomes (length, width and depth) of treatments (Absorbatox vs Control – Negative and Positive) on 20 wounds on each of 2 pigs measured after 1, 2, 3, 6, 9, 13 and 16 days.

NAME: Prof FE Steffens
Department of Statistics
Internal Consultation Service
Tel 012 420 5042

